

University of Windsor

Scholarship at UWindor

Electronic Theses and Dissertations

Theses, Dissertations, and Major Papers

2010

Tensile Behaviour and Microstructure of Permanent Mould Cast Magnesium Alloy AJ62 Subject to Corrosion

Jonathan Burns
University of Windsor

Follow this and additional works at: <https://scholar.uwindsor.ca/etd>

Recommended Citation

Burns, Jonathan, "Tensile Behaviour and Microstructure of Permanent Mould Cast Magnesium Alloy AJ62 Subject to Corrosion" (2010). *Electronic Theses and Dissertations*. 176.
<https://scholar.uwindsor.ca/etd/176>

This online database contains the full-text of PhD dissertations and Masters' theses of University of Windsor students from 1954 forward. These documents are made available for personal study and research purposes only, in accordance with the Canadian Copyright Act and the Creative Commons license—CC BY-NC-ND (Attribution, Non-Commercial, No Derivative Works). Under this license, works must always be attributed to the copyright holder (original author), cannot be used for any commercial purposes, and may not be altered. Any other use would require the permission of the copyright holder. Students may inquire about withdrawing their dissertation and/or thesis from this database. For additional inquiries, please contact the repository administrator via email (scholarship@uwindsor.ca) or by telephone at 519-253-3000ext. 3208.

TENSILE BEHAVIOUR AND MICROSTRUCTURE OF PERMANENT MOULD
CAST MAGNESIUM ALLOY AJ62 SUBJECT TO CORROSION

by
Jonathan Robert Burns

A Thesis
Submitted to the Faculty of Graduate Studies
through Engineering Materials
in Partial Fulfillment of the Requirements for
the Degree of Master of Applied Science
at the
University of Windsor

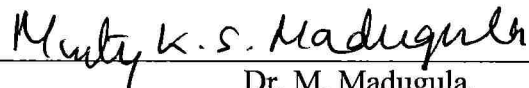
Windsor, Ontario, Canada
2010
© 2010 Jonathan Robert Burns

Tensile Behaviour and Microstructure of Permanent Mould Cast Magnesium Alloy AJ62
Subject to Corrosion

by

Jonathan Robert Burns

APPROVED BY:



Dr. M. Madugula,
Department of Civil and Environmental Engineering

Department of Mechanical, Automotive, and Materials Engineering

Dr. X. Nie, Co-Advisor
Department of Mechanical, Automotive, and Materials Engineering



Dr. H. Hu, Co-Advisor
Department of Mechanical, Automotive, and Materials Engineering

Department of Mechanical, Automotive, and Materials Engineering

September 08, 2010

DECLARATION OF PREVIOUS PUBLICATION

This thesis includes 3 original papers that have been previously published in peer reviewed proceedings, as follows:

Thesis Chapter	Publication title/full citation	Publication status
<i>Chapter 2</i>	Burns, J.R. Han, L. Hu, H. Nie, X. Effects of section thicknesses on tensile properties of permanent mould cast magnesium alloy AJ62. <i>Magnesium Technology 2010, The Minerals, Metals, and Materials Society.</i> (2010) 367-371.	<i>Published</i>
<i>Chapter 3</i>	Burns, J.R. Hu, H. Nie, X. Su, J.F. Corrosion of permanent mould cast Mg alloy AJ62 in NaCl solutions. <i>American Foundry Society.</i> (2010) Paper No. 10-022.	<i>Published</i>
<i>Chapter 4</i>	Burns, J.R. Hu, H. Nie, X. Han, L. Microstructure influence on the corrosion of permanent mould cast magnesium alloy AJ62 in engine coolant. <i>Society of Automotive Engineers.</i> (2010) Paper No. 2010-01-0412.	<i>Published</i>

I certify that I have obtained a written permission from the copyright owner(s) to include the above published material(s) in my thesis. I certify that the above material describes work completed during my registration as graduate student at the University of Windsor.

I declare that, to the best of my knowledge, my thesis does not infringe upon anyone's copyright nor violate any proprietary rights and that any ideas, techniques, quotations, or any other material from the work of other people included in my thesis, published or otherwise, are fully acknowledged in accordance with the standard referencing practices. Furthermore, to the extent that I have included copyrighted material that surpasses the bounds of fair dealing within the meaning of the Canada Copyright Act, I certify that I have obtained a written permission from the copyright owner(s) to include such material(s) in my thesis.

I declare that this is a true copy of my thesis, including any final revisions, as approved by my thesis committee and the Graduate Studies office, and that this thesis has not been submitted for a higher degree to any other University or Institution.

ABSTRACT

AJ62, containing notable amounts of strontium, exhibits a microstructure unique among aluminum-manganese based magnesium alloys. The benefit is improved high temperature mechanical performance among magnesium alloys, which are not known for this trait. Capacity for high temperature application makes AJ62 the focus of much research. The high temperature properties, coupled with the high strength to weight ratios of magnesium alloys, promise lightweight powertrain components for the automotive industry to lower fuel consumption, reduce emissions, and improve performance.

Castability of the alloy is demonstrated by its adaptation to the gravity-fed permanent mould casting process. Influential characteristics of its solidified microstructures are investigated and related to tensile and corrosion response, both independently and combined. A fine microstructure with good interdendritic eutectic phase continuity is favourable for mechanical and electrochemical properties. A recommendation for processing of the alloy is to target the benefits of a high cooling rate.

DEDICATION

This work is dedicated to Vanessa, Delores, Robert, and Kathleen whose ceaseless regimen of unconditional love and support is unsurpassed.

ACKNOWLEDGEMENTS

Dr. Hu and Dr. Nie are acknowledged for their guidance, encouragement, and fiscal support; Dr. Madugula and Dr. Bowers for offering suggestions and inspiration; John Robinson, Pat Seguin, and Andy Jenner for sharing technical knowledge and valuable time; Ontario Centres of Excellence and the Ontario Graduate Scholarship program for financial help; and lastly friends, family, colleagues, and peers for their various means of support.

TABLE OF CONTENTS

DECLARATION OF PREVIOUS PUBLICATION.....	iii
ABSTRACT.....	iv
DEDICATION.....	v
ACKNOWLEDGEMENTS.....	vi
LIST OF TABLES	x
LIST OF FIGURES	xi
LIST OF ABBREVIATIONS.....	xiii
LIST OF SYMBOLS	xiv
CHAPTER 1: INTRODUCTION	1
1.1 LITERATURE SURVEY	1
1.1.1 Pure Magnesium	2
1.1.2 Magnesium Alloys.....	3
1.1.3 Casting of Magnesium Alloys	8
1.1.4 Corrosion of Magnesium and its Alloys.....	10
1.1.5 Preceding Work	17
1.2 THESIS OBJECTIVES	20
1.3 THESIS ORGANISATION.....	21
1.4 REFERENCES	23
CHAPTER 2: EFFECTS OF SECTION THICKNESSES ON TENSILE PROPERTIES OF PERMANENT MOULD CAST MAGNESIUM ALLOY AJ62	28
2.1 INTRODUCTION	28
2.2 EXPERIMENTAL PROCEDURE	29
2.2.1 Casting Preparation.....	29
2.2.2 Tensile Testing.....	30
2.2.3 Microstructure and Fracture Analysis	30
2.3 RESULTS AND DISCUSSION	31
2.3.1 Microstructure Analysis.....	31
2.3.2 Tensile Testing.....	35
2.4 SUMMARY.....	38
2.5 REFERENCES	39
CHAPTER 3: CORROSION OF PERMANENT MOULD CAST MAGNESIUM ALLOY AJ62 IN NaCl SOLUTIONS.....	41
3.1 INTRODUCTION	41
3.2 EXPERIMENTAL PROCEDURE	42
3.2.1 Sample Preparation	42
3.2.2 Observation of Microstructure.....	43
3.2.3 Potentiodynamic Testing.....	44
3.2.4 Analysis of Potentiodynamic Findings	44
3.2.5 Observation of Corroded Surface	45
3.3 RESULTS AND DISCUSSION	45
3.3.1 Microstructure.....	45
3.3.2 Potentiodynamic Polarization	48
3.3.3 Corroded Surface	51

	3.4 CONCLUSIONS	54
	3.5 REFERENCES	55
CHAPTER 4:	MICROSTRUCTURE INFLUENCE ON THE CORROSION OF PERMANENT MOULD CAST MAGNESIUM ALLOY AJ62 IN ENGINE COOLANT	58
	4.1 INTRODUCTION	58
	4.2 IMMERSION TESTING.....	60
	4.2.1 Preparation of Specimens	60
	4.2.2 Immersion Test Procedure	61
	4.2.3 Immersion Test Results	63
	4.2.3.1 General Observations	63
	4.2.3.2 Corrosion Rate Due to Microstructure	66
	4.3 POTENTIODYNAMIC TESTING	68
	4.3.1 Preparation of Specimens	68
	4.3.2 Potentiodynamic Test Procedure	69
	4.3.3 Potentiodynamic Test Results.....	70
	4.4 CONCLUSIONS	72
	4.5 REFERENCES	73
CHAPTER 5:	CORROSION PERFORMANCE OF PERMANENT MOULD CAST MAGNESIUM ALLOY AJ62 IN AUTOMOTIVE ENVIRONMENTS	75
	5.1 INTRODUCTION	75
	5.2 EXPERIMENTAL METHODS	76
	5.3 RESULTS AND DISCUSSION	78
	5.3.1 Microstructural Analysis	78
	5.3.2 Response to Salt Solution	80
	5.3.3 Response to Engine Coolant.....	83
	5.4 CONCLUSIONS AND RECOMMENDATIONS	86
	5.5 REFERENCES	87
CHAPTER 6:	INFLUENCE OF CORROSION ON MECHANICAL PROPERTIES OF PERMANENT MOULD CAST AJ62	90
	6.1 INTRODUCTION	90
	6.2 EXPERIMENTAL METHOD.....	91
	6.2.1 Determination of Corrosion Parameters	91
	6.2.2 Corrosion of Tensile Specimens	93
	6.2.3 Tensile Response After Corrosion.....	94
	6.3 RESULTS AND DISCUSSION	94
	6.3.1 Stress Versus Strain	94
	6.3.2 Fractography	96
	6.3.3 Calculations	98
	6.4 CONCLUSIONS	100
	6.5 REFERENCES	101
CHAPTER 7:	CONCLUSIONS	104
	7.1 REVIEW OF OBJECTIVES	104
	7.2 SUMMARY OF OBSERVED RESULTS	104
	7.2.1 Mechanical Properties of Solidified AJ62.....	104

	7.2.2 Corrosion of Solidified AJ62 in NaCl Solutions	105
	7.2.3 Corrosion of Solidified AJ62 in Engine Coolant.....	106
	7.2.4 Effect of Chlorides and Inhibitors on Corrosion of Solidified AJ62.....	107
	7.2.5 Influence of Corrosion on Mechanical Properties of AJ62	108
	7.3 FINAL RECOMMENDATIONS	109
	7.4 REFERENCES	109
APPENDIX A:	CALCULATIONS FROM SECTION 6.3.3.....	110
APPENDIX B:	COPYRIGHT RELEASES FOR PREVIOUSLY PUBLISHED MANUSCRIPTS	113
VITA AUCTORIS		116

LIST OF TABLES

Table I-I	Examples of modern Mg-Al alloys and their nomenclature.....	6
Table I-II	Series of potentials for selected half-cell reactions	13
Table I-III	Dimensions of casting steps	18
Table I-IV	Thermophysical properties used to model the casting process.....	19
Table I-V	Publication information for presented manuscripts.....	23
Table II-I	Composition of AJ62 alloy in wt%	30
Table II-II	Variation of tensile properties with section thicknesses.....	36
Table III-I	Composition of AJ62 alloy in wt%	43
Table III-II	Summary of polarization curve characteristics and calculated polarization resistance	51
Table IV-I	Characteristic values for the polarization curves in Figure 4-8.....	72
Table V-I	Composition of AJ62 alloy.....	77
Table V-II	Critical values pertaining to Figure 5-6.....	81
Table V-III	Critical values pertaining to Figure 5-7	82
Table V-IV	Critical values pertaining to Figure 5-8.....	84
Table VI-I	Microstructural characteristics of various section thicknesses	91
Table VI-II	Characteristic stress-strain values for corroded PM AJ62 microstructures	96
Table VI-III	Characteristic stress-strain values for uncorroded PM AJ62 microstructures	96

LIST OF FIGURES

Fig. 1-1	Hexagonal close packed lattice structure [1].	2
Fig. 1-2	Binary aluminum-magnesium phase diagram adapted from [5].	4
Fig. 1-3	High-pressure die cast AM50 microstructure showing interdendritic eutectic material [13].	5
Fig. 1-4	Micrograph of die cast AJ62 showing the lamellar Al ₄ Sr interdendritic intermetallics [11].	7
Fig. 1-5	Schematic of resulting microstructure showing defect bands [25].	10
Fig. 1-6	Defect bands as they appear in the cross-section of an HPDC thickness [26].	10
Fig. 1-7	Concept of the galvanic cell.	11
Fig. 1-8	Effect of additions on corrosion of Mg in 3 % NaCl solution [6].	13
Fig. 1-9	Pourbaix diagram for the corrosion of Mg in water [6].	15
Fig. 1-10	Micro-galvanic corrosion progression of Mg alloy constituents [32].	16
Fig. 1-11	Illustration of the β -barrier concept showing microstructure (A) before and (B) after corrosion [9].	17
Fig. 1-12	3-dimensional rendering of the step casting with a gating and riser system [20].	18
Fig. 2-1	Schematic of casting shape.	29
Fig. 2-2	Optical micrographs from the (a) 4 mm and (b) 20 mm sections.	33
Fig. 2-3	SEM micrographs from (a) 4 mm, (b) 6 mm, (c) 10 mm, (d) 20 mm specimens.	34
Fig. 2-4	SEM image of permanent mould cast AJ62 microstructure.	34
Fig. 2-5	EDS spectrum for the matrix at location A in Figure 2-4.	35
Fig. 2-6	EDS spectrum for the cell boundary material at location B in Figure 2-4.	35
Fig. 2-7	EDS spectrum for the particle at location C in Figure 2-4.	35
Fig. 2-8	Average engineering stress-strain curves.	36
Fig. 2-9	Section thicknesses effect on UTS, YS, and E_f of permanent mould cast AJ62.	37
Fig. 2-10	Fractograph of 4 mm tensile specimen.	38
Fig. 2-11	Fractograph of 20 mm tensile specimen.	38
Fig. 3-1	This schematic represents the PM step-casting shape.	43
Fig. 3-2	This schematic shows the basic circuitry of the potentiodynamic testing set-up.	44
Fig. 3-3	The PM AJ62 alloy's microstructure includes: Primary α -Mg grains (A); Eutectic Al ₄ Sr and α (B); and Al-Mn intermetallics (C) [8].	46
Fig. 3-4	AJ62 grain size and intermetallic distribution are largely dependant on section thickness as is evident in the micrographs for the (a) 4 mm and (b) 20 mm sections.	47
Fig. 3-5	This graphic representation shows a significant difference in percent area intermetallic between the 4 mm and 20 mm section thicknesses.	48
Fig. 3-6	Potentiodynamic polarization of the AJ62 microstructures in a 0.5% NaCl solution yields this plot of potential versus current density.	49
Fig. 3-7	Potentiodynamic polarization of the AJ62 microstructures in a 1.0 % NaCl solution yields this plot of potential versus current density.	50

Fig. 3-8	The 4 mm AJ62 sample surface corroded in NaCl solution shows a morphology influenced by: (a) surface preparation, and (b) microstructure. 53	
Fig. 3-9	Corrosion morphology of the 20 mm sample was influenced more dominantly by the microstructure as in this micrograph.	53
Fig. 3-10	Micrographs of the corroded sample from the 20 mm section show oxide formation in α rich locations.....	54
Fig. 4-1	Microstructure of the permanent mould cast AJ62 alloy [5].....	59
Fig. 4-2	Step-casting shape [5].....	61
Fig. 4-3	Discoloured surface as compared with the alloy below a localised corrosion site. 66	
Fig. 4-4	Microstructure of (a) the 4mm section and (b) the 20mm section [5].....	67
Fig. 4-5	Mass loss as a function of thickness for the four durations with error accounting for instrumentation.	67
Fig. 4-6	Corrosion rate as a function of time (weeks) for different section thicknesses of the cast AJ62.	68
Fig. 4-7	Conceptual schematic of electrical circuits for potentiodynamic testing. ...	69
Fig. 4-8	Polarization curves for the permanent mould cast microstructures in engine coolant.	71
Fig. 5-1	AJ62 permanent mould step casting [13,14].	77
Fig. 5-2	Schematic of potentiodynamic test set-up [13].	78
Fig. 5-3	SEM micrograph in BSE mode showing microstructure of the 20 mm section: A, matrix; B, interdendritic eutectic; and C, Al-Mn intermetallic [18]. 79	
Fig. 5-4	SEM image in BSE mode of the (A) 4 mm and (B) 20mm section [18].....	79
Fig. 5-5	Graph of SDAS and area percent intermetallic.	80
Fig. 5-6	Potentiodynamic polarisation curves in 0.5 % NaCl [13].	81
Fig. 5-7	Potentiodynamic polarisation curves in 1.0 % NaCl [13].	82
Fig. 5-8	Potentiodynamic polarisation curves in coolant [14].	84
Fig. 6-1	Corroded sample showing depths of penetration from (A) general corrosion and (B) localised corrosion.....	93
Fig. 6-2	Engineering stress-strain for corroded PM AJ62 thicknesses.	95
Fig. 6-3	Engineering stress-strain curves of uncorroded PM AJ62 [15].....	96
Fig. 6-4	SEM micrograph of characteristic shrinkage void in thick sections showing dendrites.....	97
Fig. 6-5	SEM fractograph showing oxides in an opened discontinuity at (A) 500 x and (B) 100 x.	98

LIST OF ABBREVIATIONS

BSE	Back-Scattered Electron
CE	Counter Electrode
DAS	Dendrite Arm Spacing
E	Elastic Modulus
EDS	Energy Dispersive X-Ray Spectroscopy
HCP	Hexagonal Close Packed
HPDC	High Pressure Die Cast
PM	Permanent Mould
RE	Rare Earth Element
RE	Reference Electrode
SDAS	Secondary Dendrite Arm Spacing
SEM	Scanning Electron Microscopy
SHE	Standard Hydrogen Electrode
UTS	Ultimate Tensile Strength
WE	Working Electrode
YS	0.2 % Offset Yield Strength

LIST OF SYMBOLS

α	pro-eutectic and primary eutectic phase of HCP magnesium matrix
β	secondary eutectic phase
β_A	anodic Tafel slope
β_C	cathodic Tafel slope
η	overvoltage
a	unit cell dimension of an HCP lattice cell, radius of crack or flaw
A	cross-sectional area
A_{actual}	cross-sectional area less the area of cracks or flaws
b	distance from the edge of the section to the centre of a crack or flaw
c	unit height of an HCP lattice cell
c/a	characteristic ratio of the HCP lattice
d	average grain diameter
d_1, d_2, d_3	dimensions of a corrosion sample
E	electrochemical potential
E_{corr}	open circuit corrosion potential
E_f	elongation at fracture
f_a	term in geometry factor
f_w	term in geometry factor
F	geometry factor
i	current density, number of weeks submerged
i_{corr}	open circuit corrosion current density
k	empirical grain growth constant
K	stress intensity
m, m_0	mass, initial mass
ML, ML_0	mass loss, initial mass loss equal to 0
n	empirical grain growth exponent
N	number of cracks or flaws
R	resistance to polarisation
S	engineering stress
S_{actual}	engineering stress after accounting for reduced area
t	thickness of section, solidification time

CHAPTER 1

INTRODUCTION

This section presents a survey of literature relevant to the studies described in this thesis. The literature survey is intended to give motivation and provide an adequate technical backdrop for the subsequent experimentation and discussion. As well as a comprehensive literary survey, a concise problem statement is made and organisation of the manuscripts included in this research is described.

1.1 LITERATURE SURVEY

It must be understood that magnesium has the lowest density of structural metals [1] thus resulting a low strength-to-weight ratio, which makes its applications as base metal in modern alloys an intuitive choice. In fact, the strength-to-weight ratio of magnesium alloys is the highest [1] of all alloy groups available to design engineers. Strength-to-weight ratio is a common decision criterion used in materials selection for vehicular applications especially where packaging concerns can be set aside.

Manufacturers in the transport industries are burdened with the demand on their products for better fuel efficiency and lower emissions. In order to meet these demands while maintaining sufficient performance, one of the key areas of research is the development of lightweight materials [1-57]. Lightweight alloys offer both improved machine efficiency via reduced rotating and reciprocating masses and lowered overall vehicle weight requiring less inputted energy for propulsion.

The present study observes the properties of an alloy of interest: the permanent mould (PM) cast magnesium alloy AJ62. To deliver the experimental results, a review of some of the topics pertaining to them is presented here. These topics include: pure

magnesium, magnesium alloys, casting of magnesium alloys, corrosion of magnesium and its alloys, and other relevant preceding work.

1.1.1 Pure Magnesium

The magnesium atom has a radius of 0.160 nm and a mass of 24.31 g/mol. Crystallographic structure of pure magnesium is hexagonal close packed (HCP) as in Figure 1 with a c/a ratio of 1.623 being lower than ideal [2,3]. Strength of the magnesium crystal is based on this structure as dislocations prefer to move only through the basal planes. For the single crystal, the only other deformation mechanism at room temperature is twinning about the $\{10\bar{1}2\}$ family of planes [1]. The complex polycrystalline metal is susceptible to grain boundary sliding and all deformation mechanisms become worse at elevated temperatures.

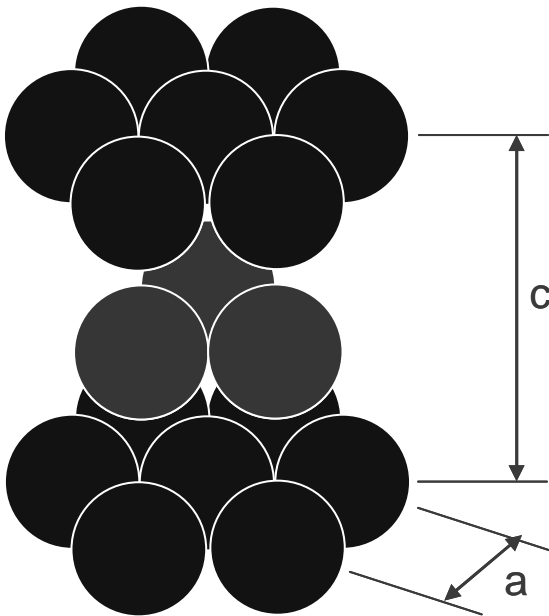


Fig. 1-1 Hexagonal close packed lattice structure [1].

In fact, high-temperature performance of the metal is detrimental to its application in automotive powertrains [4]. The melting temperature of magnesium at 1 atmosphere pressure is 650 °C [5]. This low melting temperature, relative to other structural metals,

is representative of the stability of the metal at high temperatures. Creep is generally observed in magnesium alloys at operational powertrain temperatures of about 150 °C [4] and so magnesium can be deemed unsuitable for use above this temperature.

Another poor property of the metal is its corrosion resistance [6,7]. Pure magnesium has, along with the lowest density, the lowest corrosion potential of 2.4 V with reference to the standard hydrogen electrode (SHE) [7,8]. Appearing at the bottom of the galvanic series, it is the most anodic of all metals and readily gives up Mg^{2+} ions [7]. This proneness to ionic dissolution also makes the pure metal a poor candidate for automotive application. It should also be noted that the relatively soft metal exhibits poor wear, which also restricts its use.

Therefore the significant pros and cons for selecting magnesium as an engineering material are apparent. Even for a structural component with little to no requirement for wear, the cons, which include the worst corrosion and poor high-temperature performance, markedly outweigh the beneficial strength-to-weight ratio. In general, these characteristics project themselves onto magnesium-based alloys but educated manipulation of alloying elements and microstructure can reduce or avoid their detrimental effects [4, 9].

1.1.2 Magnesium Alloys

A number of magnesium alloys exist and the most common include 3 to 10 percent aluminum by weight [10]. The reasons for this are good solubility, electrochemical similarity, and maintenance of the desirable weight advantages. The phase diagram for the binary system at 1 atm pressure is shown in Figure 1-2 with a

highlighted band indicating the commonly employed compositions. These compositions lead to a general microstructure for these alloys.

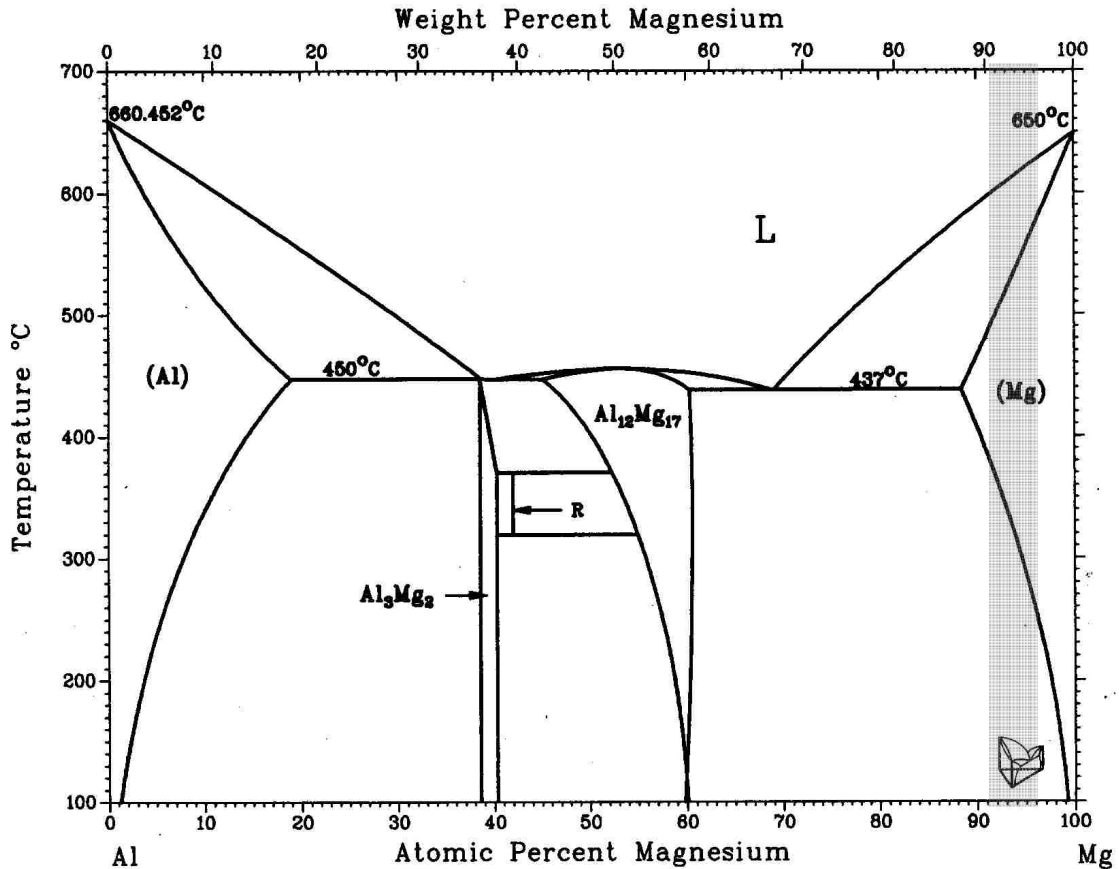


Fig. 1-2 Binary aluminum-magnesium phase diagram adapted from [5].

Observing the micrograph of a Mg-Al alloy in Figure 1-3 offers some information about this general microstructure. The cells, or matrix in the case of discontinuous boundaries, is largely magnesium with some aluminum in solid solution and regarded as the pro-eutectic α phase. The intercellular material is eutectic and is often lamellar but depends on the composition and processing. The two eutectic constituents are the Mg₁₇Al₁₂ intermetallic, referred to as the β phase, and the α magnesium. The intercellular eutectic materials including the β intermetallic phase do offer some improved strength by stopping deformation. Their influence, however, is often limited to room temperature

mechanical behaviour. This is because at elevated temperatures, the development of β particles within the matrix is discontinuous [11,12] and the existing eutectic softens.

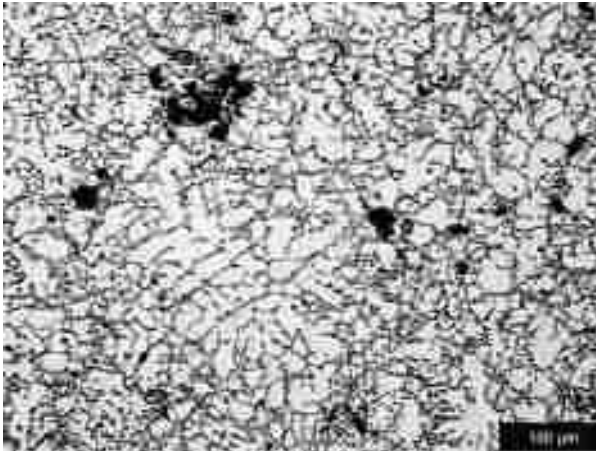


Fig. 1-3 High-pressure die cast AM50 microstructure showing interdendritic eutectic material [13].

As well as the β phase, intermetallics particles containing tertiary alloying elements can also play a large part in stopping room and elevated temperature dislocation movement [4,11]. This behaviour is a well known metallurgical principle and even some thermal treatments, *i.e.*, age or precipitation hardening, take advantage of such phase transformation. For this reason commonly employed alloys are actually ternary or better. Table I-I shows some magnesium alloys of interest and their compositions. The nomenclature includes letters for significant alloying elements other than magnesium followed by their respective percents by weight. In the case of most tertiary elements, they bond with magnesium, aluminum, or both to form small intracellular particles that can interact with dislocations [4]. For most alloys, there are usually larger aluminum-manganese intermetallics [10] as well because, as noted in Table I-I, a significant amount of manganese is present for reasons discussed later.

Table I-I Examples of modern Mg-Al alloys and their nomenclature

Alloy	Al (wt %)	Mn (wt%)	RE (wt%)	Sr (wt%)	Zn (wt%)
AE 42	~4	<0.5	~2	0	0
AE 44	~4	<0.5	~4	0	0
AJ62	~6	<0.5	0	~2	0
AM50	~5	<0.5	0	0	0
AM60	~6	<0.5	0	0	0
AZ31	~3	<0.5	0	0	<1
AZ91	~9	<0.5	0	0	<1
The balance weight percent is magnesium and small traces of other elements or impurities.					

Elevated temperature deformation in magnesium proceeds by multiple mechanisms [4]. One mechanism is diffusion creep whereby atoms use the additional thermal energy to migrate within the crystals elongating them in the direction of applied stress [4]. This is the first of three major mechanisms. Another mechanism is grain boundary sliding [14] which is actually associated with the third mechanism: dislocation movement within the crystal [1]. Dislocation movement in the crystal occurs at room temperature but is encouraged by additional thermal energy available at elevated temperatures. Therefore, the commonly observed mechanisms at the onset of creep behaviour, which is expected in powertrain application, are those associated with dislocation movement [4]. Resistance to elevated temperature deformation can be achieved if the small intermetallic particles mentioned previously are stable at high temperature and precipitate continuously within the matrix [4,11]. The benefit of the AJ alloy, however, does not rely entirely on the particles within the grain's interior but at the grain boundaries or interdendritic regions.

In earlier research, rare earth (RE) elements and silicon had been used to develop alloys targeted at improved creep resistance [4]. The mechanism lending to their success

was aluminum's greater affinity for the other elements than for the magnesium. The β phase is suppressed in these alloys allowing Al_2RE intermetallics, for example, to form that are more metallurgically stable than $Mg_{17}Al_{12}$. RE elements are aptly named and the rarity of the elements can lead to high costs that limit feasibility of those alloys for industrial application [4]. Attempting to achieve the same mechanism with some other element, researchers tried adding calcium to alloys such as AM50 and AM60 [15-17]. Unfortunately, these alloys are not well suited for casting as cracking occurs without careful mould design [4]. Strontium was explored as the new tertiary element. At present, it is the most cost effective way of handling the high temperature demands of automotive powertrains. Strontium additions successfully suppress $Mg_{17}Al_{12}$ replacing it with stable Al_4Sr at the interdendritic regions and allowing the $Mg_{17}Al_{12}$ to precipitate continuously at elevated temperatures further hindering dislocation movement [11, 12, 18]. A micrograph of the cast AJ62 microstructure is shown in Figure 1-4.

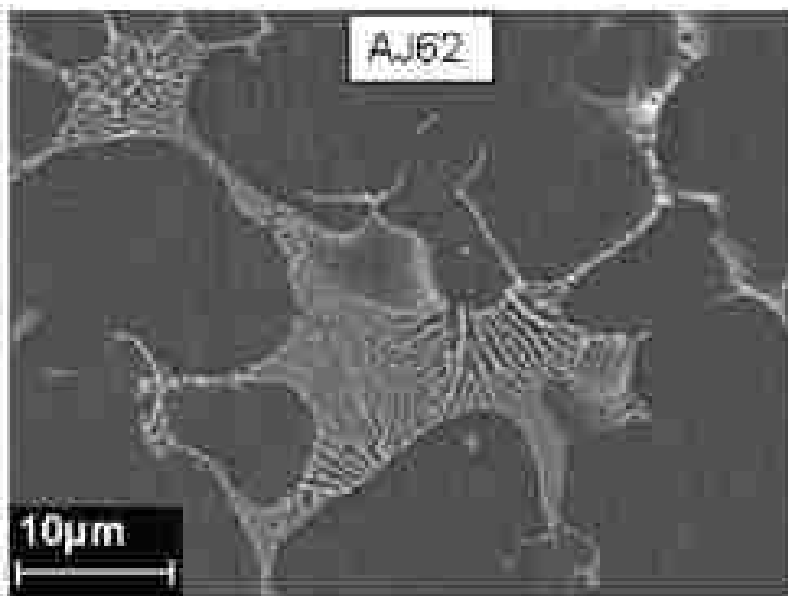


Fig. 1-4 Micrograph of die cast AJ62 showing the lamellar Al_4Sr interdendritic intermetallics [11].

1.1.3 Casting of Magnesium Alloys

The alloys discussed above are suitable mainly for high-pressure die cast (HPDC) components. It has been noted, however, that the castability of the AJ62 alloy is quite good for the currently employed HPDC processes [4]. Castability of the alloy is sufficient for the sand casting process [11]. This has led to the present studies on the feasibility of permanent mould cast components [20-23]. The PM casting process is much more primitive than that of HPDC. HPDC involves the injection of metal into a mould cavity through a narrow gate [24] at a high pressure as the name implies. Needless to say, this operation requires machinery that is costly to purchase and maintain. The benefit, however, is net shape manufacturing and very high productivity allowing mass production operations to achieve economies of scale. PM casting, in contrast, is a gravity-fed process that requires only the metal mould or die and time. Therefore, lower overhead cost is the one advantage of PM casting when anticipated production levels are relatively low.

Overhead cost is not necessarily the motivation for studying the PM process. A number of design advantages for PM castings over HPDC do exist and they result from the nature of the HPDC process. During the HPDC process metal is forced into the mould cavity under pressure as previously explained. Because the strength of HPDC parts relies on a rapidly solidified microstructure, mould temperature can be below the liquidus temperature. Therefore, as the liquid metal enters the mould, it freezes on the mould wall with a very high cooling rate [24]. This generates a fine, dense microstructure in these locations [25,26]. The metal now passing by on its way into the

mould has cooled to a semi-solid or slurry state [25]. As it shears, the frozen material it generates defect bands with high porosity [25].

The thin layer frozen along the mould wall is often referred to as the skin [27]. Skin material is assumed to be primarily responsible for an HPDC casting's integrity [28]. Because the interior region of the casting has experienced a lower cooling rate, a coarser, less dense microstructure characterises the interior or core. Recent research has shown that this concept alone does not fully explain the behaviour of HPDC components as the skin is often not uniform in thickness or hardness around the casting's perimeter [27,28]. It has been proposed that intermetallic continuity within the casting as observed in three dimensions also has a significant influence since fracture is interdendritic in nature. As poor intermetallic continuity or reduced skin to core thickness ratio occurs, mechanical integrity of the HPDC casting generally deteriorates with increasing section thickness. Furthermore, grossly machining HPDC parts would negate any mechanical advantage the skin material does have to offer. Lastly, the defect bands observed in Figures 1-6 and 1-7 do not generally allow for thermal processing of an HPDC part. Because the gas contained in the subsurface porosity bands expands at temperatures required for thermal treatment, blistering of HPDC components often occurs upon attempted heat treating [29].

The advantages of developing a successful PM cast microstructure would be to allow design of cast parts including relatively thick sections, significant machining, and thermal treatment. Thus, the AJ62 alloy could be used in a much greater range of applications. A greater range of application provides the general motivation for the present characterization of PM AJ62.

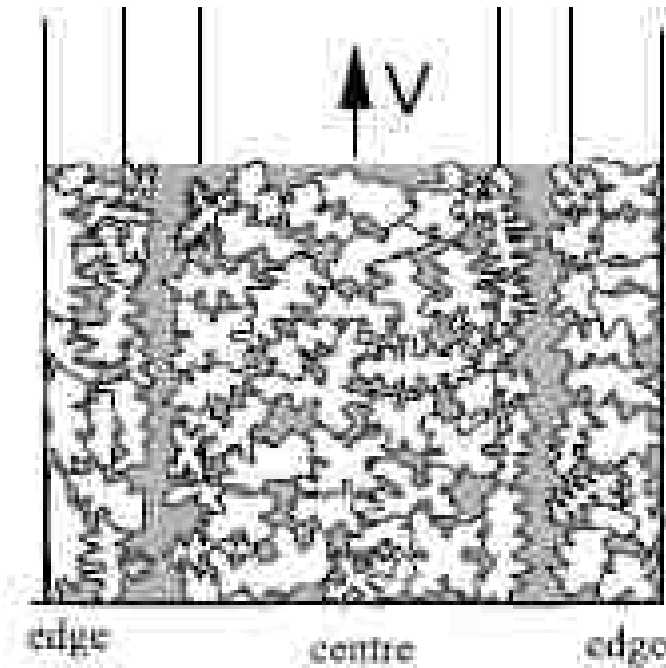


Fig. 1-5 Schematic of resulting microstructure showing defect bands [25].

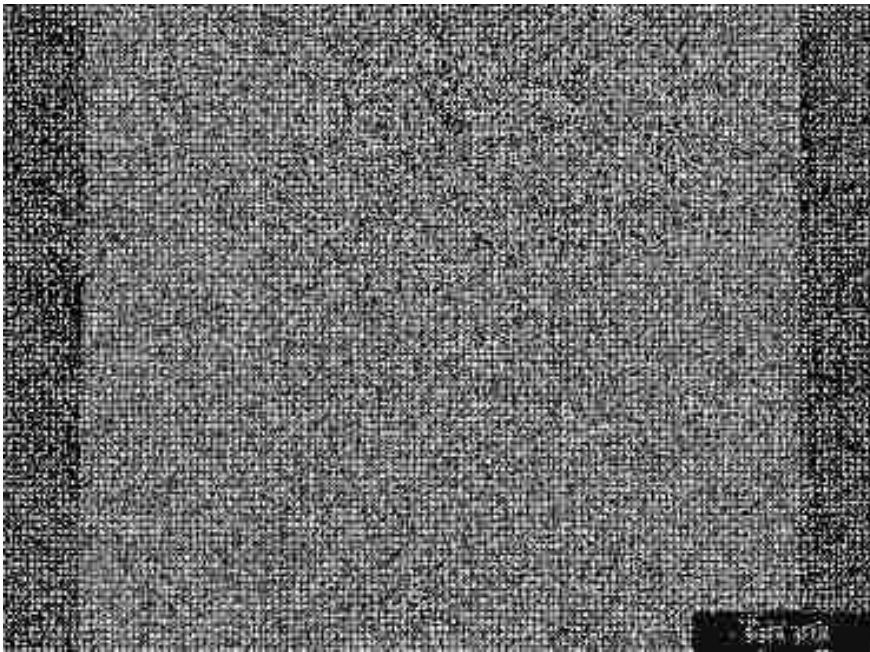


Fig. 1-6 Defect bands as they appear in the cross-section of an HPDC thickness [26].

1.1.4 Corrosion of Magnesium and its Alloys

AJ62 is well regarded among magnesium alloys for its mechanical properties but the larger issue with application of this alloy is its corrosion. As previously mentioned,

magnesium is very anodic and this relates to the corrosion of its alloys. Before discussing the electrochemistry of Mg-Al alloys, it is important to understand the corrosion of pure magnesium. Of particular interest are the chemical reactions that occur as a result of contact with water. This is because in automotive application, the largest concerns are harsh road conditions with the presence of aqueous solutions containing road salt and commercial engine coolants that contain between 30 and 70 % water [30,31]. In aqueous solutions, magnesium can develop a galvanic cell [6,7,9,24,32-34], which is shown in the diagram of Figure 1-8. Magnesium takes the role of anode where reaction 1-1 takes place. This involves the dissolution of Mg^{2+} ions into the solution and electron movement into the material [6-9,34]. Any other metal can then take on the role of cathode generating hydrogen gas [6] as indicated by reaction 1-2. Lastly, the corrosion product magnesium hydroxide forms according to reaction 1-3 between the products of the anodic and cathodic partial reactions[6].

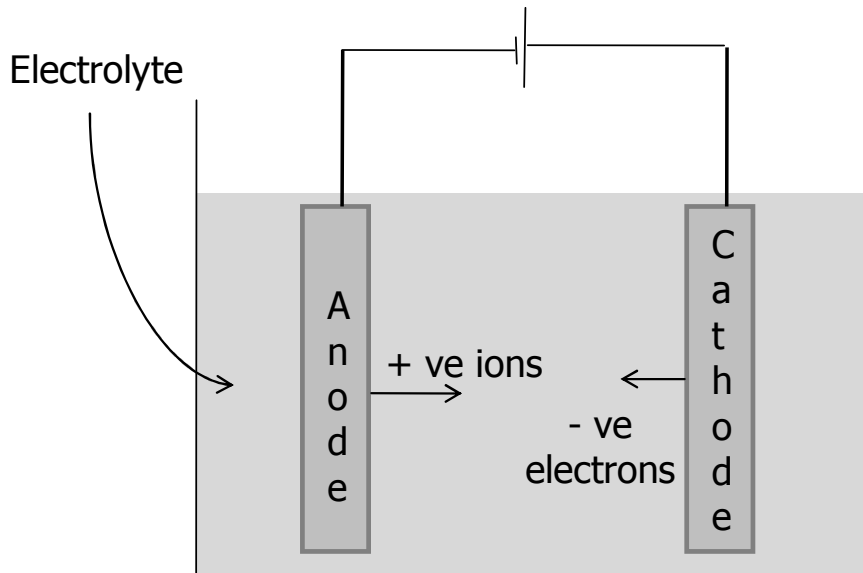
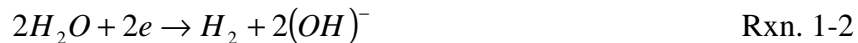


Fig. 1-7 Concept of the galvanic cell.

Table I-II, taken from reference 8, is a series of corrosion potentials, with respect to the standard hydrogen electrode, showing the ranking of some metals from typical cathodes at the top to anodes at the bottom and their respective half cell reactions. These corrosion potentials are calculated from the difference in Gibbs free energy between the reactants and products of the half cell reactions. The change in free energy of the overall galvanic reaction can be determined by combining the change for each half cell reaction [8]. Thus the difference in potential between two metals sharing an electrically conductive interface and an electrolytic medium, which relates to the change in Gibbs free energy [8,35], ultimately drives the electrochemical reaction in an attempt to reduce the system's overall energy. Magnesium therefore plays anode in extreme reactions with some common metals. For instance, iron represents the threat of severe corrosion because of its electrochemical dissimilarity to magnesium as seen in Table I-II.



Imagine an impurity, *e.g.*, an iron particle, at the surface of a magnesium casting. Clearly there is a connection allowing the free flow of electrons and if submerged in an aqueous electrolyte, hydrogen evolution begins at the impurity while dissolution of magnesium and corrosion product accumulation occurs elsewhere on the magnesium surface. This phenomenon is referred to as micro-galvanic [9] corrosion and is a serious problem for magnesium alloys. Work by researchers studying the effect of various additions has highlighted threshold values, also known as tolerance limits [6,9], above which severe micro-galvanic attack take place [6,24]. A plot of impurity level versus

corrosion rate is shown in Figure 1-9. For some impurities, this value is as low as 5 parts per million further suggesting that micro-galvanic effects can be severe and have a significant impact on the corrosion resistance of an alloy. This is why, manganese, which pulls iron atoms out of the molten metal, is often found in magnesium alloys [34].

Table I-II Series of potentials for selected half-cell reactions [8]

Electrode	Standard Electrode Potential, E^{\ominus} V (SHE)
$Au^{3+} + 3e^{-} = Au$	+ 1.50
$Cl_2 + 2e^{-} = 2Cl^{-}$	+ 1.365
$\frac{1}{2}O_2 + 2H^{+} + 2e^{-} = H_2O$	+ 1.228
$Br_2 + 2e^{-} = 2Br^{-}$	+ 1.065
$Ag^{+} + e^{-} = Ag$	+ 0.799
$Hg_2^{2+} + 2e^{-} = 2Hg$	+ 0.789
$Fe^{3+} + e^{-} = Fe^{2+}$	+ 0.771
$I_2 + 2e^{-} = 2I^{-}$	+ 0.536
$Cu^{+} + e^{-} = Cu$	+ 0.520
$Cu^{2+} + 2e^{-} = Cu$	+ 0.337
$2H^{+} + 2e^{-} = H_2$	0.000 (by definition)
$Pb^{2+} + 2e^{-} = Pb$	- 0.126
$Sn^{2+} + 2e^{-} = Sn$	- 0.136
$Ni^{2+} + 2e^{-} = Ni$	- 0.250
$Fe^{2+} + 2e^{-} = Fe$	- 0.440
$Cr^{3+} + 3e^{-} = Cr$	- 0.740
$Zn^{2+} + 2e^{-} = Zn$	- 0.763
$Al^{3+} + 3e^{-} = Al$	- 1.663
$Mg^{2+} + 2e^{-} = Mg$	- 2.370
$Na^{+} + e^{-} = Na$	- 2.714

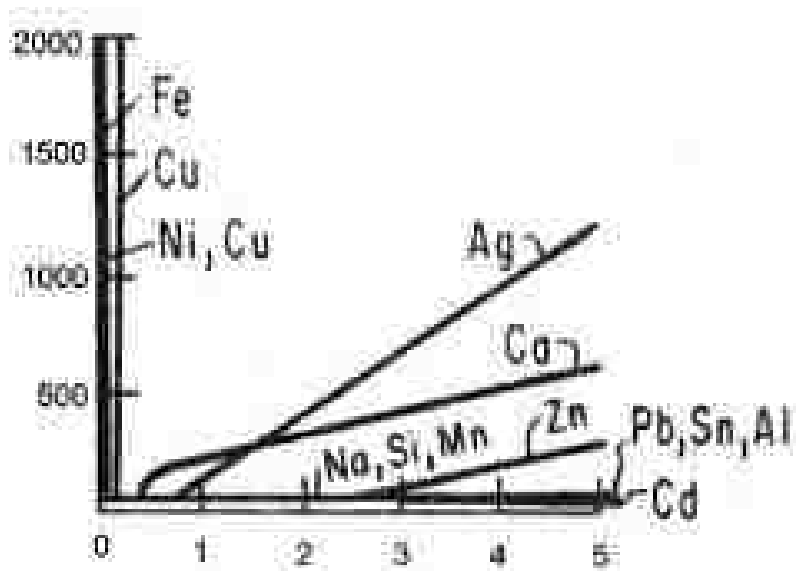


Fig. 1-8 Effect of additions on corrosion of Mg in 3 % NaCl solution [6].

In an alloy, there are more than just a few impurities but rather a number of phases and intermetallic particles present. For instance, the magnesium rich α matrix of the binary Mg-Al alloys discussed earlier makes an ideal anode while the $\text{Mg}_{17}\text{Al}_{12}$ in the eutectic boundary regions are good candidates for the cathodic counterpart. Work by Joensen *et alia* [36] has suggested the electronegativity of the β intermetallic as -0.9 V compared to -1.3 V for α versus SHE in salt solution. Therefore, a driving electrochemical force to initiate and accelerate corrosive attack is established.

Magnesium is a passivating metal that uses its magnesium hydroxide corrosion product to generate a thin film on the surface to protect the bare metal beneath [6,7,34]. It has been documented that resistance to corrosion in air is good for magnesium alloys alluding to the potential effectiveness of the passive film [6,7]. Unfortunately, in aqueous media, stabilization of $\text{Mg}(\text{OH})_2$ and thereby a film is only achievable at high pH [6,24] as shown by the Pourbaix diagram for pure magnesium shown in Figure 1-10. Compounding this problem, most environments in which engineers would like to apply magnesium alloys are not alkaline. More often they are acidic or neutral. Therefore, only in small volumes where pH is elevated by the magnesium hydroxide production itself can the passive film survive [6]. If the passive film breaks down or forms in a non-uniform manner due to increase in pH of a locally trapped electrolyte, a detrimental effect similar to the micro-galvanic effect can be created [37]. Modern engine coolants contain inhibitors that promote such films over the entire surface to stay the progression of corrosion [31]. Since the electrolytic medium cannot always be manipulated in this way, an example being external vehicular applications, researchers continue to investigate two methods of corrosion reduction. One well researched method is providing a physical

barrier by coating [7,33,38-45]. Since coatings add cost to production and, in galvanic situations, it's better to coat the cathode, some metallurgical considerations can be made, that reduces general corrosion of the bare alloy.

Knowing that the constituent phases and their electronegativity lend to general corrosion of magnesium by a micro-galvanic, or intergranular [32], mechanism has led to a number of studies on alloying additions [46-49]. Alloying additions, such as rare earth elements, can induce replacement of the β phase with other intermetallic compounds that are more compatible with the anodic matrix. This principal, however, can only contribute to a certain level of resistance in less aggressive solutions. Instead, the key to corrosion resistance of bare Mg-Al alloys is related to fine microstructure coupled with improved intermetallic continuity by the following logic.

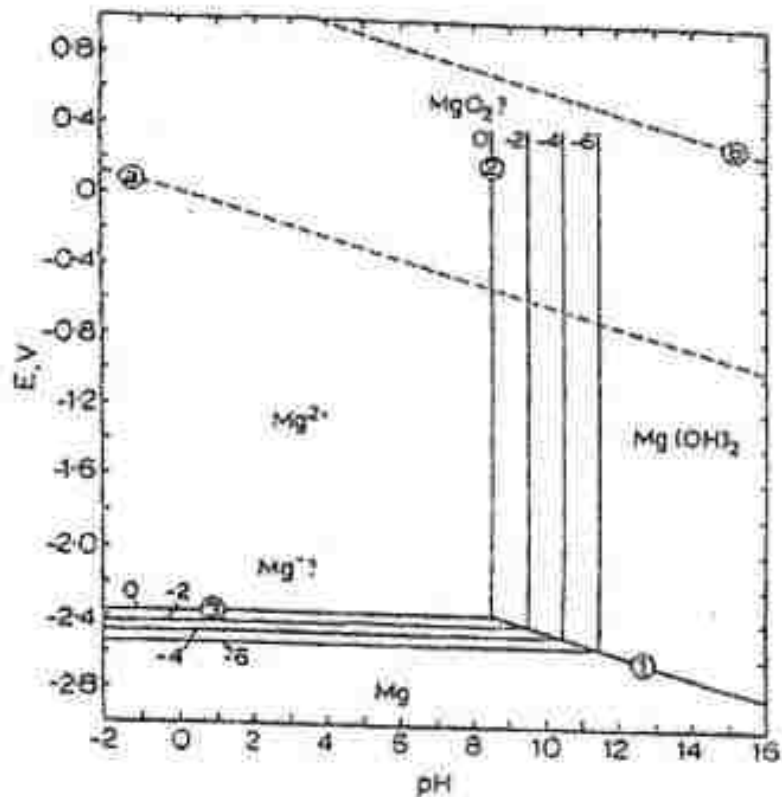


Fig. 1-9 Pourbaix diagram for the corrosion of Mg in water [6].

As corrosion of a magnesium alloy progresses, the α matrix is mined away [9,32,50,51]. A schematic of this concept is shown in Figure 1-11. Reducing the dendritic arm spacing (DAS) therefore reduces the depth of penetration suffered by the corroding alloy. If the β phase present is not continuous, corrosion cannot cease and bits of the eutectic phase are susceptible to undermining and spalling [9]. On the other hand, if the β phase is continuous, undermining and spalling are avoided and a ' β barrier' to further corrosion is developed [9,50,51]. The β barrier concept is illustrated in Figure 1-12. Understanding these mechanisms, researchers suggest that a more well-dispersed and continuous intermetallic material is capable of reducing ion exchange and thereby mass loss during immersion corrosion [9,50,51]. This suggestion is made in light of the fact that presenting more β surface area reduces resistive electrolyte length and increase the cathode to anode ratio sites that leads to corrosion [52].

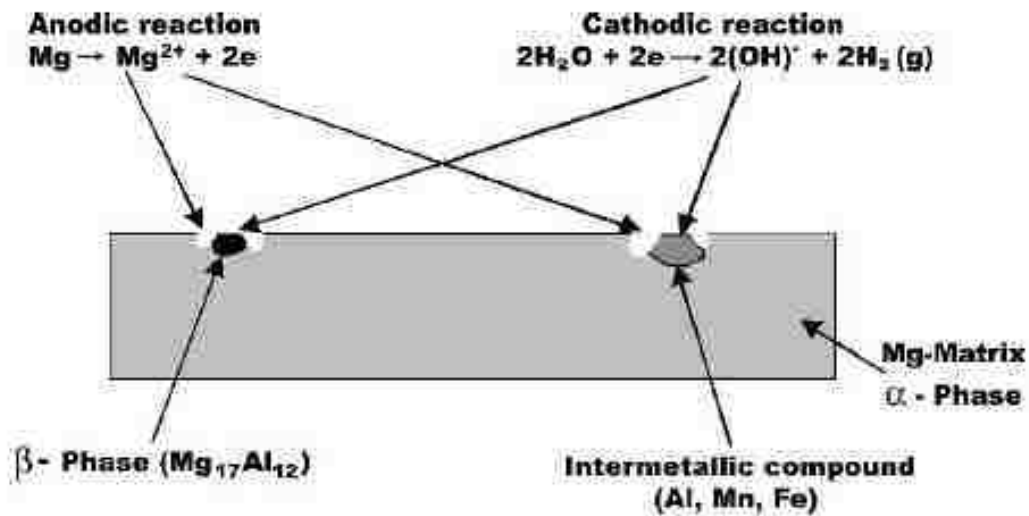


Fig. 1-10 Micro-galvanic corrosion progression of Mg alloy constituents [32].

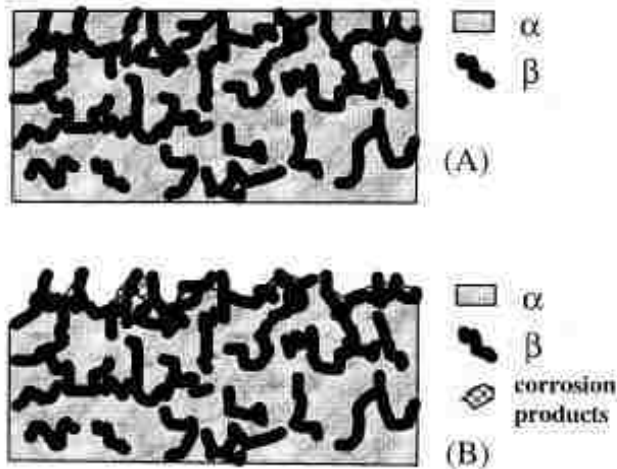


Fig. 1-11 Illustration of the β -barrier concept showing microstructure (A) before and (B) after corrosion [9].

1.1.5 Preceding Work

Characterization of the PM AJ62 casting's microstructure, as presented in the following chapters, must include documentation of the specific processing parameters used. For this reason, a summarization of the preceding work including the casting design and parameters, as well as some theoretical calculations based upon them is presented here.

To begin, the dimensions and shape of the mould cavity, *i.e.*, the yielded four-step casting, is given in Table I-III. The mould is made of steel and houses the mould cavity, risers, and the gating system less the pouring basin. A schematic of the gating system and mould cavity is given in Figure 1-13. The mould and complete gating system were designed with the aid of Magmasoft® simulation software to achieve the desired results [20]. Calculations for parameters used in the design include: the weight of the poured metal, the filling time, the average modulus, modulus of the thinnest section, and also the theoretical solidification time, which was much greater than the filling time [20]. Further calculations dictated the gating dimensions, and casting simulations using the design

were conducted observing the thermophysical properties of Table I-IV. 100 % mould filling was achieved using a high initial die temperature of 400 °C and proper gas ventilation [20]. A full account of this design process is provided by Sun *et alia* [20].

Table I-III Dimensions of casting steps

Step	Length (mm)	Width (mm)	Height (mm)
1	150	50	4
2	150	50	6
3	150	50	10
4	150	50	20

Later, experimental verification showed similar results to those obtained through simulation [20]. For the actual casting, graphite based lubrication was applied manually as a mould coating [20]. The mould was preheated with strip heaters to 400 °C and the melt had a temperature of 690 C. The molten AJ62 alloy was poured under cover of a protective gas (sulphur hexafluoride SF₆ 0.5 % + carbon dioxide CO₂). Actual cooling data observed via thermocouple indicated filling time to be in the range of 2.4 and 3.2 s [20]. Solidification times for the sections were: 20 to 80 s, which is quite fast for an unchilled mould [53].

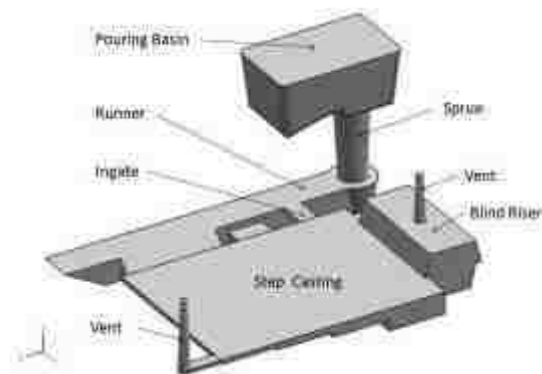


Fig. 1-12 3-dimensional rendering of the step casting with a gating and riser system [20].

Table I-IV Thermophysical properties used to model the casting process [20]

Thermal Conductivity (W/mK)	77
Specific Heat (J/kgK)	1150
Density (g/cm ³)	1.80
Latent Heat (kJ/kg)	360
Coefficient of Thermal Expansion (μm/mk)	27.3
Melting Range (C)	515 to 612

The solidification times are important to understand in the development of the microstructures presented in this thesis. An empirical relationship between the secondary dendrite arm spacing (SDAS) and the solidification time has been well established [54]. Equation 1-1 adequately describes this relationship where k is a constant unique to an alloy, and n is a constant value usually between 0.5 and 0.66 for secondary dendrites [54]. Therefore an expected microstructure for the given section thicknesses can be worked out. Other work [55] has shown that there is a significant effect of temperature gradient on this relationship due to a prolongation of the coarsening time beyond the solidification time. This concept is especially true for large gradients and low solidification velocities [55]. In reality, there is a gradient in the solidifying AJ62 step casting but the solidification velocity would be higher given the observed times. Further calculation might yield a more accurate representation of the dendritic growth. However, for this survey, the simple formula of Equation 1-1 suffices,

$$d = k \cdot t^n \quad \text{Eqn. 1-1}$$

Where d is the average grain diameter, k and n are empirical constants, and t is the solidification time.

Unfortunately, little work has been done at present to determine the constants k and n for the AJ62 alloy. Since AJ62 is largely an HPDC alloy, microstructure observations existing in the open literature cannot be related to cooling information

without consideration of the pressure effects on solidification. So without known values for the required constants and no way to extrapolate this from existing data, an approximation must be made based on other alloys. One early experiment developed the following to describe an Mg-Zn alloy: $d = 10.5 \cdot t^{0.4}$ [56]. These values would yield calculated SDAS values between 34.8 μm and 60.6 μm for the previously mentioned solidification times. Another study [57] indicated that for AM50, solidification rates of 1 $^{\circ}\text{C/s}$ and 4 $^{\circ}\text{C/s}$ resulted in SDAS values of $64.3 \pm 12.3 \mu\text{m}$ and $43.4 \pm 9.7 \mu\text{m}$, respectively. Considering that the liquidus and solidus include a range of approximately 200 $^{\circ}\text{C}$ (625 $^{\circ}\text{C}$ to 425 $^{\circ}\text{C}$ [53,57]) the rate would be between 9 $^{\circ}\text{C/s}$ and 2 $^{\circ}\text{C/s}$ giving roughly estimated SDAS values well below 40 μm , with significant scatter. This spacing can then be used in combination with empirical equations relating cell size to mechanical properties such as the Hall-Petch equation [2], for example, to gain some insight as to the mechanical strength of the alloy. As well, there are a number of SDAS effects on corrosion, as previously discussed. Of course castings always contain one or more of a number of defects including various porosity types and solidification defects. Therefore, experimental determination of the cast alloy properties for various microstructures, as in the following chapters, is required for accurate characterisation.

1.2 THESIS OBJECTIVES

The experimental work focuses mechanical and corrosion properties of PM cast AJ62 with respect to the influence of microstructural characteristics. The goal of this thesis is to evaluate and determine such properties independently, and correlate them to the microstructure that develops during solidification. Recommendations to the industry,

in light of the characterised engineering performance of the alloy, are an additional driver for this research.

1.3 THESIS ORGANISATION

This thesis combines the results of five independent manuscripts in logical progression as well as a unifying discussion to satisfy the aforementioned objectives. In the first work, a step-casting of AJ62 was produced in a gravity-fed, permanent mould to understand the effects of section thicknesses on its mechanical properties. Specimens of four varying thicknesses were prepared from respective steps in the castings, and subsequently tested in tension at room temperature. A general degradation of mechanical properties was observed as thickness increased. Evident variations in microstructure for each thickness were also observed via microstructural analysis. Changes in mechanical performance were thereby attributed to differences in microstructure evolution during solidification can be made.

Studies for the second manuscript attempt to determine the effect of NaCl concentration on microstructure-induced variations in corrosion. Experiments include potentiodynamic testing of two permanent mould cast microstructures with markedly different cell sizes in two NaCl solutions having different concentrations. The preliminary results indicate the existence of small variations in PM AJ62 corrosion based on dendrite arm spacing. Corrosion morphology on the tested surface confirms the anodic behaviour of the magnesium rich cells.

In the third manuscript's research, various permanent-mould cast AJ62 specimens with different section thicknesses were subjected to immersion corrosion in commercially-available engine coolant. The objective was to determine corrosion

behaviour variation among casting thicknesses. Corrosion product accumulation suggests passive film formation, and unlike in other media, the film exhibits certain stability. Contrasting 4 mm and 20 mm thicknesses were used to generate polarization curves for their respective microstructures in engine coolant. Variation of corrosion resistance with casting section thickness was observed in the curves. These preliminary results indicate that coarsened microstructures reduce corrosion resistance of the permanent mould cast AJ62 alloy.

Next, the results of experimentation on multiple corrosion media are examined to determine the particular effect of electrolyte chloride and inhibitor concentrations as well as the limitations of microstructural corrosion resistance. Corrosion potential for different microstructures converges as chloride concentration increases, possibly due to increased severity of the reactions and presence of resulting surface phenomena. The same is true for the corrosion current density unless, as in engine coolant, anodic inhibitors are present. Lastly, passivating behaviour is promoted by the engine coolant and the coarser microstructure with lower area percent intermetallic is benefited the greatest.

The last of the presented manuscripts details the tensile testing of corroded specimens. This study was undertaken to characterise the combined behaviour of the PM cast AJ62 alloy. Specimens from four different microstructures, due to varied casting thickness, were submerged in NaCl solution for a predetermined duration. Subsequently, the corroded specimens were observed and subjected to tensile testing. SEM observations of the fracture surfaces showed the depth of penetration by corrosion. It can be seen that the penetration of corrosion was significantly more severe for the coarser

microstructure and that this led to the acceleration of brittle fracture as confirmed by the stress-strain data.

Finally, conclusions are drawn and a preliminary model for the independent and combined response of PM cast AJ62 is developed. Recommendations for practical application in the transportation industries, especially the automotive sector are given in the final chapter as well. Table I-V highlights the original publication information for each of the manuscripts.

Table I-V Publication information for presented manuscripts

Chapter	Manuscript Title	Source
2	Effects of section thickness on tensile properties of permanent mould cast magnesium alloy AJ62	Magnesium Technology 2010. The Minerals, Metals, and Materials Society. (2010) 367-371
3	Corrosion of permanent mould cast magnesium alloy AJ62 in NaCl solutions	Proceedings of the 114 th Metal Casting Congress. American Foundry Society. (2010) Paper No. 10-022.
4	Microstructure influence on the corrosion of permanent mould cast magnesium alloy AJ62 in engine coolant	SAE World Congress 2010 Paper. Society of Automotive Engineers. (2010) Paper No. 2010-01-0412.
5	Corrosion performance of permanent mould cast magnesium alloy AJ62 in automotive environments	Unpublished
6	Influence of corrosion effects on mechanical properties of permanent mould cast AJ62	Unpublished

1.4 REFERENCES

- [1] Raynor, G.V., The physical metallurgy of magnesium and its alloys. Pergamon Press. GB. 1959.
- [2] Smith, W.F., Foundations of materials science and engineering. 3ed. McGraw-Hill. USA. 2004.
- [3] Askeland, D.R., Fulay, P.P., Essentials of materials science and engineering. 2ed. Cengage. USA. 2009.

- [4] Hu, H., Yu, A., Naiyi, L., Allison J.E., Potential magnesium alloys for high temperature die cast automotive applications: a review. *Materials and Manufacturing Processes*. 18 5 (2003) 687-717.
- [5] Massalski, T.B., Murray, J.L., Bennett, L.H., Baker, H., Binary alloy phase diagrams. American Society for Metals. USA. 1986. p 130.
- [6] Makar, G.L., Kruger, J., Corrosion of magnesium. *International Materials Reviews*. 38 2 (1993) 138-153.
- [7] Ma, Y., An investigation of the electrolytic plasma oxidation process for corrosion protection of pure Mg and Mg alloy AM50. Master Thesis. University of Windsor. 2005.
- [8] Talbot, D., Talbot, J., Corrosion science and technology. CRC Press. USA. 1998.
- [9] Song, G., Atrens, A., Understanding magnesium corrosion a framework for improved alloy performance. *Advanced Engineering Materials*. 5 12 (2003) 837-858.
- [10] Oberg, E., Jones, F.D., Horton, H.L., Ryffell, H.H., Machinery's handbook. 26ed. Industrial Press. USA. 2000.
- [11] Kunst, M., Fischersworing-Bunk, A., L'Esperance, G., Plamondon, P., Glatzel, U., Microstructure and dislocation analysis after creep deformation of die cast Mg-Al-Sr (AJ) alloy. *Materials Science and Engineering A*. 510-511 (2009) 387-392.
- [12] Pekguleryuz, M.O., Kaya, A.A., Creep resistant magnesium alloys for powertrain applications. *Advanced Engineering Materials*, 5 12 (2003) 866-878.
- [13] Sun, Z., Zhou, M., Hu, H., Naiyi, L., Strain-hardening and fracture behavior of die cast magnesium alloy AM50. *Research Letters in Materials Science*. (2007) ID: 64195.
- [14] Dargusch, M.S., Dunlop, G.L., Pettersen, K., Elevated temperature creep and microstructure of die cast Mg-Al alloys. *Magnesium Alloys and Their Applications*. Werkstoff-Informationsgesellschaft mbH. (1998) 283-288.
- [15] Luo, A.A., Powell, B.R., Tensile and compressive creep of magnesium-aluminum-calcium based alloys. *Magnesium Technology 2001*. The Minerals, Metals, and Materials Society. (2001) 137-144.
- [16] Jing, B., Yangshan, S., Shan, X., Feng, X., Tianbai, Z., Microstructure and tensile creep behavior of Mg-4Al based magnesium alloys with alkaline-earth elements Sr and Ca additions. *Materials Science and Engineering A*. 419 (2006) 181-188.

- [17] Shuping, W., Sun, Z., Hu, H., Effect of pressure levels on tensile properties of squeeze cast Mg-Al-Ca alloy. *Magnesium Technology 2008*, The Minerals, Metals, and Materials Society. (2008) 421-425.
- [18] Baril, E., Labelle, P., Pekguleryuz, M.O., Elevated temperature Mg-Al-Sr: creep resistance, mechanical properties, and microstructure. *Journal of Materials*. 55 11 (2003) 34-39.
- [20] Sun, Z., Hu, H., Burns, J., Nie, X., Han, L., Design of a step permanent mold for casting magnesium alloy AJ62. *American Foundry Society*. (2010) Paper No. 10-007.
- [21] Burns, J.R., Han, L., Hu, H., Nie, X., Effects of section thicknesses on tensile properties of permanent mould cast magnesium alloy AJ62. *Magnesium Technology 2010*, The Minerals, Metals, and Materials Society. (2010) 367-371.
- [22] Burns, J.R., Hu, H., Nie, X., Su, J.F., Corrosion of permanent mould cast Mg alloy AJ62 in NaCl solutions. *American Foundry Society*. (2010) Paper No. 10-022.
- [23] Burns, J.R., Hu, H., Nie, X., Han, L., Microstructure influence on the corrosion of permanent mould cast magnesium alloy AJ62 in engine coolant. *Society of Automotive Engineers*. (2010) Paper No. 2010-01-0412.
- [24] Avedasian, M.M., Baker, H., *ASM specialty handbook: magnesium and magnesium alloys*, ASM International. (1999)
- [25] Dahle, A.K., Sannes, S., St. John, D.H., Westengen, H., Formation of defect bands in high pressure die cast magnesium alloys. *Journal of Light Metals*. 1 (2001) 99-103.
- [26] Zhou, M., An experimental study of die and squeeze cast magnesium alloy AM50. Master Thesis, University of Windsor. 2004.
- [27] Weiler, J.P., Wood, J.T., Klassen, R.J., Berkmortel, R., Wang, G., Variability of skin thickness in an AM60B magnesium alloy die-casting. *Materials Science and Engineering A*. 419 (2006) 297-305.
- [28] Yang, K., Nagesekhar, A.V., Caceres, C.H., Section thickness and the skin effect in a high pressure die cast Mg-12% Al alloy. *Magnesium Technology 2010*, The Minerals, Metals, and Materials Society. (2010) 391-394.
- [29] Lumley, R.N., O'Doenell, R.G., Gunasegaram, D.R., Givord, M., New heat treatment for Al high pressure die castings. *Heat Treating Progress*. (2006) 31-37.
- [30] Song, G., StJohn, D., Corrosion behaviour of magnesium in ethylene glycol. *Corrosion Science*. 46 (2004) 1381-1399.

- [31] Song, G., StJohn, D.H., Corrosion of magnesium alloys in commercial engine coolants. *Materials and Corrosion*. 56 1 (2005) 15-23.
- [32] Ghali, E., Dietzel, W., Kainer, K.U., General and localized corrosion of magnesium alloys: a critical review. *Journal of Materials Engineering and Performance*. 13 1 (2004) 7-23.
- [33] Ma, Y., Hu, H., Northwood, D., Nie, X., Optimization of the electrolytic plasma oxidation processes for corrosion protection of magnesium alloy AM50 using the Taguchi method. *Materials Processing Technology*, 182 (2007) 58-64.
- [34] Revie, R.W., Uhlig, H.H., Corrosion and corrosion control. John Wiley and Sons. USA. 2008.
- [35] Ragone, D.V., Thermodynamics of materials (the MIT series in materials science and engineering), Volume I. Wiley. USA. 1994.
- [36] Joensson, M., Thierry, D., LeBozec, N., The influence of microstructure on the corrosion behaviour of AZ91D studied by scanning Kelvin probe force microscopy and scanning Kelvin probe. *Corrosion Science*. 48 (2006) 1193–1208.
- [37] Song, G., Atrens, A., StJohn, D., Wu, X., Nairn, J., The anodic dissolution of magnesium in chloride and sulphate solutions. *Corrosion Science*. 39 (1997) 1981-2004.
- [38] Liang, J., Hu, L., Hao, J., Characterisation of microarc oxidation coatings formed on AM60B magnesium alloy in silicate and phosphate electrolytes. *Applied Surface Science*. 253 (2007) 4490-4496.
- [39] Ma, Y., Nie, X., Northwood, D.O., Hu, H., Corrosion and erosion properties of silicate and phosphate coatings on magnesium. *Thin Solid Films*. 469-470 (2004) 472-477.
- [40] Reiners, G., Griepentrog, M., Hard coatings on magnesium alloys by sputter deposition using a pulsed d.c. bias voltage. *Surface and Coatings Technology* 76-77 (1995) 809-814.
- [41] Han, L., Nie, X., Hu, H., Zhang, Q. Influence of electrolytic plasma oxidation coating on tensile behaviour of die-cast AM50 alloy subjected to salt corrosion. *International Journal of Modern Physics B*. 23 6-7 (2009) 960-965.
- [42] Hosche, H., Rosenkranz, C., Delp, A., Lohrengel, M.M., Broszeit, E., Berger, C., Investigation of the macroscopic and microscopic electrochemical corrosion behaviour of PVD-coated magnesium die cast alloy AZ91. *Surface and Coatings Technology*. 193 (2005) 178-184.
- [43] Gray, J.E., Luan, B., Protective coatings on magnesium and its alloys – a critical review. *Journal of Alloys and Compounds*. 336 (2002) 88-113.

- [45] Senf, J., Broszeit, E., Wear and corrosion protection of aluminum and magnesium alloys using chromium and chromium nitride PVD coatings. *Advanced Engineering Materials*. 1 2 (199) 133-137.
- [46] Song, Y.L., Liu, Y.H., Wang, S.H., Yu, S.R., Zhu, X.Y., Effect of cerium addition on microstructure and corrosion resistance of die-cast AZ91 magnesium alloy. *Materials and Corrosion*. 58 3 (2007) 189-192.
- [47] Song, Y.L., Liu, Y.H., Yu, S.R., Zhu, X.Y., Wang, S.H., Effect of neodymium addition on microstructure and corrosion resistance of AZ91 magnesium alloy. *Journal of Materials Science*. 42 (2007) 4435-4440.
- [48] Candan, S., Unal, M., Turkmen, E., Koc, E., Turen, Y., Candan, E., Improvement of mechanical and corrosion properties of magnesium alloy by lead addition. *Materials Science and Engineering A*. 501 (2009) 115-118.
- [49] Fan, Y., Wu, G., Gao, H., Li, G., Zhai, C., Influence of lanthanum on the microstructure, mechanical property, and corrosion resistance of magnesium alloy. *Journal of Materials Science*. 41 (2006) 5409-5416.
- [50] Song, G., Atrens, A., Dargusch, M., Influence of microstructure on the corrosion of diecast AZ91D. *Corrosion Science*. 41 (1999) 249-273.
- [51] Zhao, M.C., Liu, M., Song, G., Atrens, A., Influence of β -phase morphology on the corrosion of the Mg alloy AZ91. *Corrosion Science*. 50 (2008) 1939-1953.
- [52] Liu, L.J., Schlesinger, M., Corrosion of magnesium and its alloys. *Corrosion Science*. 51 (2009) 1733-1737.
- [53] Han, L., Burns, J.R., Sun, Z., Hu, H., Unpublished work. University of Windsor. (2009).
- [54] Flemings, M.C., *Solidification Processing*. McGraw Hill. USA. 1974.
- [55] Halder, E., Exner, H.E., Coarsening of secondary dendrite arms in a temperature gradient. *Acta Metallurgica*. 36 7 (1988) 1665-1668.
- [56] Kattamis, T.Z., Holmberg, U.T., Flemings, M.C., Influence of coarsening on dendrite arm spacing and grain size of magnesium-zinc alloy. *Journal of the Institute of Metals*. 95 (1967) 343-347.
- [57] Kasprzak, W., Sokolowski, J.H., Sahoo, M., Dobrzanski, L.A., Thermal characteristics of the AM50 magnesium alloy. *Journal of Achievements in Materials and Manufacturing Engineering*. 29 2 (2008) 179-182.

CHAPTER 2

EFFECTS OF SECTION THICKNESSES ON TENSILE PROPERTIES OF PERMANENT MOULD CAST MAGNESIUM ALLOY AJ62*

2.1 INTRODUCTION

Alloy AJ62, like other magnesium alloys, is receiving much deserved attention within the automotive industry due to its high specific strength as a structural metal [1,2]. High temperature properties of the alloy promote its application in environments where magnesium alloys have been unfit to handle such elevated temperatures in the past. It has been suggested that creep resistance is achieved by two major mechanisms in high-pressure die-cast (HPDC) components [2]. Small intermetallic Al-Mn particles that are present in the α -Mg crystals hinder the movement of dislocations thereby strengthening the material. Secondly, the grain boundary eutectic phase $Mg_{17}Al_{12}$ normally observed in Mg-Al alloys, which softens at high temperatures, is suppressed in Mg-Al-Sr alloys as aluminum bonds preferentially with strontium to form a different grain boundary constituent. Aluminum content is high enough, however, that as temperatures are increased the $Mg_{17}Al_{12}$ intermetallic precipitates continuously providing small hard particles that strengthen the alloy [2,3].

While similarly desirable high temperature properties have been observed among magnesium alloys with the addition of calcium or rare earth metals, castability and cost of the AJ62 alloy sets it apart from other contending alloys [1-5]. Defect-inherent inexpensive processes such as HPDC are generally employed to minimise casting costs for most applications of high temperature magnesium alloys. Despite their low cost and

* Contents of this chapter have been reprinted with permission from Magnesium Technology 2010, © 2010 TMS. See Appendix B for copyright details.

capability of net-shape manufacturing, they are often infeasible for engineers to design components with thicker sections, as cast quality deteriorates severely with large thicknesses [6]. Thermal treatments are not applicable either, since porosity bands due to high velocities during casting [7] lead to blistering at treatment temperatures. In an effort to afford notable creep resistance in a magnesium alloy component with thick sections produced via some relatively inexpensive method, gravity-fed permanent mould AJ62 step-castings were manufactured in the present study. In particular, the purpose of this work was to relate microstructure formation and mechanical properties of the alloy to casting section thickness.

2.2 EXPERIMENTAL PROCEDURE

2.2.1 Casting Preparation

A mould, machined from steel, was used to create four-step castings as in Figure 2-1. The step-castings produced had four distinct sections with thicknesses of 4 mm, 6 mm, 10 mm, and 20 mm. AJ62 ingots purchased from an industrial supplier (Magnesium Elektron) were used for preparing the step-castings without any additions. The chemical composition for this alloy is presented in Table II-I.

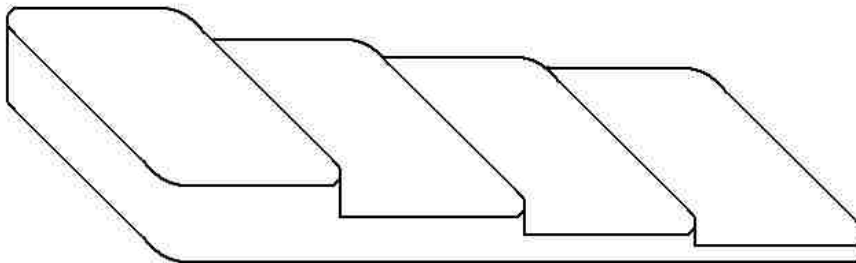


Fig. 2-1 Schematic of casting shape.

Table II-I Composition of AJ62 alloy in wt%

Alloy	Al	Sr	Mn	Si	Zn	Others
AJ62	6.00	2.82	0.28	0.02	<0.01	<0.002

2.2.2 Tensile Testing

Subsize rectangular tension specimens were prepared according to a modified ASTM standard B557M [8]. The gauge length and width of the specimens were machined to 25 mm and 6 mm, respectively. The thickness, however, was determined by the salvageable thickness of each step after any defects in the as cast surface were machined away. Each sample was polished to avoid stress concentrations and cross-section dimensions were measured.

After preparation, the samples were tested at room temperature on an Instron 8562 universal testing machine equipped with a data acquisition system at a strain rate of 0.5 mm/s. The outputted data, including displacement measured by extensometer, and tensile load, were then analyzed. The average Young's moduli (E) for each thickness were determined using ASTM standard E111 [9] for non-linear relationships. The average 0.2% offset yield (YS) as well as highest observed ultimate tensile strength (UTS) and % elongation (E_f) were also determined for each thickness.

2.2.3 Microstructure and Fracture Analysis

Specimens representing the gauge cross-section were mounted and polished according to standard metallurgical procedures for each thickness. An optical light microscope was used to note general trends in secondary dendrite arm spacing (SDAS) before the samples were observed using scanning electron microscopy (SEM). SEM images were generated to identify porosity and phases within the samples. Phases were identified with the aid of energy dispersive x-ray spectroscopy (EDS). SEM fractographs

were also prepared to identify any variations in the failure mode among the different casting thicknesses.

2.3 RESULTS AND DISCUSSION

2.3.1 Microstructure Analysis

Marked variation in the coarseness of the microstructures is evident in Figure 2-2. Parts (a) and (b) of Figure 2 show optical micrographs from the 4 mm and 20 mm sections. Average cell size escalates from $\sim 10 \mu\text{m}$ for the 4 mm specimens to $\sim 24 \mu\text{m}$ for the 20 mm thickness. Greater total thermal energy in the thicker sections of liquid metal requires more time for removal during solidification if thermal conductivity of the mould is the same for both thin and thick sections. The longer the time spent at elevated temperatures, the greater the effects of diffusion in terms of solute atom rejection leading to larger phases and particles. Summarizing this logical progression, a thicker section cast in a similar mould to a thin section, experienced a slower cooling rate, and ultimately has a coarser microstructure as demonstrated by the 20 mm sections compared with the 4 mm in the present study. Figure 2-3 parts (a) through (d) were generated by SEM at a magnification of 500 x for samples from the 4 mm, 6 mm, 10 mm, and 20 mm thicknesses, respectively. Along with the obvious variation in coarseness, the micrographs of Figure 2-3 demonstrate a decrease in cell boundary continuity as section thickness increases that is accompanied by a more massive congregation of intermetallics at the cell boundaries. This difference in microstructural arrangement can also be attributed to the variation in cooling rate of the sections. These micrographs also indicate that while coarseness of the microstructure and distribution of the intermetallics changes with thickness, the microstructural constituents remain similar.

The microstructure of permanent mould cast AJ62 resembles most other Mg-Al alloys. Figure 2-4 shows a micrograph from the centre of the 20 mm thickness. As seen in Figure 2-4, Mg rich pro-eutectic α cells (dark) are surrounded by eutectic phases (light gray) developed during non-equilibrium cooling. In most Mg-Al alloys an intermetallic compound $Mg_{17}Al_{12}$, often referred to as the β phase, presents itself at the cell boundaries [2-5,10-14]. In locations where cell boundary area is greater, a lamellar structure is visible in SEM micrographs. EDS of the matrix and cell boundary locations generated the spectra shown in Figures 2-5 and 2-6, respectively. Unsurprisingly high counts of magnesium in Figure 2-5 confirm that the matrix, or cells, consists almost entirely of Mg. The cell boundary's spectrum in Figure 2-6, however, suggests a significant concentration of Sr. In the case of sufficient Sr additions to Mg-Al alloys, the common $Mg_{17}Al_{12}$ cell boundary β phase is suppressed due to Al's greater affinity for Sr than Mg which creates an Al_4Sr intermetallic. This tendency has been observed in die cast components by a number of authors [2-4,13] and is confirmed here for the permanent mould casting process as well. This result is desirable as it indicates that the permanent mould cast material will possess the high temperature integrity reflective of its HPDC counterpart although the thermodynamics of the two processes are very different.

In terms of the room temperature behaviour studied in the present work, the intermetallic cell boundary constituents undoubtedly affect deformation. Another feature of the microstructure important to deformation for posing challenge to the movement of crystallographic dislocations are the intermetallic particles formed within the matrix. The bright globule-shaped particle in Figure 2-4 represents the intermetallic particles found throughout the alloy's microstructure. The observation of Al-Mn intermetallic particles

is common in such die-casting alloys as AM50 and AM60 [11-13]. Noting in Table II-I that there is a significant, 0.28 wt%, presence of Mn in the AJ62 alloy, the formation of similar particles is expected. Figure 2-7, the EDS spectrum for the particle shown in Figure 2-4 having notable counts of Al and Mn, indicates that the particles observed in the permanent mould cast AJ62 are most likely the same Al-Mn intermetallic as in Mg-Al-Mn alloys.

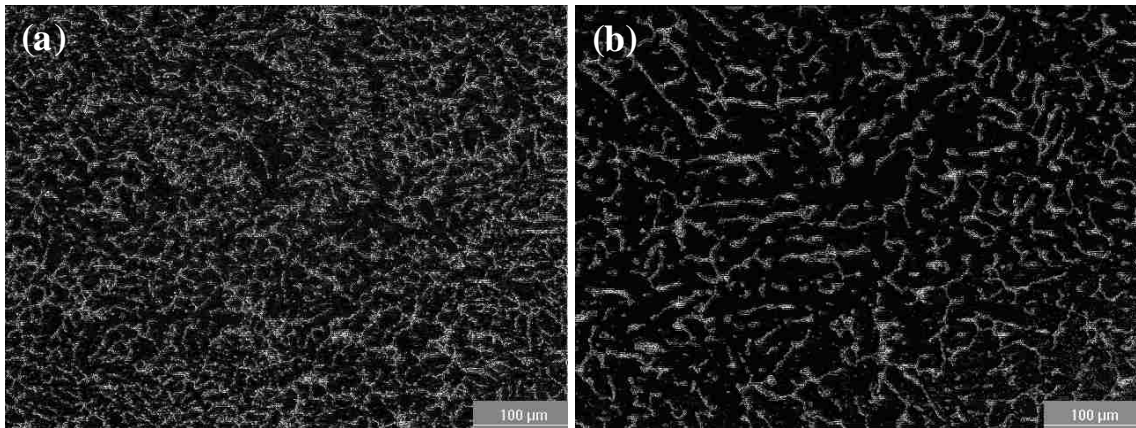


Fig. 2-2 Optical micrographs from the (a) 4 mm and (b) 20 mm sections.

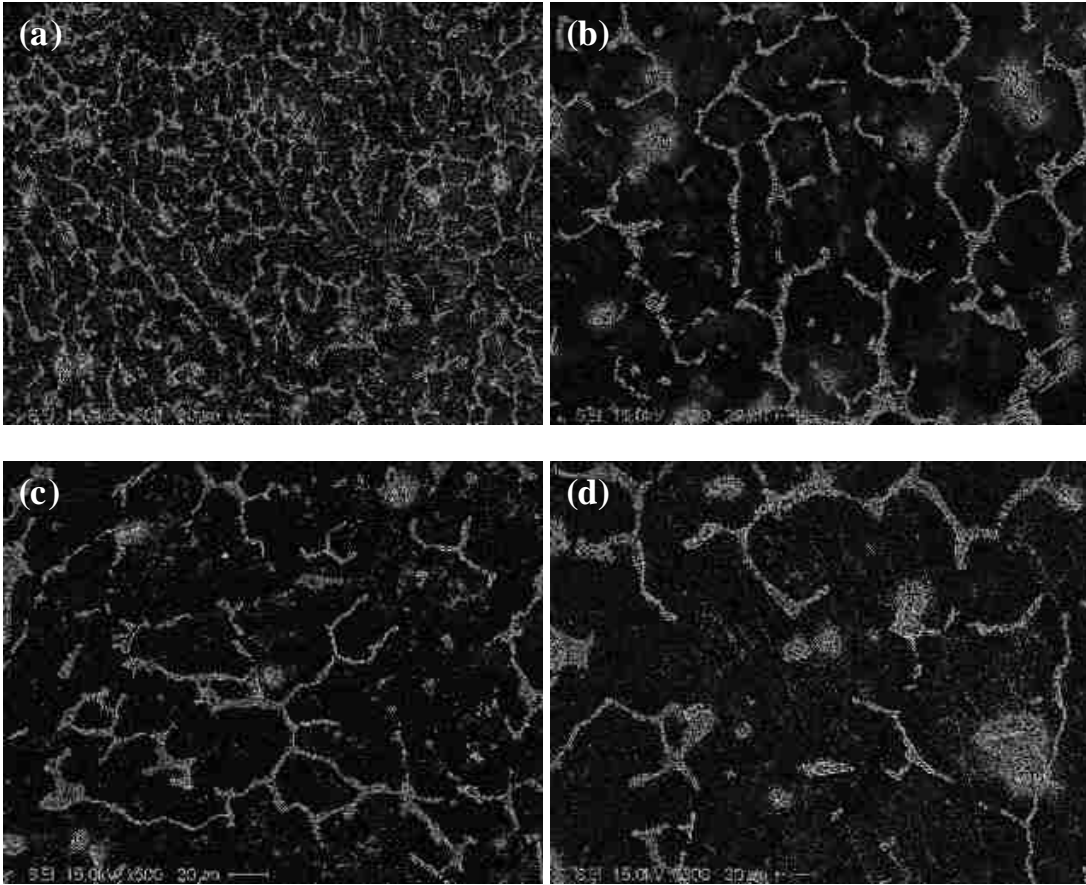


Fig. 2-3 SEM micrographs from (a) 4 mm, (b) 6 mm, (c) 10 mm, (d) 20 mm specimens.



Fig. 2-4 SEM image of permanent mould cast AJ62 microstructure.

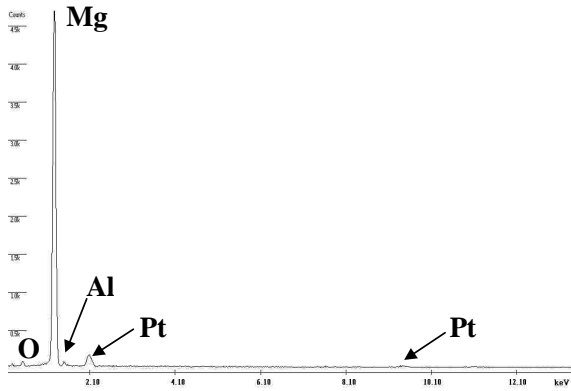


Fig. 2-5 EDS spectrum for the matrix at location A in Figure 2-4.

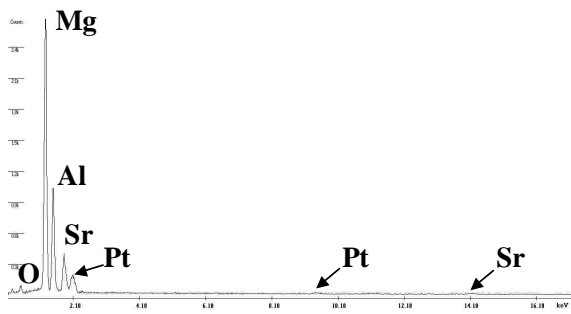


Fig. 2-6 EDS spectrum for the cell boundary material at location B in Figure 2-4.

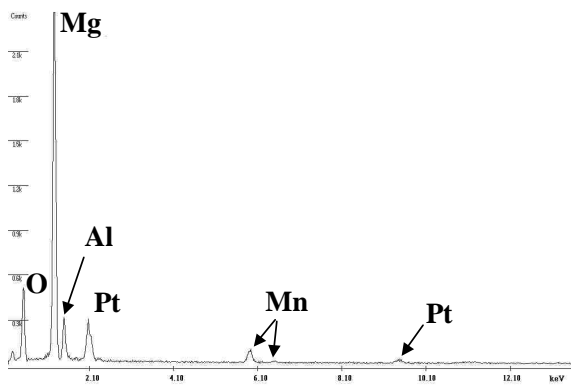


Fig. 2-7 EDS spectrum for the particle at location C in Figure 2-4.

2.3.2 Tensile Testing

Figure 2-8 shows the representative stress-strain curves for each of the thicknesses studied. The curves show that under tensile loading, the alloy deformed elastically first. Then, once the yield point reached, plastic deformation of the alloy set in.

It is obvious that the ultimate tensile strength, yield strength, and elongation of the 10 and 20 mm thick samples are lower than the 4 and 6 mm specimens. The effect of section thicknesses on tensile properties of permanent-mould cast AJ62 alloy is shown in Table II-II and Figure 2-9. It can be seen from the results that a decrease in the section thickness brings a significant improvement in UTS and YS, and some improvement in E_f . The UTS, YS and E_f of the 4 mm thick AJ62 section are 153.6 MPa, 93.1 MPa and 2.71%, respectively, which results in increases of 24% in UTS, 14% in YS, and 36% in elongation over the 20 mm thickness. The improvement in tensile properties as the thicknesses decrease should be attributed to fine cell structure and massive well-dispersed intermetallics.

Table II-II Variation of tensile properties with section thicknesses

T (mm)	E (GPa)	YS (MPa)	UTS (MPa)	E_f (%)
4	38.7 ±2.3	93.1 ±2.0	153.6 ±9.4	2.71 ±0.50
6	35.8 ±6.4	91.0 ±2.0	153.2 ±8.1	2.84 ±0.33
10	34.3 ±8.0	87.7 ±1.1	131.2 ±2.7	1.79 ±0.14
20	33.3 ±6.3	81.8 ±1.2	123.9 ±3.3	1.99 ±0.23

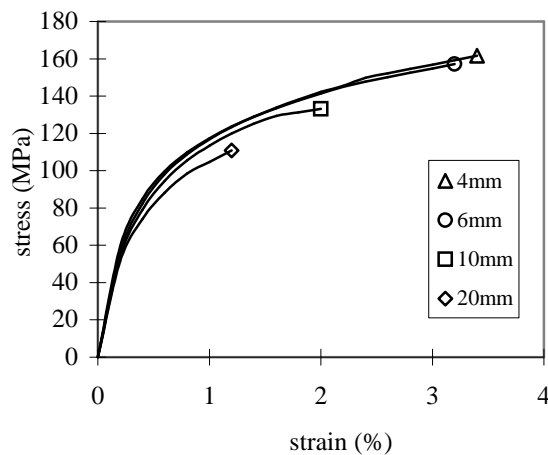


Fig. 2-8 Average engineering stress-strain curves.

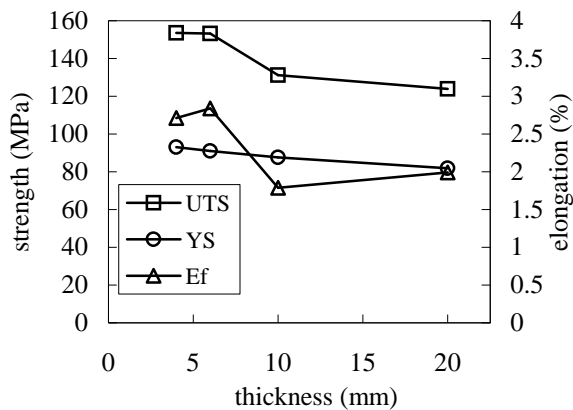


Fig. 2-9 Section thicknesses effect on UTS, YS, and E_f of permanent mould cast AJ62.

As the results show, the microstructure variation from one section to another has a large effect on the mechanical properties. This is especially true for the most prominent of the mechanical property degradations mentioned earlier: the elongation. A severe embrittlement of the as-cast material with increasing section thickness was observed. Fractographs in Figures 2-10 and 2-11 exemplify the range in fracture behaviour between the 4 mm and 20 mm thick specimens. Figure 2-10 demonstrates a ductile fracture surface containing dimples as the most observed feature and dramatic height variations resulting from the elongated nature of the surface. In contrast, Figure 2-11 illustrates brittle fracture with the dominating presence of plateau-like flat surfaces as a result of the crystallographic shearing effect. Such embrittlement phenomena have been well documented elsewhere [6,11,12] for squeeze and die cast magnesium alloys including AM50. Resemblance of the permanent mould cast specimens' behaviour to that of squeeze cast specimens is not unexpected as neither casting process exhibits significant gradients in cell size or porosity throughout a given thickness. Fracture behaviour, just as

the mechanical properties of the permanent mould cast specimens, relies primarily on the distribution of intermetallics.

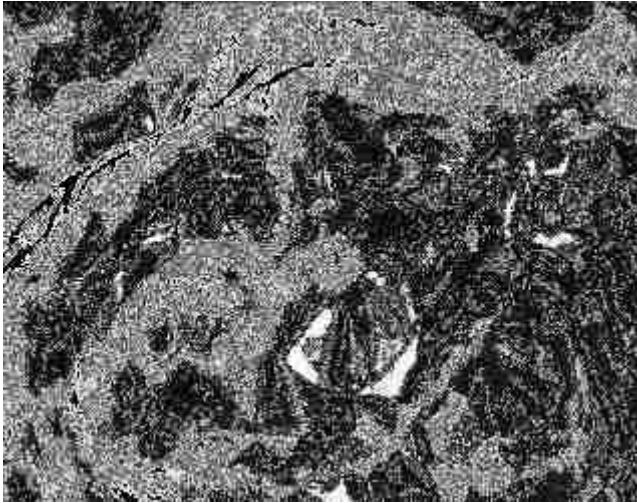


Fig. 2-10 Fractograph of 4 mm tensile specimen.

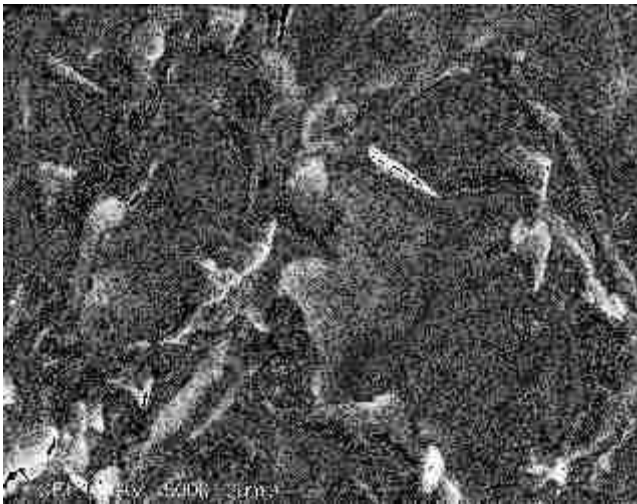


Fig. 2-11 Fractograph of 20 mm tensile specimen.

2.4 SUMMARY

1. The characteristics of the permanent mould cast AJ62 microstructure prominently affected by casting section thickness include coarseness, cell boundary continuity, and distribution of intermetallics.

2. In terms of constituent phases, the microstructure of the permanent mould cast AJ62 alloy does not vary from that observed for other casting processes: α -Mg makes up the matrix; eutectic Al₄Sr appears at the cell boundaries; and globule Al-Mn particles are common within the matrix.
3. The section thickness plays a large role in the mechanical performance of permanent mould cast AJ62. Most notable is the reduction by over 30 % in elongation from 4 mm thicknesses to 20 mm.
4. The well-noted transition from ductile to brittle fracture among specimens of increasing casting thickness can be attributed to the cell size and intermetallic distribution.

2.5 REFERENCES

- [1] Hu, H., Yu, A., Naiyi, L., Allison J.E., Potential magnesium alloys for high temperature die cast automotive applications: a review. *Materials and Manufacturing Processes*. 18 5 (2003) 687-717.
- [2] Kunst, M., Fischersworing-Bunk, A., L'Esperance, G., Plamondon, P., Glatzel, U., Microstructure and dislocation analysis after creep deformation of die cast Mg-Al-Sr (AJ) alloy. *Materials Science and Engineering A*. 510-511 (2009) 387-392.
- [3] Jing, B., Yangshan, S., Shan, X., Feng, X., Tianbai, Z., Microstructure and tensile creep behavior of Mg-4Al based magnesium alloys with alkaline-earth elements Sr and Ca additions. *Materials Science and Engineering A*. 419 (2006) 181-188.
- [4] Kielbus, A., "The influence of casting temperature on castability and structure of AJ62 alloy," *Archives of Materials Science and Engineering*, 28 (6) (2007) 345-348.
- [5] Baril, E., Labelle, P., Pekguleryuz, M.O., Elevated temperature Mg-Al-Sr: creep resistance, mechanical properties, and microstructure. *Journal of Materials*. 55 11 (2003) 34-39.
- [6] Sun, Z., Zhou, M., Hu, H., Naiyi, L., Strain-hardening and fracture behavior of die cast magnesium alloy AM50. *Research Letters in Materials Science*. (2007) ID: 64195.

- [7] Dahle, A.K., Sannes, S., St. John, D.H., Westengen, H., Formation of defect bands in high pressure die cast magnesium alloys. *Journal of Light Metals*. 1 (2001) 99-103.
- [8] ASTM Standard B577M, 2007e1, "Standard test methods for tension testing wrought and cast aluminum- and magnesium-alloy products (metric)," ASTM International, 2007, DOI 10.1520/B0557M-07E01.
- [9] ASTM Standard E111, 2004, "Standard Test Method for Young's Modulus, Tangent Modulus, and Chord Modulus," ASTM International, 2004, DOI 10.1520/E0111-04.
- [10] Gordon, A.W., "Comparison of methods for characterizing porosity in die castings," Engineering Research Center for Net Shape Manufacturing, (1991).
- [11] Zhou, M., An experimental study of die and squeeze cast magnesium alloy AM50. Master Thesis, University of Windsor. (2004).
- [12] Zhou, M., Hu, H., Li, N., Lo, J., "Microstructural and tensile properties of squeeze cast magnesium alloy AM50," *Journal of Materials Engineering and Performance*, 14 (2005) 539-545.
- [13] Wang, S., "Microstructure and tensile properties of squeeze cast Mg-Al-Sr Alloys" Thesis, University of Windsor. (2007).
- [14] Tang, B., Wang, X.S., Li, S.S., Zeng, D.B., Wu, R., "Effects of Ca combined with Sr additions on microstructure and mechanical properties of AZ91D magnesium alloy," *Materials Science and Technology*, 21(2005) 574-578.

CHAPTER 3

CORROSION OF PERMANENT MOULD CAST MAGNESIUM ALLOY AJ62 IN NaCl SOLUTIONS*

3.1 INTRODUCTION

Magnesium alloy AJ62 is receiving increased interest from the automotive industry due to its high specific strength [1,2]. High-temperature properties of the alloy promote its application in environments where magnesium alloys have been unfit to handle such elevated temperatures in the past. Creep resistance is achieved by two major mechanisms in high-pressure die-cast (HPDC) components. Small intermetallic Al-Mn particles having a diameter of 6 ± 3 nm are present in the α -Mg crystals and interact with dislocations thereby strengthening the material [2]. Secondly, the grain boundary eutectic phase $Mg_{17}Al_{12}$ normally observed in Mg-Al alloys, which softens at high temperatures, is suppressed in Mg-Al-Sr alloys as aluminum bonds preferentially with strontium to form an Al_4Sr intermetallic. Aluminum content is high enough, however, that as temperatures are increased the $Mg_{17}Al_{12}$ intermetallic precipitates continuously providing small hard particles near the interdendritic regions that also interact with dislocations [2,3].

While other high-temperature alloys have been developed, castability and cost of the AJ62 alloy sets it apart from other contending alloys [1-5]. Defect-inherent inexpensive processes such as HPDC are generally employed to minimise casting costs for most applications of high temperature magnesium alloys. Despite their low cost and capability of net-shape manufacturing, they often prevent engineers from designing

* Contents of this chapter have been reprinted with permission from AFS Paper No. 10-022, © 2010 AFS. See Appendix B for copyright details.

components with thicker sections, as casting quality deteriorates severely with large thicknesses [6]. Thermal treatments are not applicable either, since porosity bands due to high velocities during casting [7] lead to blistering at treatment temperatures. As such, the feasibility of a PM variant was investigated.

In a previous study [8], a permanent mould AJ62 step-casting was successfully poured to evaluate the mechanical properties imparted by the process. This has opened another window of opportunity for characterization of the alloy. The present work is a preliminary investigation of the PM cast alloy's electrochemical behaviour. Many automotive powertrain components are not only subjected to high temperatures but also the corrosive environment of salty winter road conditions. As well, any strong but lightweight alloy such as AJ62 is a candidate for chassis and suspension components. These too are subject to the potentially harsh road conditions. Since the variation of microstructure with PM casting section thickness [8] is likely to be exposed due to post-cast machining, a further understanding of PM AJ62's microstructural influence on corrosion in varied NaCl solutions was sought.

3.2 EXPERIMENTAL PROCEDURE

In order to fulfill the objective of this work, execution of the experiment proceeded in five steps. These include: sample preparation, observation of microstructure, potentiodynamic testing, analysis of the polarization findings, and finally observation of corroded microstructures.

3.2.1 Sample Preparation

Two samples were used for the potentiodynamic testing. They were extracted from the two extreme thicknesses of a step casting, represented in Figure 3-1, prepared in

a steel mould. The thicknesses of these two sections were 4 mm and 20 mm for the thin and thick sections, respectively. Composition of the alloy used in the step casting, which was supplied by Magnesium Elektron, is given in Table III-I.

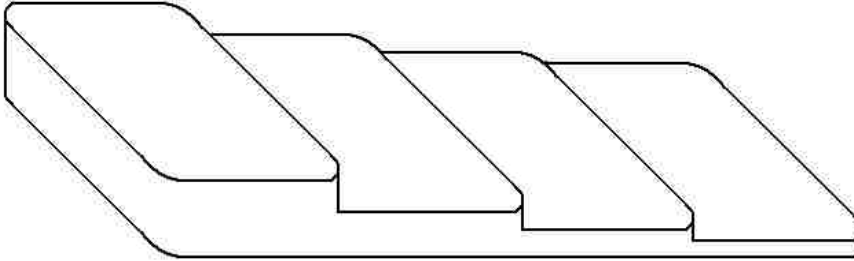


Fig. 3-1 This schematic represents the PM step-casting shape.

Table III-I Composition of AJ62 alloy in wt%

Alloy	Al	Sr	Mn	Si	Zn	Others
AJ62	6.00	2.82	0.28	0.02	<0.01	<0.002

Thin rectangular samples were taken from the casting allowing sufficient surface area as required for the testing procedure. The samples were polished with abrasive papers up to 600 grit both before and in between individual tests. Although polishing the samples between tests removed material from the sample, it had been observed previously [8] that the microstructure within the permanent mould cast sections varies little, if at all, throughout the thickness.

3.2.2 Observation of Microstructure

Representative samples for the two thicknesses were mounted and polished following standard metallographic procedures. Constituent phases and their distribution were observed by scanning electron microscopy (SEM). Population and distribution of microstructure constituents that may act as cathode sites for micro-galvanic corrosion can

have a large effect on the corrosion characteristics of an alloy. For this reason, the area percent of intermetallics observed was determined using ASTM standard E562-08 [9].

3.2.3 Potentiodynamic Testing

Potentiodynamic polarization testing was carried out exposing 0.7854 cm² of sample surface area to the electrolytic media. In this case, each sample was tested using two different NaCl solutions: 0.5 % and 1 %. Two electrodes were submerged in the electrolyte: a counter electrode, CE, near the sample surface, and a reference electrode, RE, elsewhere in the solution. The set-up shown in Figure 3-2 describes the system.

Prior to each test, the specimens were held in the salt solution allowing the open circuit potential, E_{corr} , to settle to a constant value. Using a Bio-Logic SP-150 potentiostat, the current required to maintain a given voltage across the surface was measured for a range of potentials from 0.5 mV below E_{corr} to -0.5 mV with respect to the reference electrode.

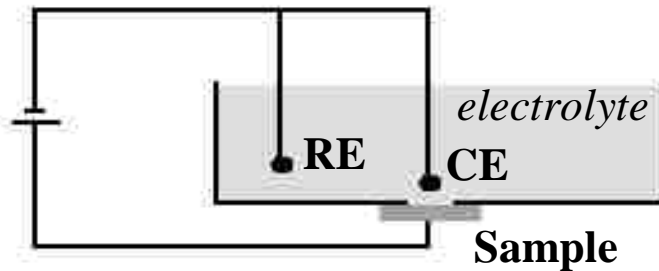


Fig. 3-2 This schematic shows the basic circuitry of the potentiodynamic testing set-up.

3.2.4 Analysis of Potentiodynamic Findings

The overvoltage, η , was plotted versus logarithmic current values, $\log i$, for each test. Using the Tafel fitting capabilities of the EC-Lab® software [10], the corrosion current density, i_{corr} , which represents corrosion rate, was approximated. As well, the

anodic and cathodic Tafel slopes: β_A and β_C , respectively, were calculated. These slopes describe the polarization behaviour as follows:

$$\begin{aligned} \eta &= E_{corr} + \beta_A \log(i/i_{corr}), \eta > E_{corr} \\ \eta &= E_{corr} - \beta_C \log(i/i_{corr}), \eta < E_{corr} \end{aligned} \quad \text{Eqn. 3-1}$$

Using the gathered values, Equation 2 was used to determine the polarization resistance [11,12].

$$R = \frac{\beta_A \beta_C}{2.303 i_{corr} (\beta_A + \beta_C)} \quad \text{Eqn. 3-2}$$

The polarization resistance was taken as another criterion with which to assess the variation among fine and coarse microstructures in both of the NaCl concentrations. Other general observations such as the voltage at which ion exchange is sustained at the surface, E_{corr} , and the passivation behaviour were made.

3.2.5 Observation of Corroded Surface

Micrographs of each sample were taken after potentiodynamic testing in NaCl solution. Initially, images of the surface were generated in the direction normal to the surface. Subsequently, the samples were sectioned and prepared to yield micrographs showing sub-surface behaviour.

3.3 RESULTS AND DISCUSSION

3.3.1 Microstructure

Microstructural constituents of the casting confirmed elsewhere [8] include: the proeutectic α -Mg matrix; Al₄Sr and eutectic α -Mg at the interdendritic regions; and large Al-Mn intermetallic particles. These are labeled as 'A', 'B', and 'C', respectively in Figure 3-3. The large Al-Mn particle size in Figure 3-3 suggests that the observed Al-Mn particles are too large to interact with dislocations at elevated temperatures unless some

smaller Al-Mn particles are still present within the crystals. However, the advantages of continuous $Mg_{17}Al_{12}$ precipitation may maintain the elevated temperature performance of the PM cast alloy. Further research to that end is recommended.

With respect to the microstructure variation between the 4 mm and 20 mm sections, the thermodynamic effect of varied section thicknesses during the casting process is primarily noticed in dendritic cell size. The micrographs of Figure 3-4 highlight the variation in coarseness of the microstructure between the two casting thicknesses studied. Secondary dendrite arm spacing (SDAS) in the 4 mm and 20 mm sections has been estimated as $\sim 10 \mu m$ and $\sim 24 \mu m$, respectively. Microstructure of an alloy can affect its corrosion resistance in two ways.

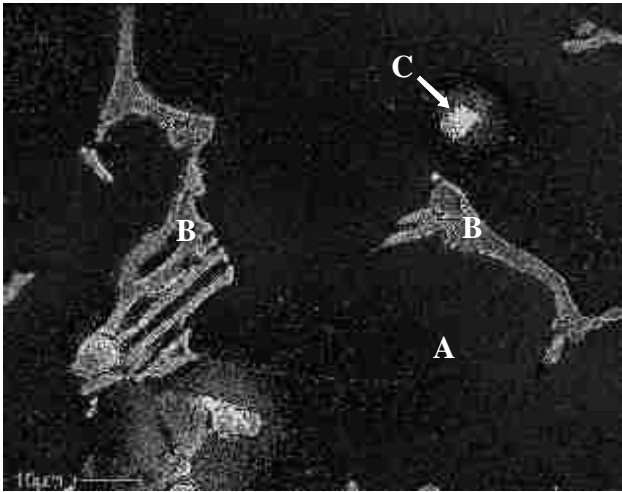


Fig. 3-3 The PM AJ62 alloy's microstructure includes: Primary α -Mg grains (A); Eutectic Al_4Sr and α (B); and Al-Mn intermetallics (C) [8].

First, multiple phases can lead to the generation of a micro-galvanic cell. The most electronegative, anode, phase will move into solution as ions while other phases act as cathode sites to complete the cell. This concept has been well demonstrated in AZ91 and other magnesium alloys [13-16]. In the case of magnesium alloys, it is apparent that the α phases are dissolved preferentially due to the electronegativity of pure magnesium.

Therefore, the ratio of constituents is important. The percent area of the intermetallic phases present in the representative microstructures of Figure 3-4, are given in Figure 3-5. Since the material is largely made up of the α phase, cathodic sites often limit the number of microgalvanic cells [13]. Thus, a lower percent area of Al_4Sr and other intermetallics is desirable in one respect. This theory would suggest using the microstructure of the 20 mm section to combat micro-galvanic corrosion as it's intermetallic area is reduced by over 50 %. This is especially true since the longer cooling time of the thicker section not only produces the low percent area of intermetallics but also means greater solubility of Al in the matrix. This will yield a smaller difference in electronegativity and, as a result, a slightly lessened driving force for the galvanic reactions.

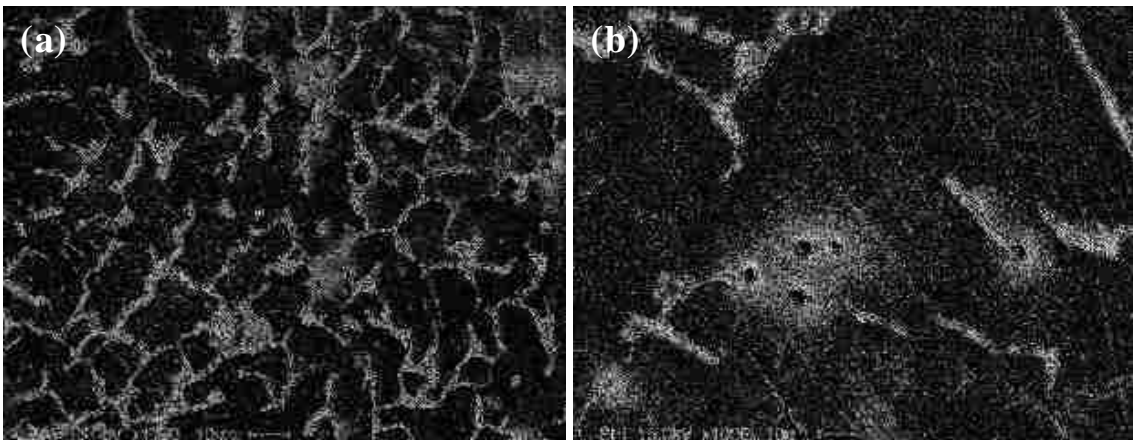


Fig. 3-4 AJ62 grain size and intermetallic distribution are largely dependant on section thickness as is evident in the micrographs for the (a) 4 mm and (b) 20 mm sections.

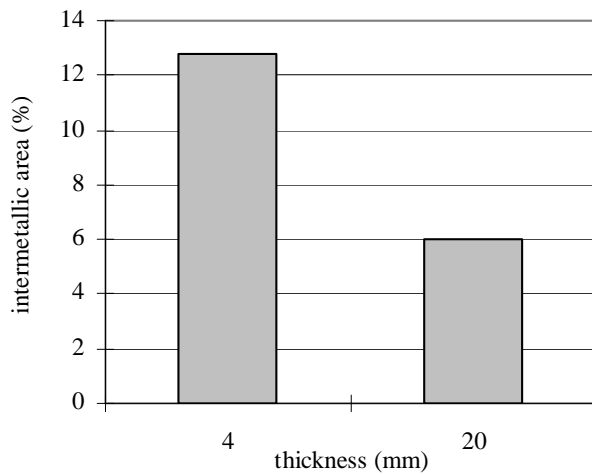


Fig. 3-5 This graphic representation shows a significant difference in percent area intermetallic between the 4 mm and 20 mm section thicknesses.

Another factor is continuity of the intermetallics. Continuous intermetallic phases can form a barrier to further corrosion when the α grains have been mined away [14,15]. This theory of microstructural corrosion inhibition argues convincingly that a greater percentage of secondary phases would be preferential. Observing Figure 3-4 shows that good intermetallic phase continuity characterises the finer structure but not the coarse. This leads to counteracting microstructural considerations with respect to corrosion.

3.3.2 Potentiodynamic Polarization

Potentiodynamic testing results yielded the polarization curves shown in Figures 3-6 and 3-7 for the 0.5 % and 1.0 % NaCl solutions, respectively. From initial observation, variations in the current density at i_{corr} , as well as the anodic and cathodic Tafel slopes cannot be seen clearly. Open circuit corrosion potentials, which give an indication of the alloy's galvanic behaviour, are varied significantly in the more dilute solution. The EC-Lab® software [10] aided Tafel fitting values and the polarization resistance as calculated by Equation 3.2 are summarised in Table III-II.

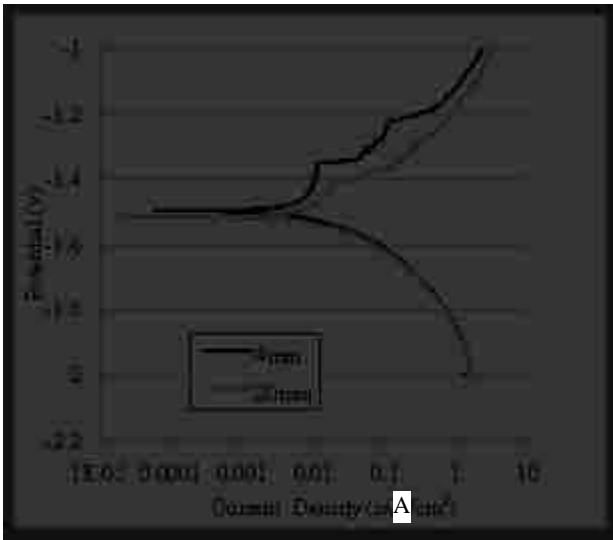


Fig. 3-6 Potentiodynamic polarization of the AJ62 microstructures in a 0.5% NaCl solution yields this plot of potential versus current density.

The low E_{corr} of the alloy is more negative for the coarser microstructure as was observed in both electrolytes and is more noticeable in the weaker solution. This indicates that for the case of galvanic corrosion, the AJ62 alloy will behave more severely as an anode if its microstructure is coarse. Large variations observed in Table III-II were that of the corrosion current density. Observing these values, it is clear that the effect of a coarser microstructure is to increase the corrosion current, which is a representation of the open circuit corrosion rate. This is most likely caused by the greater area of the more electrochemically active α phase present in the coarse microstructure. Divergence of the corrosion current appears to accompany a decrease in NaCl concentration. The polarisation resistance is lower for the coarser microstructure as a result of its inverse proportionality to corrosion current. Variation in calculated resistance is more appreciable in the weaker solution. Values presented for the polarization resistance rely on the values β_A and β_C , which are difficult to determine with high precision due to the lack of observable linear regions on the polarization curves. As

well, it should also be noted that as corrosion continues, products deposited on the surface would affect the potentiodynamic responses documented in the present work. That is to say corrosion may become more or less aggressive as a result of prolonged exposure. Therefore, the resistance values given in this work should be regarded for the general trend they show but not as an indication of performance as would be seen in an immersion corrosion test. Further testing, such as mass loss or salt spray testing, is recommended to better understand the performance of these microstructures.

Han *et alia* [12] recorded nearly no difference in the behaviour of the HPDC AJ62 skin and interior microstructures in a severe 3.5 % NaCl solution but a small noticeable change when engine coolant was used. The present work confirms that such findings are partially a result of the chloride concentration. When elevated, the chlorides promote such aggressive attack that the influence of microstructure becomes inconsequential.

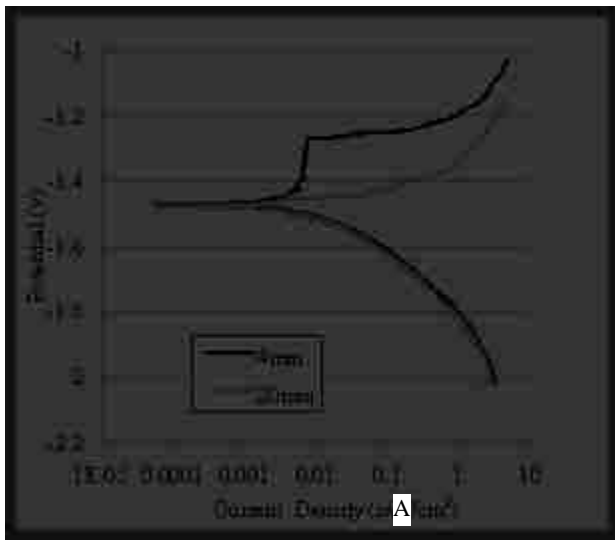


Fig. 3-7 Potentiodynamic polarization of the AJ62 microstructures in a 1.0 % NaCl solution yields this plot of potential versus current density.

Also of interest, and not yet discussed, is the passivation behaviour of the alloy. In Figure 3-6, the response to anodic polarization shows a region of unstable passivity for

both microstructures. The inability to develop a stable passive film in the solutions considered here is due to the pH. Many researchers concerned with the corrosion of Mg and its alloys have determined that passivity of these materials is only stable in very alkaline solutions that are uncommon in most operating environments [11, 16]. It has been noted [16], that a coarser Mg microstructure often shows less propensity for passive film formation and that this effect is magnified with increased chloride concentration. The plot in Figure 3-7 would support a similar principle for the AJ62 alloy as the coarser microstructure is much more susceptible to breakdown of passivity. So while the microstructural influence on corrosion rate and resistance of AJ62 is reduced by the presence of chlorides, the influence on passivation behaviour is accentuated.

Table III-II Summary of polarization curve characteristics and calculated polarisation resistance

		β_A (V)	β_C (V)	i_{corr} ($\mu\text{A}/\text{cm}^2$)	E_{corr} (V)	R ($\text{k}\Omega\cdot\text{cm}^2$)
0.5 % NaCl	4mm Sample	0.067	0.046	2.254	1.498	5.23
	20mm Sample	0.066	0.045	3.311	1.516	3.51
1.0 % NaCl	4mm Sample	0.065	0.040	1.342	1.472	8.01
	20mm Sample	0.065	0.039	1.463	1.480	7.21

3.3.3 Corroded Surface

The corroded areas of the surface displayed a distinct discolouration after potentiodynamic testing. This is most likely due to deposits of corrosion products on the surface. For this alloy, such a deposit would mainly include Mg and O with traces of Al, C, and Cl as discovered by Han [12]. Authors on the topic of Mg corrosion suggest that a passive film would be made up largely of the hydroxide $\text{Mg}(\text{OH})_2$ and the oxide MgO is another compound likely to deposit on the surface given the right conditions [16]. The presence of these elements on the corroded surfaces is therefore expected. Nonetheless,

the discolourations observed give some indication of the corrosion morphology. Figure 3-8 shows the morphology of the finer microstructure, which indicated two preferential corrosion morphologies.

In Figure 3-8 (a), the corrosion pattern tends to follow the striations generated in preparing the uncorroded surface. The microstructure that can be seen does not seem to strongly influence the corrosion morphology. Tendency for the corrosion to follow the striations from abrasive papers has been observed in other materials as well. Wu *et alia* [17] observed that abraded surfaces lead to more uniform corrosion patterns not congruent with specimen microstructure in aluminum 7075. Since the anodic process of metal dissolution can be described by thermodynamic considerations [18], it is no surprise that deformation energies [19], such as those imparted by abrasion, would effect the corrosion pattern. Wu found that a tendency for deeper, localised pitting congruent with surface microstructure was associated with smooth, lapped surfaces and thermal processing [17]. However, Figure 3-8 (b) of the present work shows the anticipated microstructure-influenced corrosion pattern at another location on the 4 mm sample. pH of an electrolyte has an effect on passive film breakdown on a metal surface [16,19] and could explain the variation in corrosion pattern. It is apparent that local pH of the electrolyte, surface conditions, perhaps even the ratio of the SDAS to surface roughness, or a combination thereof have an effect on corrosion of the PM cast AJ62 alloy. It is, however, beyond the scope of this study to characterise such behaviour.

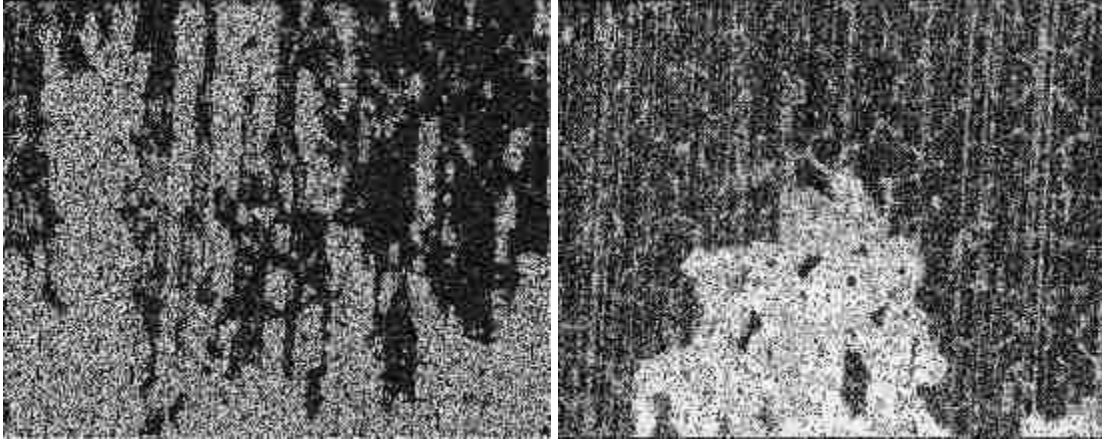


Fig. 3-8 The 4 mm AJ62 sample surface corroded in NaCl solution shows a morphology influenced by: (a) surface preparation, and (b) microstructure.

Figure 3-9 shows that for the coarser microstructure, its influence on the corrosion morphology may be somewhat increased. Unlike the 4 mm sample, there were no locations identified on the 20 mm sample that supported corrosion patterns congruent with surface preparation. The contours of the corrosion pattern on the 20 mm sample surface strongly suggest preferential dissolution of the Mg rich α phase. This would substantiate the theories for intergranular micro-galvanic or response due to electrochemical dissimilarity.

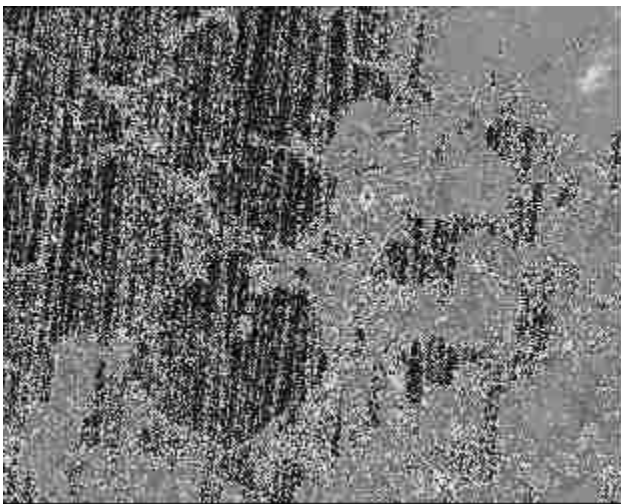


Fig. 3-9 Corrosion morphology of the 20 mm sample was influenced more dominantly by the microstructure as in this micrograph.

To investigate this further, the 20 mm sample was sectioned and metallographically polished to generate the optical images shown in Figure 3-10. It can be clearly seen from Figure 3-10 (a) that congregation of corrosion products takes place in the Mg rich α locations. An intermetallic corrosion barrier as suggested in the referenced literature [14,15] is also apparent. In Figure 3-10 (b), the less anodic intermetallic material can be seen within the deposit, lamellar structure still intact. This would indicate that the intercellular material has not moved. These micrographs of corrosion product formation foreshadow the α phase dissolution and intermetallic spalling most likely to characterise more advanced corrosion of the AJ62 alloy.

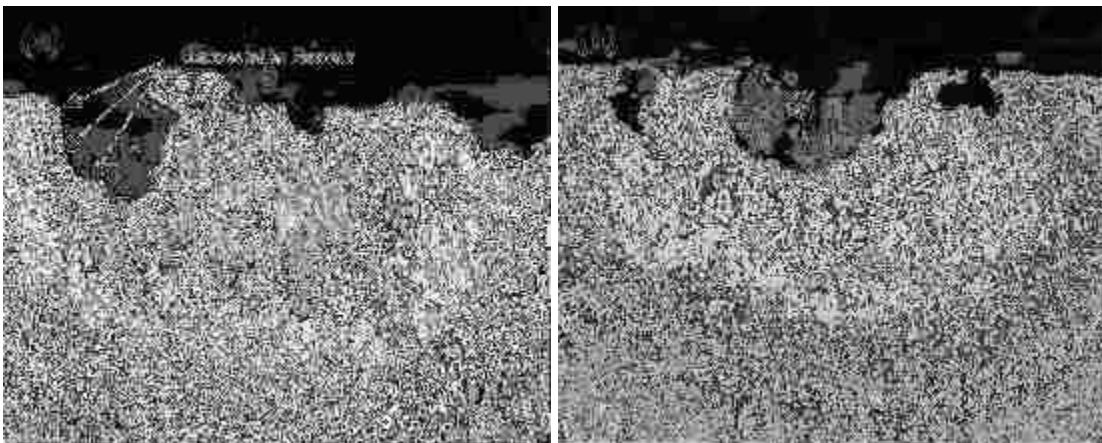


Fig. 3-10 Micrographs of the corroded sample from the 20 mm section show oxide formation in α rich locations.

3.4 CONCLUSIONS

- Variations in microstructure of the PM AJ62 alloy due to casting section thickness are evident. These include: SDAS, intermetallic continuity, and intermetallic distribution.
- The 4 mm section's finer microstructure had good intermetallic continuity for providing a barrier to corrosion. Reduction in cathodic sites on the order of 50% could limit the micro-galvanic effect of the 20 mm section.

- Results generated with the use of weaker NaCl solutions support existing theories that suggest a finer microstructure is more desirable to resist corrosion. However, little variation in the microstructure's response to polarization can be observed. This variation also becomes significantly smaller with increased chloride concentration.
- Unstable passivation response to anodic polarization deteriorates significantly with increased chloride concentration for the coarser microstructure.
- A buildup of corrosion products on the tested surface is visible with an unaided eye. These deposits most likely consist of Mg and O, while traces of other elements are possible.
- The corrosion morphology shows preferential corrosion of α grains when viewing normal to the surface. This is more evident for the coarser microstructure since the finer microstructure corroded via a surface preparation influenced pattern.
- Replacement of α cells with corrosion product deposits can be observed below the corroded surface and suggests preferential dissolution and boundary spalling as the likely mechanisms of mass loss.
- The recommendations that have been made are to develop: a better understanding of the PM cast AJ62 elevated temperature mechanical performance, and an account of PM cast AJ62 corrosion behaviour using experimentation such as mass loss due to immersion corrosion.

3.5 REFERENCES

- [1] Hu, H., Yu, A., Li, N., Allison, J.E., "Potential magnesium alloys for high temperature die cast automotive applications: a review," *Materials and Manufacturing Processes*, 18 (2003) 687-717

- [2] Kunst, M., Fischersworing-Bunk, A., L'Esperance, G., Plamondon, P., Glatzel, U., "Microstructure and dislocation analysis after creep deformation of Mg-Al-Sr (AJ) alloy," *Materials Science and Engineering A*, 510-511 (2009) 387-392.
- [3] Jing, B., Yangshan, S., Shan, X., Feng, X., Tianbai, Z., Microstructure and tensile creep behavior of Mg-4Al based magnesium alloys with alkaline-earth elements Sr and Ca additions. *Materials Science and Engineering A*. 419 (2006) 181-188.
- [4] Kielbus, A., "The influence of casting temperature on castability and structure of AJ62 alloy," *Archives of Materials Science and Engineering*, Volume 28 Issue 6 (2007) 345-348.
- [5] Baril, E., Labelle, P., Pekguleryuz, M.O., Elevated temperature Mg-Al-Sr: creep resistance, mechanical properties, and microstructure. *Journal of Materials*. 55 11 (2003) 34-39.
- [6] Sun, Z., Zhou, M., Hu, H., Naiyi, L., Strain-hardening and fracture behavior of die cast magnesium alloy AM50. *Research Letters in Materials Science*. (2007) ID: 64195.
- [7] Dahle, A.K., Sannes, S., St. John, D.H., Westengen, H., Formation of defect bands in high pressure die cast magnesium alloys. *Journal of Light Metals*. 1 (2001) 99-103.
- [8] Burns, J.R., Han, L., Hu, H., Nie, X., Effects of section thicknesses on tensile properties of permanent mould cast magnesium alloy AJ62. *Magnesium Technology 2010*, The Minerals, Metals, and Materials Society. (2010) 367-371.
- [9] ASTM Standard E562, 2008, "Standard Test Method for Determining Volume Fraction by Systematic Manual Point Count", ASTM International, 2008, DOI 10.1520/E0562-08.
- [10] EC-Lab® Software Version 9.45, Bio-Logic Science Instruments, Released December 14, 2007.
- [11] Revie, R.W., Uhlig, H.H., *Corrosion and corrosion control*. John Wiley and Sons. USA. 2008.
- [12] Han, L., Nie, X., Ni, J., Zhang, Q., Zhang, P., Hu, H., "Effect of grain size on corrosion behavior of high-pressure cast AJ62 magnesium alloy in salt solution and automotive coolant," *Magnesium Technology 2009*, The Minerals, Metals, and Materials Society, (2009).
- [13] Liu, L., Schlesinger, M., "Corrosion of magnesium and its alloys," *Corrosion Science*, 51 (2009) 1733-1737.
- [14] Song, G., Atrens, A., "Understanding magnesium corrosion," *Advanced Engineering Materials*, 5 (2005) 837-858.

- [15] Song, G., Atrens, A., Dargush, M., "Influence of microstructure on the corrosion of diecast AZ91D," *Corrosion Science*, 41 (1999) 249-273.
- [16] Makar, G.L., Kruger, J., "Corrosion of magnesium," *International Materials Reviews*, 38 (1993) 138-153.
- [17] Wu, T.I., Wu, J.K., "Effect of surface finish on the corrosion behavior of commercial 7075 Al alloy," *Scripta Metallurgica et Materialia*, 27 (1992) 875-880.
- [18] Talbot, D., Talbot, J., *Corrosion science and technology*, CRC Press, 1998.
- [19] Kolodii, B.I., "Influence of the strain energy of a metal on its interaction with corrosive media," *Materials Science*, 38 2 (2002) 243-249.

CHAPTER 4

MICROSTRUCTURE INFLUENCE ON THE CORROSION OF PERMANENT MOULD CAST MAGNESIUM ALLOY AJ62 IN ENGINE COOLANT*

4.1 INTRODUCTION

Magnesium alloy AJ62 has recently been developed as an advantageous option among structural automotive powertrain materials. This alloy is characterised not only by a high strength-to-weight ratio synonymous with magnesium alloys but also by a relative mechanical integrity at elevated temperatures [1-3]. Its high temperature performance has led engineers to suggest exploitation of this alloy as an engine block material.

Numerous studies have been made on high-pressure die-cast (HPDC) and squeeze cast AJ62 specimens or components. The alloy's die-castability has been well noted among other die-casting magnesium alloys [4]. This has led to investigations on the alloy's ability to be cast by the gravity fed permanent mould process. Early success with this seemingly more primitive method has been demonstrated [5].

Constituents of the microstructure reflect those in the HPDC and squeeze cast alloy leading to the assumption that permanent mould casting the alloy will not greatly affect its high temperature performance [1-3,5]. The permanent mould cast microstructure is shown in Figure 4-1 where locations A, B, and C are the magnesium rich matrix, the eutectic intermetallic containing Al₄Sr, and intermetallic Al-Mn particles, respectively [5].

* Contents of this chapter have been reprinted with permission from SAE Paper No. 2010-01-0412, © 2010 SAE International. See Appendix B for copyright details.

One concern still remains, however, and that is magnesium alloys' susceptibility to corrosion. As magnesium is the most anodic of all metals [6], its alloys suffer severe corrosive attack in most environments. Ceramic coatings have been suggested as the optimal combatant to magnesium alloy corrosion in relevant literature [6-8]. Detrimental levels of corrosion have been observed for surfaces exposed to salt solutions. Therefore, surfaces exposed to salty road conditions would likely require such coatings. Conversely, on the interior of an engine block, corrosion is not assumed to be as severe because modern engine coolants will not behave well as an electrolyte. Corrosion inhibitors are used to block ion movement from metal surfaces and stay the progression of corrosion [9]. The main objective of the present study was to scientifically understand the corrosion behaviour of permanent mould cast AJ62 immersed in engine coolant.

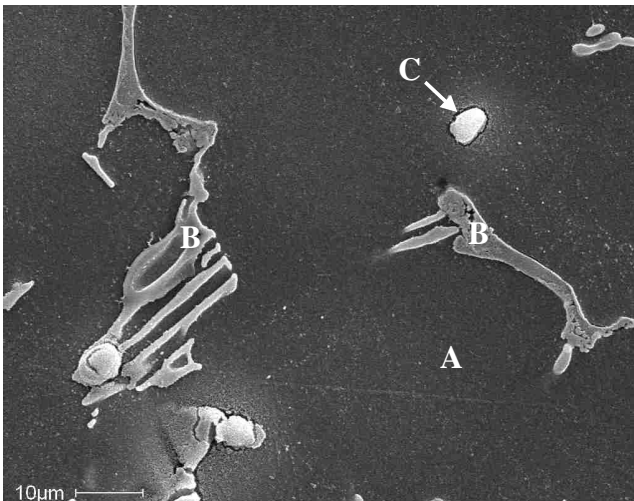


Fig. 4-1 Microstructure of the permanent mould cast AJ62 alloy [5].

Adding complexity to the problem of AJ62 corrosion in engine coolant is the significant effect of alloy microstructure on corrosion behaviour. After potentiodynamic testing, it was documented by Han *et alia* [10] that corrosion potential of the HPDC alloy varies based on microstructure coarseness. This was especially true for tests where

engine coolant was the electrolytic medium. Previous study of AJ62 corrosion in NaCl solutions suggests that this is primarily due to the microgalvanic effect dictated by the anode to cathode ratio observable in electrolytes with low chloride concentrations [11]. The second objective of the current study was to observe this phenomenon for permanent mould cast AJ62 and relate the corrosion of immersed specimens to the potentiodynamic variation.

4.2 IMMERSION TESTING

4.2.1 Preparation of Specimens

Specimens were prepared for both immersion corrosion and potentiodynamic testing. All of the specimens were taken from simple step-castings as the variation in casting thickness leads to variations in cell size [5,11]. Length and width of each step were 150 mm and 50 mm, respectively. The casting thicknesses of the step-castings were 4 mm, 6 mm, 10 mm, and 20 mm yielding geometry similar to that shown in the diagram of Figure 4-2. Magnesium AJ62 with a melt temperature of 690 °C was poured into steel mould preheated to a temperature of approximately 390 °C [12]. To avoid burning or excessive oxidation, protective gas was used during both the melt and pour (sulfur hexafluoride SF₆ 0.5% + carbon dioxide CO₂) [12].

Prior to testing, one coupon was extracted from each of the casting thicknesses for microscopy. These coupons were then compression mounted in diallyl phthalate. The mounted coupons were subsequently polished using standard metallographic procedures first with increasingly finer abrasive papers and then using polishing wheels and alumina abrasives. Final particle size used for polishing was 0.05 µm. Having been sufficiently polished, the microstructures were examined via scanning electron microscopy (SEM).

The purpose for this was to note the variation in microstructure, particularly the secondary dendrite arm spacing (SDAS) and thereby understand its effect on the corrosion test results.

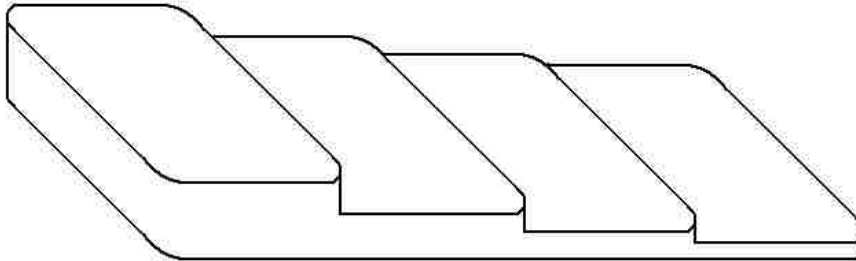


Fig. 4-2 Step-casting shape [5].

Test specimens for the immersion test were taken from locations central to the casting steps. Four small specimens for each thickness, totalling sixteen specimens in all, were prepared. The specimens were approximately 10 mm in both width and length and their heights were slightly less than their respective casting thicknesses. All surfaces were polished with 320 grit abrasive papers to avoid the entrapment of H_2 and other gasses on the surface as the submerged specimens were corroded. The final dimensions and mass of each specimen was measured and recorded for the calculation of mass loss after the test.

4.2.2 Immersion Test Procedure

Specimens were submerged in Prestone® engine coolant intended for all makes and models, which is claimed to satisfy ASTM D3306 and D4985 [13,14]. This engine coolant, chosen for its wide range of applicability in the industry, was used as an analogue to the “typical” commercially available coolant compatible with most common automotive metals. Specimens were submerged in a large volume of coolant, 2 L

specifically, to avoid significant pH increase or saturation of reaction products due to the corrosion process. Such phenomena may have otherwise affected the corrosiveness of the engine coolant. While local coolant volumes within automotive engine block geometries may not be sufficiently large to completely avoid these phenomena, movement of the engine coolant during regular operation would.

ASTM standard G3172 suggests a better replication of immersion corrosion than those that reintroduce specimens after being cleaned and weighed, as the latter is not an accurate analogue to the corrosion process [15]. Therefore, one specimen of each thickness was left in the coolant for each of the 1, 2, 3, and 4 week durations. These durations were chosen as they might show existing changes in the corrosion rate well after initial submersion. After being removed from the coolant, the specimens were wiped to cease the progress of corrosion and remove any corrosion products from the surface. Some immersion corrosion studies employ chemical specimen cleaning [15]. Due to the electrochemical sensitivity of magnesium alloys and the limited severity of corrosion in engine coolant, the use of such means has been avoided here. Thickness and distribution of the surface deposits, noted in the next section, did not require the use of chemicals for removal. Once cleaned, the specimens were weighed and their mass was recorded for calculations.

Calculation of mass lost, ML , for each specimen was achieved via Equation 4-1 as follows:

$$ML = \frac{(m_0 - m)}{A} \quad \text{Eqn. 4-1}$$

Here m_0 is the initial mass of the specimen in grams, m is the mass after corrosion, and A is the surface area of the specimen given by Equation 4-2 using the initial dimensions: d_1 , d_2 , and d_3 .

$$A = 2d_1d_2 + 2d_2d_3 + 2d_1d_3 \quad \text{Eqn. 4-2}$$

Corrosion rates in units of $\text{g/mm}^2/\text{year}$ were approximated in terms of mass loss for the four intervals by Equation 4-3 below.

$$\text{rate} = (ML_i - ML_{i+1})(52) \quad \text{Eqn. 4-3}$$

The term, i , in Equation 4-3 is the number of weeks the specimen removed at the beginning of the interval had been submerged. Of course, for the first interval $i=0$ and $ML_0=0$.

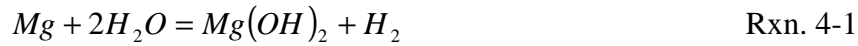
4.2.3 Immersion Test Results

In addition to the calculated results mentioned in the procedures above, some general observation of the corrosion process took place. These observations are presented here before discussion of the other quantifiable results.

4.2.3.1 General Observations

At initial exposure to the engine coolant corrosion medium, reactions were obviously taking place. This was suggested by the relatively aggressive generation of bubbles during the first few days compared with the rest of the experiment. Visible hydrogen evolution is often associated with the corrosion of magnesium and its alloys [8]. In water, corrosion of magnesium and its alloys proceeds according to three partial reactions. The anodic reaction includes the dissolution of magnesium cations, the cathodic reaction involves the evolution of hydrogen gas, and a third reaction forms

magnesium hydroxide from products of the above reactions. The overall reaction can therefore be written as:



For this reason, researchers have been able to use the volume of hydrogen gas evolved to determine mass lost in known solutions [17]. Corrosion in engine coolant involves many more chemical constituents and therefore reactions. In fact, the exact composition of the engine coolant remains undisclosed by the manufacturer. Collection and measurement of evolved gasses is futile without a complete understanding of the governing equations. Most coolants are made up in large part by ethylene glycol and water while a small concentration of chemical inhibitors are also present [18]. Therefore the evolved gas is most likely hydrogen, a product of the aforementioned cathodic reaction, although it cannot be quantifiably related to magnesium ion movement in this case.

At most naturally occurring environmental potentials, magnesium is a passivating metal though its passive layer can only be stabilised at high pH [8]. However, elevation of pH by the $Mg(OH)_2$ corrosion product in the volume of coolant used would have taken a significant amount of time and is unlikely. Any reactions required in stabilizing this, or some other, surface film using inhibitors would require alternate chemical reactions. Because this too would take some time, it is assumed that during the initial stages of corrosion a passive layer is not yet stable on the exposed magnesium matrix and rapid corrosion of the bare metal is expected. This might explain the surge of gas evolution that directly followed the submersion of the specimens.

Another general observation was a dark pigmentation of the metal surface within the first few days. This surface condition was not a substantial build-up of any product on the surface, as seen during corrosion of the AJ62 alloy in NaCl solutions [10,11], since the striations of the prepared surface were still visible by eye. Cause of this discolouration is likely related to the chemical inhibitors promoting or creating a minute protective film to stop ion movement. Upon further investigation, it was noted that the dark pigmentation was restricted to the magnesium rich locations of the microstructure. In Figure 4-3, shapes on the surface that are apparently unsusceptible to the discolouration may be congruent with intermetallic constituents although the surface preparation does not allow conclusive identification of the microstructure.

Lastly, a highly localised build-up of corrosion products was noticed on most specimens but only in a few locations. The corrosion products were not identified as they were easily wiped away for the measurement of mass. Underneath the build-up, the bare metal had the colour and luster of its prepared form. It is expected that the corrosion products were similar to those found on the alloy corroded in salt solution although any additive or impurity in the coolant could contribute to the composition of the buildup. The presence of such deposits would accompany any localised corrosion due to the inhomogeneous nature of the alloy. As an example, an unseen porosity or surface defect could induce corrosion processes associated with small electrolyte volumes. This would create a local surface different from the bulk surface and thereby some microgalvanic effect [8]. Suppression of these micro-galvanic effects by the coolant's inhibitors after prolonged exposure is probable as evidence of localised corrosion was most prominent on the specimens subjected to shorter immersion durations. Such localised phenomena do

not characterise the general corrosion of the magnesium alloy AJ62 but may be a result of the permanent mould process. The image in Figure 4-3 shows the discolouration of the corroded AJ62 surface, as mentioned previously, compared with a location on the surface that was covered by corrosion products.

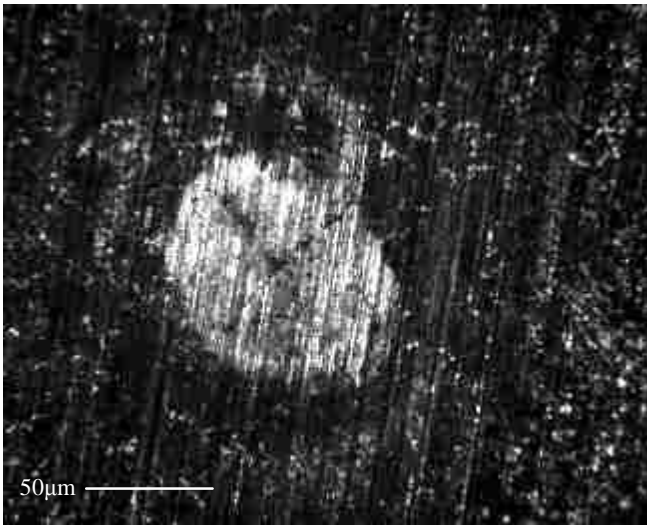


Fig. 4-3 Discoloured surface as compared with the alloy below a localised corrosion site.

4.2.3.2 Corrosion Rate Due to Microstructure

It has been noted elsewhere [5], that the secondary dendrite arm spacing of the 4mm section is double that of the 20 mm thick sections. This is clearly seen in the SEM micrographs of Figure 4-4 as initial observation suggests a SDAS of $\sim 20 \mu\text{m}$ for the 4 mm section and $\sim 40 \mu\text{m}$ for the 20 mm section. As shown by potentiodynamic investigation in previous works [11], variation of corrosion rate is most evident in electrolytic media with low chloride concentrations. This phenomenon was replicated here by the immersion test results. As Figure 4-5 points out, the mass loss not only increases with duration as expected but also increases with microstructure coarseness. Figure 4-6 highlights the variation in corrosion rate with duration and section thickness.

While individual trends for each thickness are not apparent, it can be seen that the initial corrosion rate is much higher than the corrosion rate observed for subsequent weeks. These results quantify the corrosion indicated by aggressive hydrogen evolution occurring just after submersion as well as its tendency to subside. This is especially true for the thicker sections with coarser microstructure.

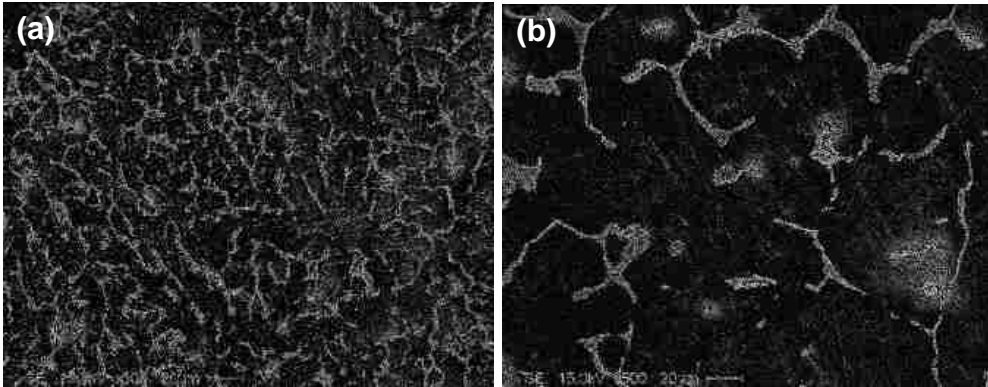


Fig. 4-4 Microstructure of (a) the 4mm section and (b) the 20mm section [5].

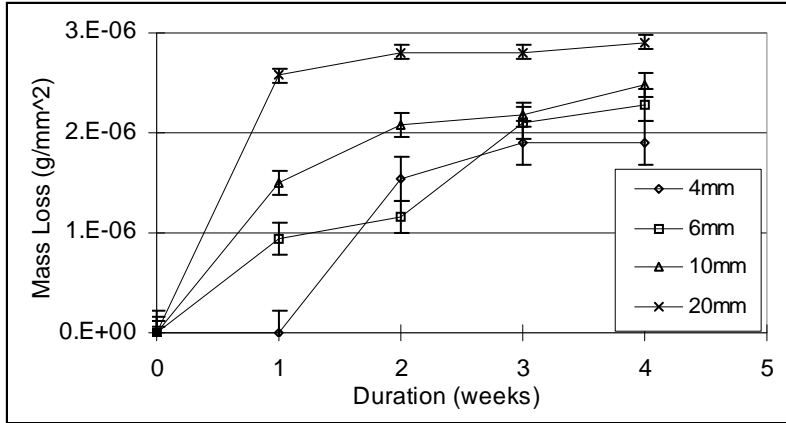


Fig. 4-5 Mass loss as a function of thickness for the four durations with error accounting for instrumentation.

Variation in mass loss and corrosion rate by week of the thinner sections, particularly the 4 mm and 6 mm specimens, appears to be more linear overall than that of the thicker sections. While this is an interesting observation, it could be a false trend generated by the precision of the instrumentation used as it relates to the specimens'

overall size. This error in mass measurement has been shown in the figures and also accounts for the lack of any mass loss being indicated for the smallest specimen at the shortest, 1 week, duration. The undesirable effect on the reported result for that specimen would be due to its larger error coupled with its superior corrosion resistance. To make conclusive statements regarding these trends with sufficient confidence and gather a more accurate representation of the mass loss for smaller specimens, the testing of multiple samples for each datum is recommended in future experimentation. Nonetheless, it is important to note that the corrosion rate decreases with time, but never ceases, for the durations of exposure examined here. Also, these results are in agreement with previous studies [10,11,17] claiming that finer microstructures exhibit better corrosion resistance than their coarser counterparts.

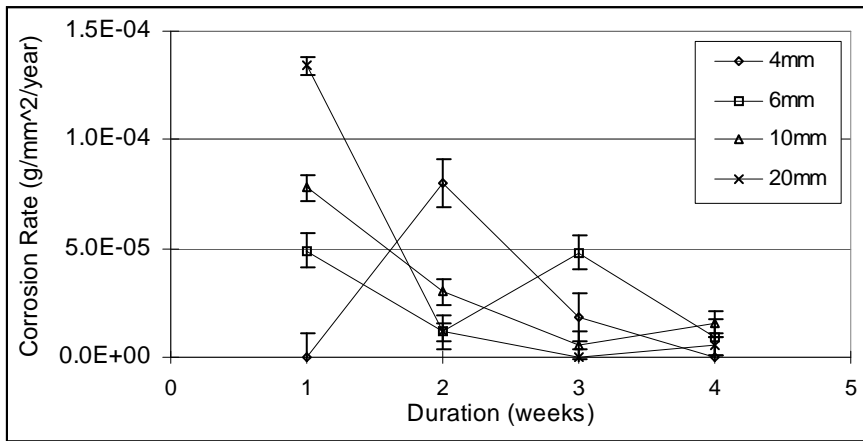


Fig. 4-6 Corrosion rate as a function of time (weeks) for different section thicknesses of the cast AJ62.

4.3 POTENTIODYNAMIC TESTING

4.3.1 Preparation of Specimens

Similar to the specimens for immersion corrosion testing, potentiodynamic specimens were taken from locations central to the casting steps. Two specimens were

prepared: one from the 4 mm thickness and one from the 20 mm thickness. The specimens were approximately 20 mm in width, 30 mm in length, 4 mm in height for the fine microstructure specimen and 8 mm for the coarse microstructure specimen. One of the two large flat surfaces was polished with gradually finer abrasive papers up to 600 grit. Metallographic preparation of these specimens with finer abrasive papers than those used for immersion testing was conducted because bubbles are much more detrimental to the accuracy of potentiodynamic testing.

4.3.2 Potentiodynamic Test Procedure

The each specimen, one 4 mm and one 20 mm, was mounted in the testing apparatus individually. The apparatus exposed exactly 0.7854 cm^2 of the specimen's prepared surface to the electrolytic medium. Prestone® engine coolant, as in the immersion tests, was used as an electrolyte. Temperature and pH of the coolant was not measured or monitored but initial conditions prior to both potentiodynamic tests were constant. The apparatus allowed a maximum electrolyte volume of 300 mL, the entirety of which was exploited for the potentiodynamic testing to limit excessive pH variation. A counter electrode (CE) was placed in the coolant directly above the specimen's surface while a reference electrode (RE) was placed in the coolant away from the counter electrode. This arrangement created the circuitry as shown in Figure 4-7.

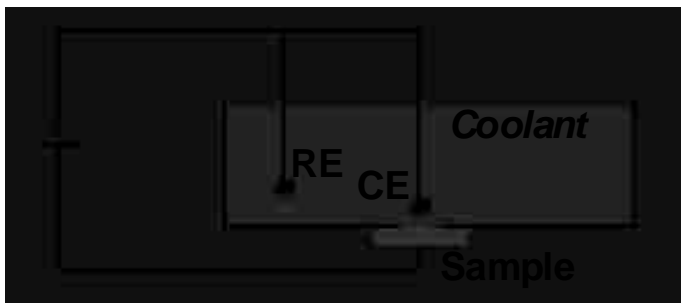


Fig. 4-7 Conceptual schematic of electrical circuits for potentiodynamic testing.

Using a Bio-Logic potentiostat, the potential across the surface was increased continuously from 0.5 V below the open circuit potential to -0.5 V with respect to the reference electrode at a rate of 1 mV/s. Results were used to determine the anodic and cathodic Tafel slopes (β_A and β_C , respectively). Obtaining these in a consistent manner for both tests allows calculation of corrosion potential and current (E_{corr} and i_{corr} , respectively) for both microstructures that can later be compared although the certain Tafel slope values are not easily discernable. To do this EC-Lab® software [16] was used to analyze the polarization curves.

4.3.3 Potentiodynamic Test Results

The polarization curves for the AJ62 microstructures are given in Figure 4-8. These show a similar pattern to results obtained from previous studies [10]. Cathodic polarization is characterised by unstable passivation although the passive film breakdown occurs at much higher potentials than it does in NaCl solutions [10,11]. This improvement in passivation behaviour beyond that observed in other media is likely due to a compounding effect. Not only does the coolant contain inhibitors that hinder Mg^{2+} ion dissolution but also the volume restrictions of the potentiodynamic testing apparatus mentioned earlier may cause an increase in pH. This increase would cause higher pH during the final portion of testing when passivation behaviour is being recorded. Since electrolytes of high pH stabilise passive films [8], the behaviour induced by chemical inhibitors is thereby promoted. It should be noted that the region of passivation on the curves in Figure 4-8 is greater for the thicker casting section than that for the thinner section, which is most likely a result of greater α magnesium surface area where passivation will occur. Another characteristic is the apparent variation in corrosion

potential. This suggests that the effects of galvanic corrosion in practical application will be significantly more severe because its driving force is related to the difference between the corrosion potential, observed in Figure 4-8, and that of any cathodic metal present [9]. Since the coarser microstructure displays a more anodic corrosion potential and it is most likely that other metals present in a galvanic reaction will have a higher potential [8], the finer microstructure is much more desirable.

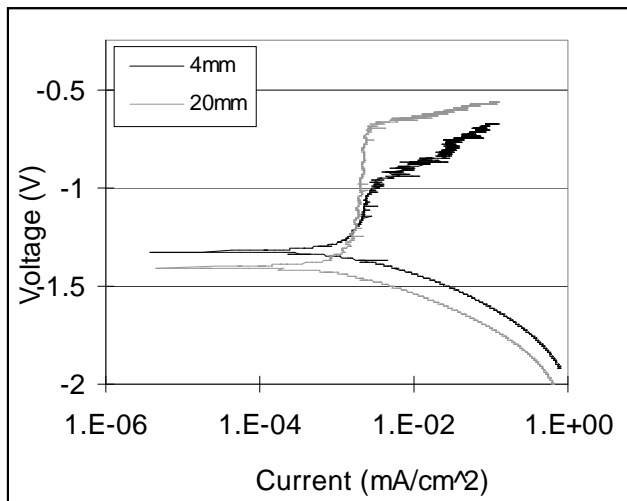


Fig. 4-8 Polarization curves for the permanent mould cast microstructures in engine coolant.

Most important for this study, in relating the potentiodynamic findings to the immersion test results, is the corrosion current which represents the rate of ion exchange. Table IV-I highlights this and other outputs of the EC-Lab Tafel fitting. The Tafel slopes are often used to characterise polarization curves [9-11]. Unfortunately the AJ62 alloy studied in the present work does not demonstrate any noticeable range of linear behaviour. This limits the accuracy of the slope values, as some judgment is required in analyzing the curves. However, the slopes are required to calculate an accurate value for corrosion current. For this reason, the Tafel slopes were generated using similar locations for both curves. The slope values have been recorded to demonstrate their similarity and that a

consistent means of determining the corrosion current has been employed. Corrosion current is conclusively higher for the thicker casting section although the difference is very small. In fact, the difference is unclear by simply observing the polarization curves in Figure 4-8. This confirms the immersion test results although the rates do not easily relate mathematically. Corrosion rate predicted by the polarization curves varies by 7 % between the thin and thick sections with respect to the thinner specimen. Meanwhile, the corrosion rate for the first week of immersion showed a more marginal variation between the 4 mm and 20 mm specimens. In fact, corrosion of the 4 mm specimen was unnoticed during the first week of immersion as was discussed earlier. This difference signifies a change in the kinetics of corrosion during the first week and that change has varied effects on different microstructures. Its association with the marked decrease in hydrogen evolution and the change in surface characteristics is likely.

Table IV-I Characteristic values for the polarization curves in Figure 4-8

Specimen	I_{corr} (mA/cm²)	E_{corr} (V)	β_A	β_C
4 mm	0.199	-1.329	56.7	37.2
20 mm	0.213	-1.409	76.7	36.1

4.4 CONCLUSIONS

Permanent mould cast thickness for the AJ62 magnesium alloy has been shown to have a significant effect on the alloy microstructure. This is especially true for the microstructural coarseness and intermetallic continuity. This study has shown that the corrosion of permanent mould cast AJ62 in engine coolant intensifies with increases in casting thickness. Also, while the corrosion of the alloy does continue with prolonged exposure to engine coolant, the initial corrosion during the first week is responsible for the majority of the mass loss. This is particularly true for the thicker casting sections.

Initial corrosion may proceed according to reactions that govern the corrosion of the alloy in water as most engine coolants contain notable amounts of water. Hydrogen evolution and corrosion product deposits can be seen for a period following submersion into the coolant suggesting that this may be the case. After this period but prior to one week of exposure, all specimen surfaces had developed a dark appearance. In combination with the reduction in hydrogen evolution this suggests the stabilization of a passive film most likely attributed to or accelerated by chemical inhibitors in the coolant. Polarization testing of the extreme thicknesses indicated that corrosion behaviour of the alloy varies significantly with microstructure in the coolant. However it may not relate to the corrosion properties exhibited after passive film stabilization on the magnesium rich cells.

4.5 REFERENCES

- [1] Kunst, M., Fischersworing-Bunk, A., L'Esperance, G., Plamondon, P., Glatzel, U., Microstructure and dislocation analysis after creep deformation of Mg-Al-Sr (AJ) alloy, *Materials Science and Engineering A*, 510-511 (2009) 387-392.
- [2] Jing, B., Yangshan, S., Shan, X., Feng, X., Tianbai, Z., Microstructure and tensile creep behavior of Mg-4Al based magnesium alloys with alkaline-earth elements Sr and Ca additions, *Materials Science and Engineering A*, 419 (2006) 181-188.
- [3] Baril, E., Labelle, P., Pekguleryuz, M.O., Elevated temperature Mg-Al-Sr: creep resistance, mechanical properties, and microstructure, *Journal of Materials*, 55 (11) (2003) 34-39.
- [4] Kielbus, A., The influence of casting temperature on castability and structure of AJ62 alloy, *Archives of Materials Science and Engineering*, 28 (6) (2007) 345-348.
- [5] Burns, J.R., Han, L., Hu, H., Nie, X., Effects of section thicknesses on tensile properties of permanent mould cast magnesium alloy AJ62, *Magnesium Technology 2010 Conference Proceedings*, The Minerals Metals and Materials Society, Accepted (2010).
- [6] Ma, Y., Hu, H., Northwood, D.O., Nie, X., Optimization of the electrolytic plasma oxidation processes for corrosion protection of magnesium alloy AM50 using Taguchi method, *Journal of Materials Processing Technology*, 182 (2007) 58-64.

- [7] Gary, J.E., Laun, B., Protective coatings on magnesium and its alloys – a critical review, *Journal of Alloys and Compounds*, 336 (2002) 88-113.
- [8] Makar, G.L., Kruger, J., Corrosion of magnesium, *International Materials Reviews*, 38 (1993) 138-153.
- [9] Talbot, D.E.J., Talbot, J.D.R., *Corrosion science and technology*, Taylor Francis and Group, 2007, Boca Raton, FL, USA.
- [10] Han, L., Nie, X., Ni, J., Zhang, Q., Zhang, P., Hu, H., Effect of grain size on corrosion behavior of high-pressure cast AJ62 magnesium alloy in salt solution and automotive coolant, *Magnesium Technology 2009 Conference Proceedings*, The Minerals Metals and Materials Society, (2009), 21-25.
- [11] Burns, J.R., Hu, H., Nie X., Su, J.F., Corrosion of Permanent Mould Cast Mg Alloy AJ62 in NaCl Solutions, 114th World Metalcasting Congress, American Foundry Society, Accepted (2010).
- [12] Sun, Z, Hu, H., Burns, J., Nie, X., Han, L., Design of a Step Permanent Mold for Casting Magnesium Alloy AJ62, 114th World Metalcasting Congress, American Foundry Society, Accepted (2010).
- [13] ASTM Standard D3306, 2008, “Standard Specification for Glycol Base Engine Coolant for Automobile and Light-Duty Service”, ASTM International, 2008, DOI 10.1520/D3306-08A.
- [14] ASTM Standard D4958, 2009, “Standard Specification for Low Silicate Ethylene Glycol Base Engine Coolant for Heavy Duty Engines Requiring a Pre-Charge of Supplemental Coolant Additive (SCA)”, ASTM International, 2009, DOI 10.1520/D4985-09.
- [15] ASTM Standard G31-72, 2009, “Standard Practice for Laboratory Immersion Corrosion Testing of Metals”, ASTM International, 2009, DOI 10.1520/G0031-72R04.
- [16] EC-Lab® Software Version 9.45, Bio-Logic Science Instruments, Released December 14, 2007.
- [17] Song, G., Atrens, A., Understanding magnesium corrosion a framework for improved alloy performance, *Advanced Engineering Materials*, 5 (12) (2003) 837-858.
- [18] Song, G., StJohn, D., Corrosion behaviour of magnesium in ethylene glycol, *Corrosion Science*, 46 (2004) 1381-1399.

CHAPTER 5

CORROSION PERFORMANCE OF PERMANENT MOULD CAST MAGNESIUM ALLOY AJ62 IN AUTOMOTIVE ENVIRONMENTS

5.1 INTRODUCTION

Within the field of lightweight alloys, those based on the metal magnesium are among the most desirable for future automotive application. Benefiting from the low density of magnesium, these alloys exhibit the greatest strength-to-weight ratio of any engineering metals [1]. Future products of the transportation industries are expected to consume less fuel while maintaining or exceeding their current level of performance. By lowering the weight of a vehicle, its energy, and thereby fuel, requirements, are lessened. This reduced fuel requirement highlights the importance of strength-to-weight ratio as a criterion for material selection. Development of magnesium alloys has primarily been focused on improvement of mechanical performance at elevated temperatures [2-8]. One alloy that has been successful in this regard is the magnesium-aluminum-strontium alloy AJ62. Its unique microstructure includes an Al_4Sr intermetallic at the interdendritic regions rather than the $Mg_{17}Al_{12}$ common to other magnesium-aluminum alloys. In other respects, the microstructure of the AJ62 alloy resembles the common magnesium-aluminum-manganese alloys such as AM50 and AM60. Recent publications [2-5] indicating the creep resisting mechanisms of this microstructure tout the elevated temperature superiority of this alloy among other magnesium alloys.

The majority of magnesium alloy applications are high-pressure die-cast (HPDC) components. The HPDC process prohibits many designs that include heat-treating [9] and thicker cast sections due to the formation of a skin layer and subsurface defect band [10-12]. Moderate castability has characterised the AJ62 alloy in HPDC experiments

leading to investigation of alternate processing. Permanent mould (PM) casting, a gravity-fed process offers thick casting sections potentially suitable for heat-treated components. While unable to offer the economies of scale achievable through high volume HPDC production, the PM process would yield a greater range of applicability available at a lower overhead cost. Integral to adapting an alloy to a new process is the characterization of its performance in a number of potential environments. Susceptibility of magnesium to corrosion is a cause for concern in many operating environments [13-17]. Thus the observed response of permanent mould cast AJ62 microstructures to corrosion is of particular interest to the automotive industry. The current research documents and compares the corrosion of AJ62 in two media common to automotive environments, engine coolant and salt solution. The goal is to build a more comprehensive understanding of the alloy.

5.2 EXPERIMENTAL METHODS

Step castings, as in Figure 5-1 taken from reference 18 were produced via the permanent mould casting process in a steel mould. The composition of the AJ62 castings was that indicated in Table V-I. Four thicknesses were cast in all: 4 mm, 6 mm, 10 mm, and 20 mm. Of these, the two extreme thicknesses of 4 mm and 20 mm were subsequently sectioned taking a rectangular coupon from the centre of each. These samples were polished with abrasive papers up to 600 grit. This polishing operation was done to avoid trapping bubbles of evolved hydrogen gas on the surface and to expose the microstructure to the electrolytic medium.

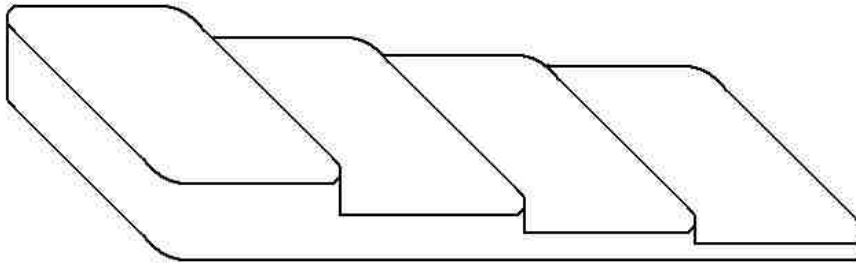


Fig. 5-1 AJ62 permanent mould step casting [13,14].

Table V-I Composition of AJ62 alloy

Alloy	Al	Sr	Mn	Si	Zn	Others
AJ62	6.00	2.82	0.28	0.02	<0.01	<0.002

Once prepared, the samples were assembled into an apparatus for potentiodynamic testing and subjected to polarisation tests one at a time with the first medium: a 0.5 % sodium chloride solution. This polishing and testing was repeated twice for each sample to observe the response to other electrolytes: a 1.0 % sodium chloride solution and a commercial engine coolant. The coolant used was Prestone® antifreeze engine coolant suited for use in any make or model and to be mixed with any other coolant. This product was chosen to represent the commercially available generic engine coolants. The potentiodynamic testing apparatus included a Bio-Logic potentiostat connected to the sample, or working electrode (WE), and two other electrodes suspended in the electrolyte: a counter electrode (CE) placed directly above the sample surface, and a reference electrode (RE) located elsewhere in the electrolyte. A schematic of the set-up has been given in Figure 5-2 [13]. Before beginning each test, the open circuit potential (E_{corr}) was allowed to converge on a single value. The test was executed recording the

current density (i) required to sustain a potential drop (E) ranging from 0.5 V below the E_{corr} to -0.5 V with respect to the RE.

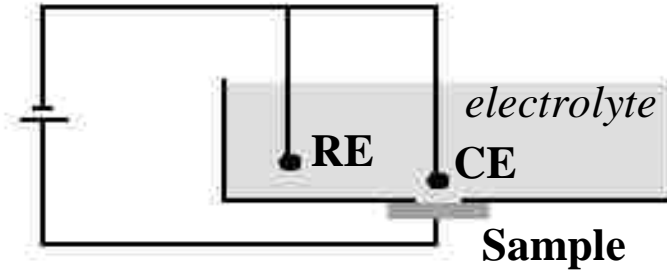


Fig. 5-2 Schematic of potentiodynamic test set-up [13].

Such experimentation has already been completed and documented elsewhere [13,14] but a comparison of the variation in corrosion response to the different media has yet to be made. In the present work, a general understanding and explanation for the varied responses has been developed after presenting the findings of the previous works.

5.3 RESULTS AND DISCUSSION

5.3.1 Microstructural Analysis

Microstructure of the permanent mould cast alloy includes magnesium rich α matrix and the Al_4Sr intermetallic in between the dendrite arms with intracellular aluminum-manganese particles [15,18]. This general microstructure as observed by scanning electron microscopy (SEM) in back-scattered electron (BSE) mode in the 20 mm thick section is presented in Figure 5-3. These alloy constituents have been confirmed by energy dispersive x-ray spectroscopy (EDS) in previous work [18]. The differences in microstructure presented by the 4 mm and 20 mm sections include greater secondary dendrite arm spacing (SDAS), less continuous intermetallic material, and less area percent intermetallic material exhibited in the 20 mm section [13,14,18]. This variation can be observed comparing the micrographs of Figure 5-4. Whereas subsurface

intermetallic continuity has influence during immersion testing [17], the intermetallic continuity, SDAS, and the area percent intermetallic on the corroding surface are of great consequence in potentiodynamic polarisation testing [13,14]. A visual comparison of these values for the two section thicknesses can be made from the graph in Figure 5-5.

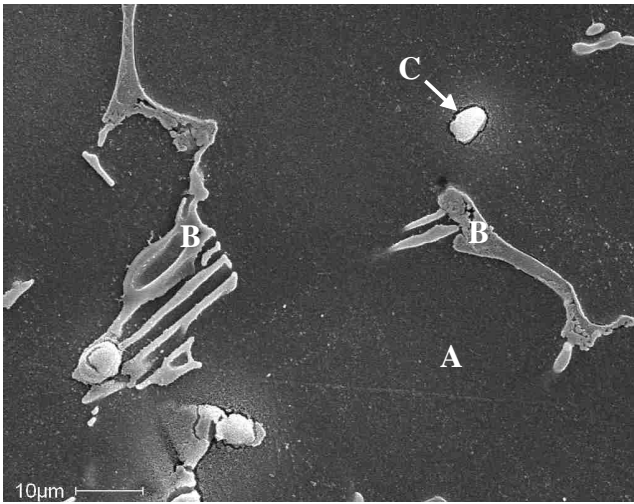


Fig. 5-3 SEM micrograph in BSE mode showing microstructure of the 20 mm section: A, matrix; B, interdendritic eutectic; and C, Al-Mn intermetallic [18].

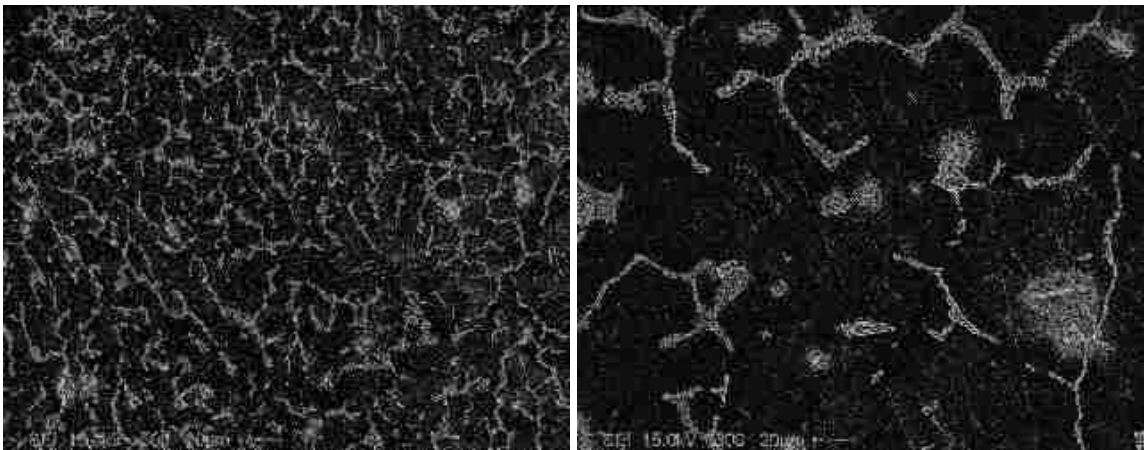


Fig. 5-4 SEM image in BSE mode of the (A) 4 mm and (B) 20mm section [18].

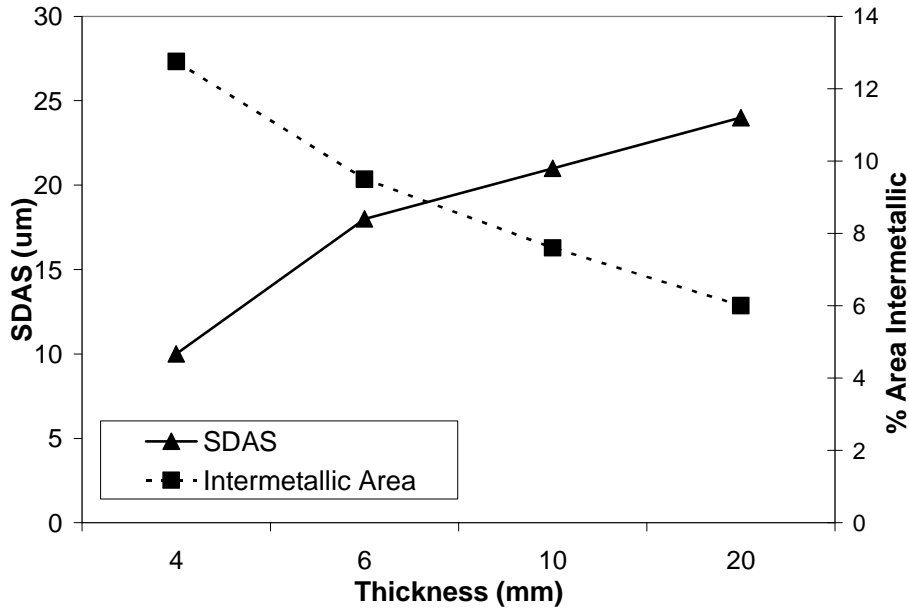


Fig. 5-5 Graph of SDAS and area percent intermetallic.

5.3.2 Response to Salt Solution

Using the 0.5 % and 1.0 % NaCl solutions as the electrolytic media for potentiodynamic testing, the response to polarization of the two microstructures was observed as in Figure 5-6 and Figure 5-7, respectively. Critical values describing these curves have been presented in Tables V-II and V-III. Noteworthy was the dependence of the current density for ion exchange at the open circuit potential. Given a higher concentration of chloride ions, the difference in the current density between the different microstructures became less noticeable albeit on a small scale [13]. This tendency is most likely due to the aggressive rate of corrosion in aqueous salt solution. In increasingly detrimental environments, the small microstructural variations have a lessened effect on the corrosion.

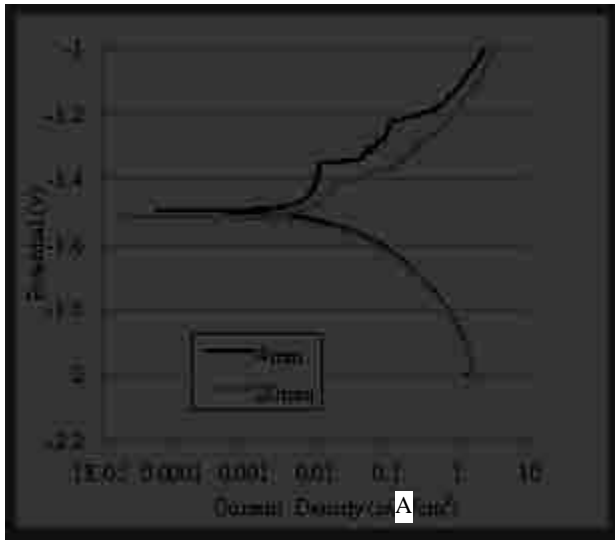


Fig. 5-6 Potentiodynamic polarisation curves in 0.5 % NaCl [13].

Table V-II Critical values pertaining to Figure 5-6

		β_A (V)	β_C (V)	i_{corr} ($\mu\text{A}/\text{cm}^2$)	E_{corr} (V)	R ($\text{k}\Omega \cdot \text{cm}^2$)
0.5 % NaCl	4mm Sample	0.067	0.046	2.254	-1.498	5.23
	20mm Sample	0.066	0.045	3.311	-1.516	3.51

The variation in the current density observed when fewer chlorides are in the electrolytic solution is due to the area percent intermetallic. In general, the area comprised of α matrix is the working surface from which the positively charged ions are preferred to flow. Therefore the thicker section, having a coarser microstructure and less intermetallic area, has a greater working surface area than the thinner casting section for a given area on the specimen surface. Higher chloride concentrations have the effect of reducing the microstructure-influenced difference in current density [15]. This reduction in variation of current is due to the chlorides in solution promoting movement of ions in solution thus facilitating accelerated hydrogen and/or oxide production reactions.

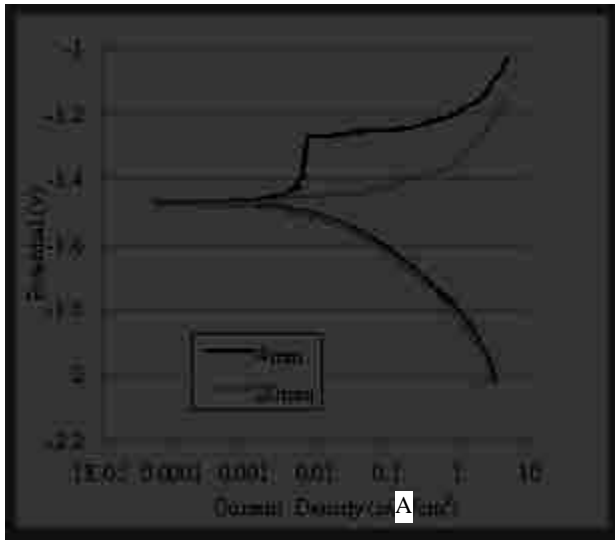


Fig. 5-7 Potentiodynamic polarisation curves in 1.0 % NaCl [13].

Table V-III Critical values pertaining to Figure 5-7

		β_A (V)	β_C (V)	i_{corr} ($\mu\text{A}/\text{cm}^2$)	E_{corr} (V)	R ($\text{k}\Omega \cdot \text{cm}^2$)
1.0 % NaCl	4mm Sample	0.065	0.040	1.342	-1.472	8.01
	20mm Sample	0.065	0.039	1.463	-1.480	7.21

Corrosion potential, E_{corr} , of the two microstructures also became more similar as the percent NaCl of the solution was increased. In the case of magnesium and its alloys this value is often near -1.4 V [13-15] resulting from its extreme anodic behaviour. For the thicker casting section studied, its greater percent area α yields a more electronegative surface as this matrix has a significantly lower corrosion potential than the intermetallic materials. In fact, the corrosion potentials of the α magnesium and $\text{Mg}_{17}\text{Al}_{12}$ intermetallic are -1.3 V and -0.9 V with respect to the standard hydrogen electrode in NaCl solution [19], and clearly show an effect in the 0.5 % NaCl solution. In the 1.0 % NaCl solution, however, this effect is less noticeable. This too was attributed to the severity of the corrosion process as hydrogen production and oxide deposits on the

surface generated more rapidly in the stronger solution may be masking the variation between the fine and coarse microstructures.

Finally, the passivation behaviour of the microstructure was observed. Magnesium is widely accepted as a well passivating metal. It has been documented to have significant corrosion resistance in air that is largely attributed to its passivating behaviour [16]. Expelled magnesium cations, Mg^{2+} , react with hydroxyl anions, $(OH)^-$, remaining from the cathodic hydrogen evolution reaction to form magnesium hydroxide $Mg(OH)_2$ [16]. In aqueous solution, this passive layer of magnesium hydroxide is only stable at high pH [16]. Most common environments for application are not so basic and in NaCl solution, chlorides promote the movement of the charged magnesium ions away from the surface. Thus, it is no surprise that the passive regions existing on the polarisation curves are observably small. Passivation, and the breakdown thereof, are phenomena dependant upon a number of seemingly uncontrollable variables, very local pH being a good example, and are often characterised by a level of unpredictability. A good demonstration of this is the near immediate breakdown of passivation observed with the 20 mm sample in the 1.0 % NaCl solution.

5.3.3 Response to Engine Coolant

The response of an alloy to engine coolant is a far more complex concept than the response to NaCl solution. This complexity is not only because engine coolants contain between 30 and 70 % ethylene glycol to avoid freezing in cold climates, but because many inhibitors are also present [20]. The chemical additions used, and number of them, also vary from one coolant producer to another and are not information readily disclosed. Polarisation curves generated by the aforementioned methodology for AJ62 in a

commercial engine coolant are presented in Figure 5-8. Accompanying values that characterise the curves are given in Table V-IV. Continuing with the theme proven in research, using NaCl solutions that lower chloride concentrations accentuated the differences between the varied microstructures, the three most easily noted characteristics of the polarisation curve were examined: current density, electrochemical potential, passivation, and corrosion resistance.

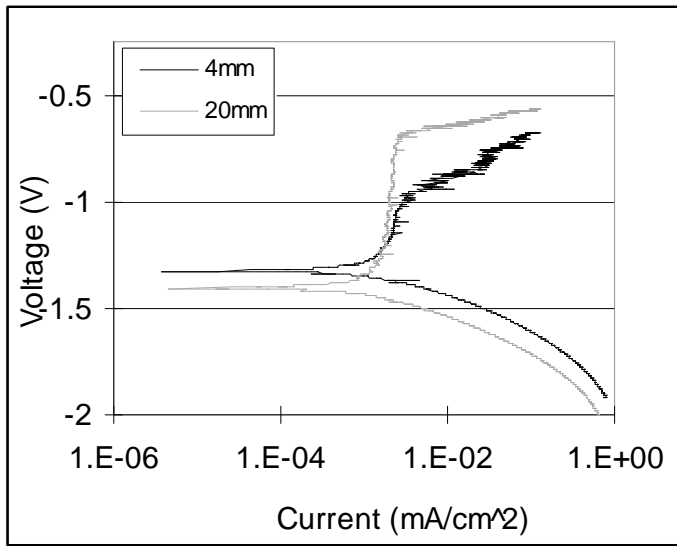


Fig. 5-8 Potentiodynamic polarisation curves in coolant [14].

Table V-IV Critical values pertaining to Figure 5-8 from [14]

Specimen	i_{corr} (mA/cm ²)	E_{corr} (V)	β_A (V)	β_C (V)	R (kΩ•cm ²)
4mm	0.199	-1.329	56.7	37.2	49.0
20mm	0.213	-1.409	76.7	36.1	50.0

Current density for ion exchange at E_{corr} , representative of the physical corrosion rate, is far lower than the values observed in NaCl solution. Anodic inhibitors in the engine coolant are primarily responsible for this behaviour [21]. Blocking the movement of ions from the surface [20,21], these chemical additions clearly do their job. With a lowered chloride concentration, the expectation is to see a large difference in the current

density between the fine and coarse microstructures. This variation, however, is less noticeable than that observed in the salt solutions, which is counterintuitive. Again this behaviour is due to the inhibitors present in the coolant. Since the mechanism by which they afford protection of the alloy is to stop anodic behaviour at the anodic surface, the area of that surface becomes irrelevant if the concentration of inhibitors is sufficient. Therefore the variation in current density cannot be attributed as was previously to the difference in percent area α magnesium.

E_{corr} values are changed very little in the engine coolant as it appears in the same range near -1.4 V [14]. What has changed is the variation between the E_{corr} for the fine and coarse microstructures. Inhibitors, as they were described above, stop flow of ions but do not change the electrochemical potential of the metal they are protecting. In the engine coolant, without the oxides forming as in water or salt solution, the true effect of α area versus intermetallic area is clearly seen. Having a surface heavily populated with the anodic metal clearly influences the E_{corr} and this influence is not masked by severe corrosion in the case of engine coolant.

Lastly, the relevant discussion must include the passivation behaviour in the engine coolant. As well as containing additions to stop ion migration away from the surface, additions in engineered engine coolants are clearly used to promote passive behaviour. This passivation can be seen above the E_{corr} on the curves in Figure 5-9 where the passive regions are appreciably larger than those seen using the NaCl solutions. Characterizing these regions is a “jagged” appearance especially noticeable well above the E_{corr} . This may be a result of a pitting corrosion response to the polarisation or non-uniform development of the passive film that can lead to a transfer of anodic behaviour

from one region to another. The latter hypothesis is based on a potentially detrimental effect similar to the micro-galvanic effect that has been documented [16]. If local variations in the passive film can induce a pseudo micro-galvanic effect, its effects are likely seen in the response to polarisation as well. Whatever the cause of this passive region characteristic, its mechanism most likely operates in a localised manner. Ignoring the “jagged” appearance of the passive region, it is clear that the passivation is more prominent in the thicker section with coarser microstructure. Passivation occurs on the active anode. Since the anodic area is larger for the coarser microstructure, passivation is achievable on a greater area for the 20 mm casting section.

5.4 CONCLUSIONS AND RECOMMENDATIONS

This industrially relevant work suggests the metallurgical concepts that may have an effect on the corrosion resistance of future PM AJ62 components. It has been clearly presented that finer microstructures have a significant advantage over their coarser counterparts in terms of corrosion. This advantage includes reduced current density for ion exchange as well as less negative open circuit potentials.

For exposure to environments where the electrolytic medium is uncontrolled, *i.e.*, external vehicular applications, developing a finer microstructure via thin sections, greater cooling rates, or some thermal treatment would be beneficial. These efforts are, however, undermined should the corrosive environment include a significant chloride concentration. Therefore, the resources required in developing a desirable microstructure should be weighed against the achievable corrosion resistance. Other methods of corrosion resistance might include coating technologies for such applications. Depending on the type of coating, microstructure of the substrate may influence the performance of

the coating. Thus in most circumstances some attempt to generate a fine microstructure should be made for application in uncontrolled environments.

In a controlled environment where the corrosive medium is a commercial engine coolant, chloride concentrations are low but anodic inhibitors make metallurgical considerations unappreciable in terms of ion exchange current. So the other two considerations are left: corrosion potential and polarization. Achieving a fine structure reduces the galvanic driving forces significantly with respect to the coarser microstructure. If there is a cathodic surface in the coolant that lends to severe galvanic corrosion a finer microstructure becomes more desirable. Meanwhile, the coarser microstructure passivating more easily with the help of the chemical additions in the coolant is desirable as well. But, it should be remembered, though, that passivation could lead to unexpected results in local, small, trapped volumes of electrolyte. This liability and the galvanic considerations ultimately lead to the recommendation of some effort in reducing SDAS for components exposed to coolant as well.

5.5 REFERENCES

- [1] Raynor, G.V., The physical metallurgy of magnesium and its alloys. Pergamon Press. GB. 1959.
- [2] Hu, H., Yu, A., Li, N., Allison, J.E., Potential magnesium alloys for high temperature die cast automotive applications: a review. *Materials and Manufacturing Processes*. 18 5 (2003) 687-717.
- [3] Baril, E., Labelle, P., Pekguleryuz, M.O., Elevated temperature Mg-Al-Sr: creep resistance, mechanical properties, and microstructure. *Journal of Materials*. 55 11 (2003) 34-39.
- [4] Kunst, M., Fischersworing-Bunk, A., L'Esperance, G., Plamondon, P., Glatzel, U., Microstructure and dislocation analysis after creep deformation of die cast Mg-Al-Sr (AJ) alloy. *Materials Science and Engineering A*. 510-511 (2009) 387-392.

- [5] Luo, A.A., Powell, B.R., Tensile and compressive creep of magnesium-aluminum-calcium based alloys. *Magnesium Technology 2001*. The Minerals, Metals, and Materials Society. (2001) 137-144.
- [6] Dargusch, M.S., Dunlop, G.L., Pettersen, K., Elevated temperature creep and microstructure of die cast Mg-Al alloys. *Magnesium Alloys and Their Applications*. Werkstoff-Informationsgesellschaft mbH. (1998) 283-288.
- [7] Jing, B., Yangshan, S., Shan, X., Feng, X., Tianbai, Z., Microstructure and tensile creep behavior of Mg-4Al based magnesium alloys with alkaline-earth elements Sr and Ca additions. *Materials Science and Engineering A*. 419 (2006) 181-188.
- [8] Pekguleryuz, M.O., Kaya, A.A., Creep resistant magnesium alloys for powertrain applications. *Advanced Engineering Materials*, 5 12 (2003) 866-878.
- [9] Lumley, R.N., O'Donnell, R.G., Gunasegaram, D.R., Givord, M., New heat treatment for Al high pressure die castings. *Heat Treating Progress*. (2006) 31-37.
- [10] Dahle, A.K., Sannes, S., St. John, D.H., Westengen, H., Formation of defect bands in high pressure die cast magnesium alloys. *Journal of Light Metals*. 1 (2001) 99-103.
- [11] Weiler, J.P., Wood, J.T., Klassen, R.J., Berkmortel, R., Wang, G., Variability of skin thickness in an AM60B magnesium alloy die-casting. *Materials Science and Engineering A*. 419 (2006) 297-305.
- [12] Yang, K., Nagesekhar, A.V., Caceres, C.H., Section thickness and the skin effect in a high pressure die cast Mg-12% Al alloy. *Magnesium Technology 2010*, The Minerals, Metals, and Materials Society. (2010) 391-394.
- [13] Burns, J.R., Hu, H., Nie, X., Su, J.F., Corrosion of permanent mould cast Mg alloy AJ62 in NaCl solutions. *American Foundry Society*. (2010) Paper No. 10-022.
- [14] Burns, J.R., Hu, H., Nie, X., Han, L., Microstructure influence on the corrosion of permanent mould cast magnesium alloy AJ62 in engine coolant. *Society of Automotive Engineers*. (2010) Paper No. 2010-01-0412.
- [15] Han, L., Nie, X., Hu, H., Zhang, Q., Influence of electrolytic plasma oxidation coating on tensile behaviour of die-cast AM50 alloy subjected to salt corrosion. *International Journal of Modern Physics B*. 23 6-7 (2009) 960-965.
- [16] Makar, G.L., Kruger, J., Corrosion of magnesium. *International Materials Reviews*. 38 2 (1993) 138-153.
- [17] Song, G., Atrens, A., Understanding magnesium corrosion a framework for improved alloy performance. *Advanced Engineering Materials*. 5 12 (2003) 837-858.

- [18] Burns, J.R., Han, L., Hu, H., Nie, X., Effects of section thicknesses on tensile properties of permanent mould cast magnesium alloy AJ62. *Magnesium Technology 2010*, The Minerals, Metals, and Materials Society. (2010) 367-371.
- [19] Joensson, M., Thierry, D., LeBozec, N., The influence of microstructure on the corrosion behaviour of AZ91D studied by scanning Kelvin probe force microscopy and scanning Kelvin probe. *Corrosion Science*. 48 (2006) 1193–1208.
- [20] Song, G., StJohn, D., Corrosion behaviour of magnesium in ethylene glycol. *Corrosion Science*. 46 (2004) 1381-1399.
- [21] Revie, R.W., Uhlig, H.H., *Corrosion and corrosion control*. John Wiley and Sons. USA. 2008.

CHAPTER 6

INFLUENCE OF CORROSION ON MECHANICAL PROPERTIES OF PERMANENT MOULD CAST AJ62

6.1 INTRODUCTION

In the transport industries, especially the automotive sector, there are great demands for both better fuel efficiency and lower emissions [1]. In an effort to meet such demands, manufacturers are turning to new lightweight alloys. Magnesium is among the most desirable base metals for modern alloys particularly because of its low density of 1.74 g/cm³ [1,2]. Such a low density translates to a high strength-to-weight ratio, which is a common criterion in component design [2]. To apply magnesium based alloys in automobile design, a number of issues must be addressed. These include magnesium's poor elevated temperature mechanical performance, poor corrosion resistance, and poor wear characteristics that all plague its alloys [1,3-14]. One alloy, AJ62, has become the centre of much academic and industrial focus due to its high temperature stable intermetallic phases and good castability [3-6].

The previous studies on permanent mould (PM) cast AJ62 [10,11,15] show that its microstructure consists of α -Mg dendritic cells, an Al₄Sr intermetallic compound in the interdendritic regions, and aluminum-manganese particles. However, the section thickness can yield a significant microstructural variation as in Table VI-I. This variation is expected since metallurgical principles dictate that dendritic growth relates to the cooling rate, or solidification time [16-20]. The two quantitative measurements that highlight the microstructural variation of four section thicknesses (4, 6, 10, and 20 mm) [10,11,15,21] are secondary dendrite arm spacing (SDAS) and percentage of intermetallic area. The increase in microstructural coarseness and decrease in intermetallic area that

result from slow solidification as section thicknesses increase are accompanied by an observable degradation of intermetallic continuity [10,11,15].

Table VI-I Microstructural characteristics of various section thicknesses

Thickness (mm)	4	6	10	20
SDAS (μm)	10	18	21	24
Intermetallic Area (%)	12.75	9.50	7.60	6.00

The mechanical and corrosion response of the alloy both depend on microstructure as examined in the previous literature [10,11,15]. In both cases, a finer microstructure that was yielded by high cooling rates of the thin PM cast sections was preferable in terms of overall performance [10,11,15]. Industrial application of a PM AJ62 material would likely pose mechanical and corrosion requirements on the alloy not just independently but also in combination. Hence, the current research attempts to relate the cast microstructures to the mechanical engineering performance of as-cast PM AJ62 alloy subject to corrosion, and determine the compounding effect of corrosion-degraded and solidification-dictated microstructure on tensile properties of the alloy.

6.2 EXPERIMENTAL METHOD

6.2.1 Determination of Corrosion Parameters

To highlight any compounding effects as desired in this study, a two-step test procedure was followed by observation. Tensile specimens extracted from permanent mould castings [15] were to be corroded to generate small pits acting as stress intensifiers and effective area reduction during tensile loading in the second step. To understand the level of corrosion the specimens might encounter, rectangular samples of the poorest performing coarse microstructure were corroded by immersion and observed. Corrosion media in previous studies included 0.5 % NaCl [10], 1.0 % NaCl [10], and engine coolant

[11]. Observed corrosion in engine coolant had shown that the chemical inhibitors successfully arrest the movement of Mg^{2+} ions from the alloy surface [21]. Therefore, attention was turned to the NaCl solutions which promote much more aggressive attack. While variation in corrosion response is more notable in the weaker, 0.5 %, NaCl solution during potentiodynamic testing [10], such a weak solution digresses from the likely operational environments of exposed structural automotive components. In addition, the 1.0 % NaCl solution was chosen as it would expedite the initial step of testing. Thus four samples from AJ62 cast into a 20 mm section were immersed in 1.0 % NaCl solution for 1, 2, 3, and 4 days at room temperature.

The sample that experienced the worst corrosion, 4 days, was sectioned for subsurface observation and quantification of penetration depth. After mounting and rough grinding through 400 grit silicon carbide, the sample was observed using light microscopy. A resulting micrograph is given in Figure 6-1. Shown in this image is a general dissolution of surface grains, which leads to defects approximately 25 μm in depth congruent with the alloy's microstructure. There is also a larger pit formed by localised corrosion appearing to penetrate to a depth of approximately 250 μm . These surface defects are likely to generate some stress concentration effect but not excessively reduce the cross section of a 4 mm section. Therefore, this concentration and duration, 1.0 % and 4 days respectively, were chosen for the subsequent testing.

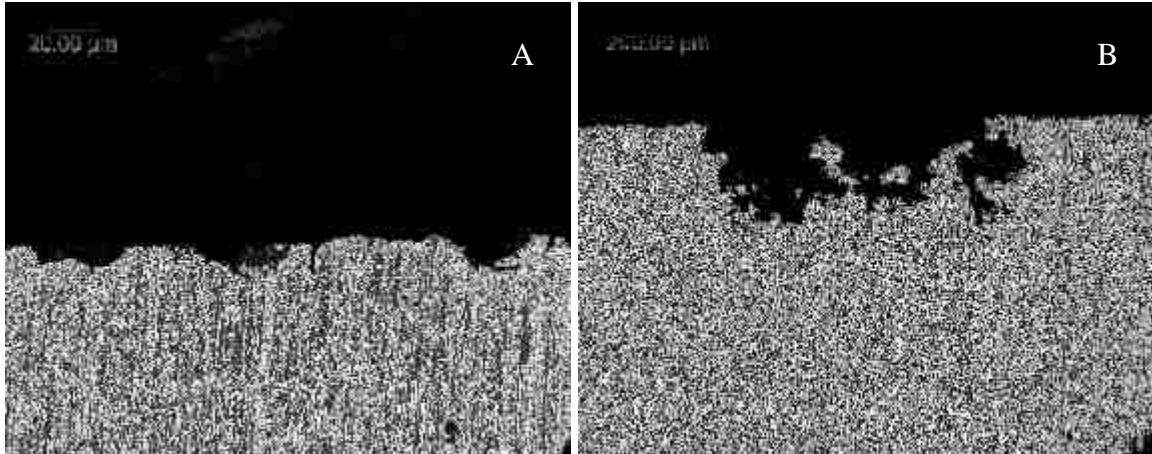


Fig. 6-1 Corroded sample showing depths of penetration from (A) general corrosion and (B) localised corrosion.

6.2.2 Corrosion of Tensile Specimens

Specimens subjected to this testing were sub-size specimens according to ASTM standards extracted from cast thicknesses of 4, 6, 10, and 20 mm. Once machined from the castings, the specimens were polished with papers up to 400 grit to avoid machining marks and any other initial defects. After preparation, each specimen was immersed in 1.0 % NaCl solution. They were placed in separate containers and suspended in the medium to avoid preferential corrosion of surfaces. An ample amount of water, 1 L, was used to avoid effects of pH increase due to corrosion products. The solution used for corrosion was mixed together prior to dividing it into the individual containers to ensure a for each specimen a level of control on the corrosion parameters, *e.g.*, initial pH, temperature, unavoidable impurities.

H₂ evolution begins shortly after the specimens are submerged and continues for the 4 day duration of the test. After removing the specimens from the solution, it is clearly seen that the level of corrosion on the thicker specimens is clearly seen to be similar to that observed previously when determining the corrosion parameters. After

removal from the solution, the specimens were each rinsed with distilled water and dried to halt further progression of the corrosion reactions. They were then marked and measured for the second step of testing.

6.2.3 Tensile Response After Corrosion

The tensile specimens were pulled in tension within 1 hour after being extracted from the solution. An Instron universal tensile testing machine elongated the specimens at a rate of 0.5 mm/min with a data sampling rate of 10 Hz. An extensometer and built-in load cell were employed to monitor the applied force and displacement. Data acquisition yielded the force-displacement curves, from which the engineering stress strain curves were measured.

Once fractured, a representative specimen was chosen from each thickness to provide SEM fractographs. Using these observations and calculations based on the earlier corrosion samples, conclusions were made on the dominant weakening effect of the corrosion process observed by comparing the stress-strain data to that of uncorroded specimens.

6.3 RESULTS AND DISCUSSION

6.3.1 Stress Versus Strain

Engineering stress and strain resulting from the tensile testing can be observed in Figure 6-2. Characteristic values for these curves are presented in Table VI-II. These curves can be compared to those of uncorroded specimens, in Figure 6-3 and Table VI-III from [15]. Elastic modulus, E , which is dictated by the constituent phases and their distribution, has not changed during corrosion. While yield strength, YS , is also dictated by constituent phases, the YS as calculated from a tensile test is understated if large voids

are present. There does not seem to be a significant difference in the yield strengths of the corroded and uncorroded materials.

Elongation, E_f , of 20 mm specimens decreased after corrosion, while elongation and ultimate tensile strength, UTS, of the specimens with finer microstructure remains unchanged. Given the sample size, and scatter in UTS representative of cast metals, conclusions cannot be drawn from the observed changes for corroded thinner sections. The sample size and scatter explains the small increase in elongation suggested for the 6 mm sections. The variation of the thicker sections from uncorroded to corroded, however, is substantial and should be noted. Such degradation suggests that corrosion has affected the mechanical strength. In order to understand the fracture of the specimen and the interaction of corrosion with the fracture mechanism, SEM fractographs were generated.

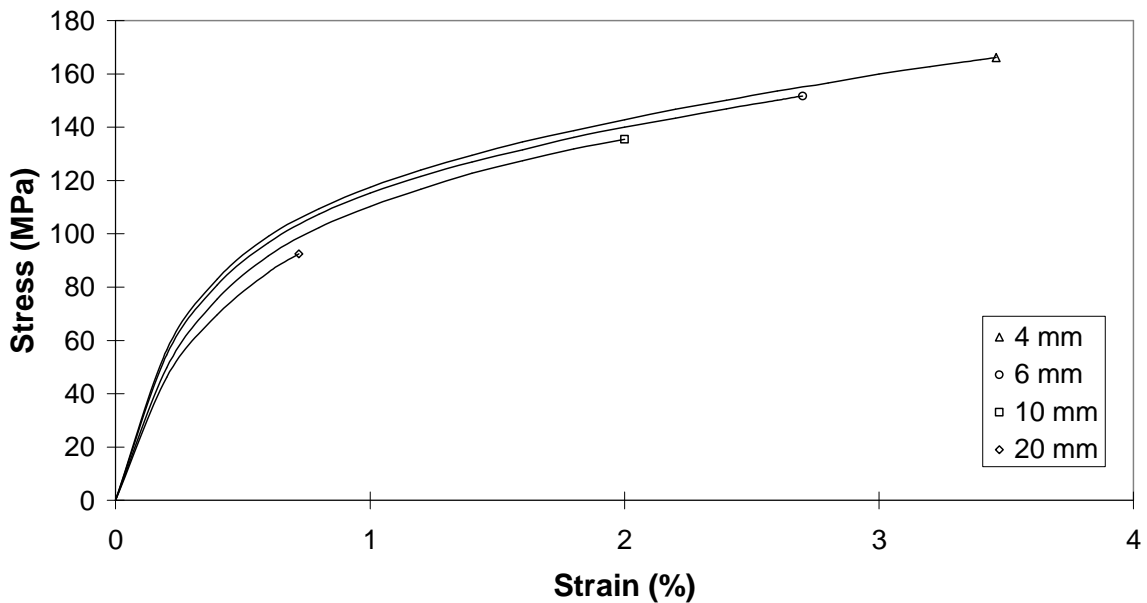


Fig. 6-2 Engineering stress-strain for corroded PM AJ62 thicknesses.

Table VI-II Characteristic stress-strain values for corroded PM AJ62 microstructures

Thickness (mm)	E (GPa)	YS (MPa)	UTS (MPa)	E _f (%)
4	35.9 ±0.7	88.2 ±1.4	168.5 ±2.4	3.64 ±0.19
6	34.3 ±1.5	87.1 ±2.1	155.4 ±8.8	3.00 ±0.33
10	30.5 ±1.1	84.1 ±0.3	139.0 ±6.8	2.21 ±0.17
20	28.4 ±0.6	79.8 ±1.8	98.51 ±7.8	0.89 ±0.19

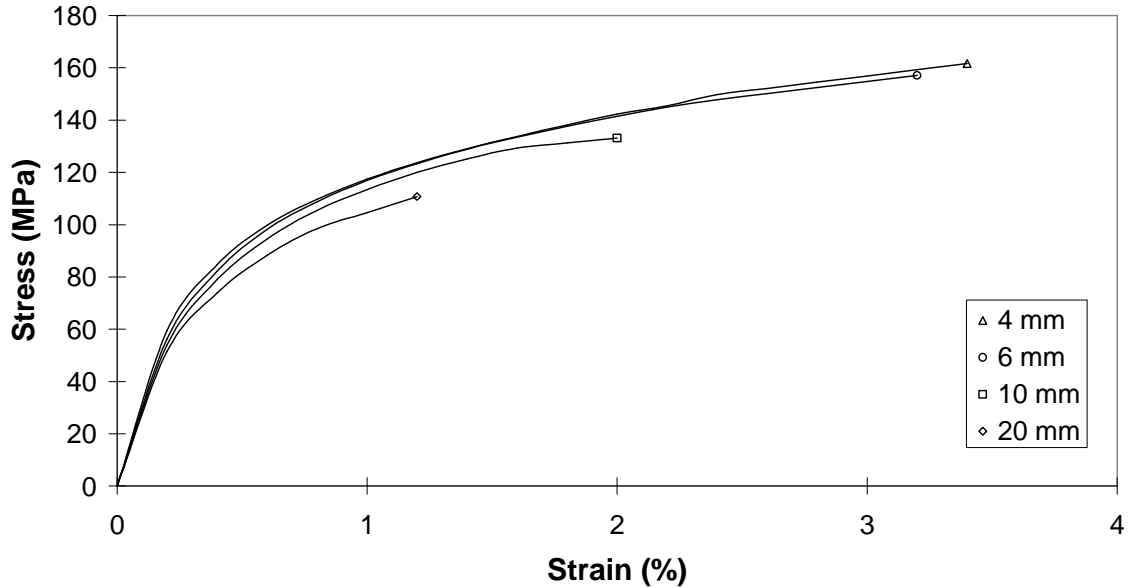


Fig. 6-3 Engineering stress-strain curves of uncorroded PM AJ62 [15].

Table VI-III Characteristic stress-strain values for uncorroded PM AJ62 microstructures [15]

Thickness (mm)	E (GPa)	YS (MPa)	UTS (MPa)	E _f (%)
4	38.7 ±2.3	93.1 ±2.0	153.6 ±9.4	2.71 ±0.50
6	35.8 ±6.4	91.0 ±2.0	153.2 ±8.1	2.84 ±0.33
10	34.3 ±8.0	87.7 ±1.1	131.2 ±2.7	1.79 ±0.14
20	33.3 ±6.3	81.8 ±1.2	123.9 ±3.3	1.99 ±0.23

6.3.2 Fractography

In general, examination of thinner specimens with finer microstructure showed no apparent anomalies to indicate pre-existing voids or corrosion penetration into the specimens. In contrast, the thicker sections showed two types of discontinuous fracture

surface. On the interior of the thicker casting section, shrinkage type voids with indicative dendritic surfaces as in Figure 6-4 were observed.

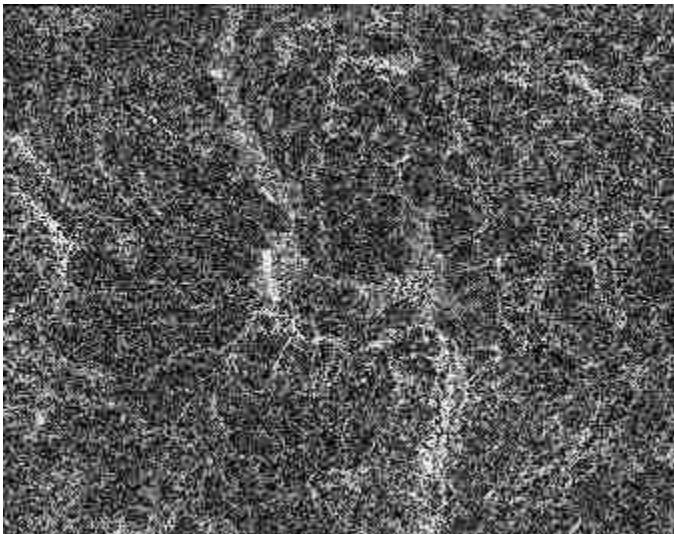


Fig. 6-4 SEM micrograph of characteristic shrinkage void in thick sections showing dendrites.

Other locations show potential corrosion penetration interacting with specimen fracture. On the fracture surface of a 20 mm section, development of oxides in a uniquely shaped void was observed. These oxides are shown in Figure 6-5. The brightly energised crystalline formations on the wall of the observed void indicate the presence of an oxide. While metal oxides do present themselves within the cast material, the oxides shown in Figure 6-5 suggest a corrosion product that did not exist prior to the corrosion step. Therefore, it is likely that a subsurface discontinuity was somehow affected by the corrosion process.

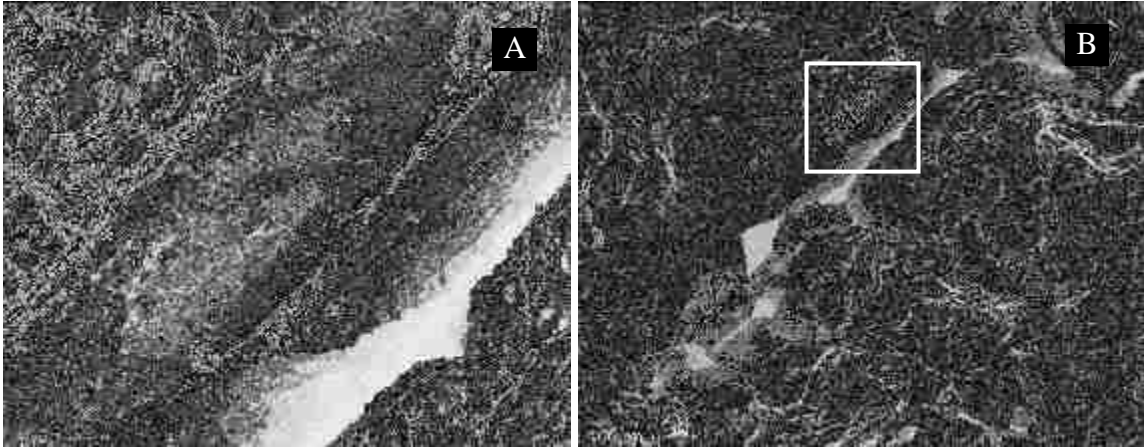


Fig. 6-5 SEM fractograph showing oxides in an opened discontinuity at (A) 500 x and (B) 100 x.

6.3.3 Calculations

Pitting that occurs as a result of general corrosion can have one of two influences on the UTS. If the pit geometry resembles a semicircular flaw, it can lead to a stress intensification at the surface making a tensile specimen fail at a lower UTS than expected. Stress intensification is described by Equation 6-1 where K is the intensity factor to be compared with fracture toughness, S is the applied stress, a is the length of the crack, and F is a geometry factor given by Equations 6-2 through 6-4 for the geometry of interest [22]. To calculate the geometry factor, a is again the crack length and t is the thickness of the specimen, and b is the distance of the crack centre from the edge of the specimen.

$$K = FS\sqrt{\pi a} \quad \text{Eqn. 6-1}$$

$$F = f_a f_w \frac{2}{\pi} \quad \text{Eqn. 6-2}$$

$$f_a = \left(1.04 + 0.2017 \left(\frac{a}{t} \right)^2 - 0.1061 \left(\frac{a}{t} \right)^4 \right) \left(1.1 + 0.35 \left(\frac{a}{t} \right)^2 \right) \quad \text{Eqn. 6-3}$$

$$f_w = \sqrt{\sec \left(\frac{\pi a}{2b} \sqrt{\frac{a}{t}} \right)} \quad \text{Eqn. 6-4}$$

Combating this concept, if the pit is large enough, the reduction in area would mean that the engineering stress calculated for a tensile test is slightly lower than the actual stress being sustained by the material. To gauge this reduction in area effect, Equation 6-5 can be used for calculation of the actual stress. The actual area can be calculated as in Equation 6-6.

$$S_{actual} = S \cdot \frac{A}{A_{actual}} \quad \text{Eqn. 6-5}$$

$$A_{actual} = A - N \frac{\pi a^2}{2} \quad \text{Eqn. 6-6}$$

where S_{actual} is the actual stress, S is the stress according to the stress strain curve, A is the nominal area, A_{actual} is the actual area, a is crack length, *i.e.*, penetration depth, and N is the number of pits.

Calculating the stress intensification and reduced area using the highest observed stress in the 20 mm specimens of ~110 MPa, the largest observed pit dimension of 250 μm , and assuming there are about 10 pits around the circumference, intensified stress yields just $K=2.24 \text{ MPa}\cdot\text{m}^{0.5}$ and reduced area only yields $S_{actual} = 111 \text{ MPa}$. A full account of these calculations can be found in Appendix A. According to previous research [23], a similar alloy containing 10.7 % by weight Al and 0.13 % by weight Mn, has a fracture toughness of $\sim 9 \text{ MPa}\cdot\text{m}^{0.5}$. This fracture toughness is expected to be a higher value than that of the machined PM AJ62 due to the presence of a densified squeeze cast microstructure in the Mg-10.7 wt.% Al alloy. Nonetheless, since the calculated intensity factor and actual stress of the reduced area is quite low, the reason for premature failure of the corroded specimen cannot be attributed to either theory for

corrosion effect. This logic fails to explain the variation in UTS from uncorroded to corroded.

However, shrinkage porosity and other pre-existing inherent casting defects that are more abundant in the thicker sections can be larger than 250 μm , potentially up to 1mm as seen in Figures 6-4 and 6-5, and do not result from the corrosion process. Figure 6-5 shows an internal void or discontinuity that has begun to develop an oxide layer. This may indicate that the corrosion pitting on the side of the specimen penetrated deep enough to interact with a discontinuity in the thick cast section or that corrosion penetration is deeper than previously measured. Thereby, a large surface defect or crack is generated where $a=1.25$ mm and $K=4.84$ $\text{MPa}\cdot\text{m}^{0.5}$. Although this value has been determined making the assumption that the flaw is semicircular and it is still marginally lower than 9 $\text{MPa}\cdot\text{m}^{0.5}$. As such, the possibility remains for a drastic increase in stress intensity factor with compound flaws, *i.e.*, combined corrosion and casting induced defects, remains. This intensification could result in premature failure of the brittle material and can be worse if there are multiple corrosion induced imperfections.

6.4 CONCLUSIONS

Samples were successfully corroded and parameters were chosen for the corrosion portion of the combined corrosion and mechanical response evaluation. The chosen sample showed pits having up to 250 μm radii. Specimens were then corroded and subsequently measured and pulled. Engineering stress-strain curves demonstrated that corrosion of specimens leads to a marked reduction in achievable elongation. Two theories based on widely accepted concepts, stress intensification and area reduction, do not necessarily explain the premature failure of the corroded specimens without

consideration of pre-existing sub-surface defects apparent on the fracture surface. Oxides forming in what appears to be an opened casting defect indicate that premature failure of corroded thick sections may be three-fold. Thick sections in PM AJ62 (i) fail in a brittle manner, (ii) have more large internal defects inherent to the processing, and (iii) suffer greater corrosion because of their microstructure. All of these conditions together allow for crack initiation by way of internal void and corrosion pit interaction. This interaction is unique to the combination of casting parameters, corrosion parameters, and alloy used in this study. A fine microstructure is therefore recommended for PM AJ62 regardless whether service life requires resistance to mechanical loading, corrosion, or a combination thereof.

6.5 REFERENCES

- [1] Hu, H., Yu, A., Li, N., Allison, J.E., Potential magnesium alloys for high temperature die cast automotive applications: a review. *Materials and Manufacturing Processes*. 18 5 (2003) 687-717.
- [2] Raynor, G.V., *The physical metallurgy of magnesium and its alloys*. Pergamon Press. GB. 1959.
- [3] Baril, E., Labelle, P., Pekguleryuz, M.O., Elevated temperature Mg-Al-Sr: creep resistance, mechanical properties, and microstructure. *Journal of Materials*. 55 11 (2003) 34-39.
- [4] Kunst, M., Fischersworing-Bunk, A., L'Esperance, G., Plamondon, P., Glatzel, U., Microstructure and dislocation analysis after creep deformation of die cast Mg-Al-Sr (AJ) alloy. *Materials Science and Engineering A*. 510-511 (2009) 387-392.
- [5] Luo, A.A., Powell, B.R., Tensile and compressive creep of magnesium-aluminum-calcium based alloys. *Magnesium Technology 2001*. The Minerals, Metals, and Materials Society. (2001) 137-144.
- [6] Dargusch, M.S., Dunlop, G.L., Pettersen, K., Elevated temperature creep and microstructure of die cast Mg-Al alloys. *Magnesium Alloys and Their Applications*. Werkstoff-Informationsgesellschaft mbH. (1998) 283-288.

- [7] Jing, B., Yangshan, S., Shan, X., Feng, X., Tianbai, Z., Microstructure and tensile creep behavior of Mg-4Al based magnesium alloys with alkaline-earth elements Sr and Ca additions. *Materials Science and Engineering A*. 419 (2006) 181-188.
- [8] Pekguleryuz, M.O., Kaya, A.A., Creep resistant magnesium alloys for powertrain applications. *Advanced Engineering Materials*, 5 12 (2003) 866-878.
- [9] Joensson, M., Thierry, D., LeBozec, N., The influence of microstructure on the corrosion behaviour of AZ91D studied by scanning Kelvin probe force microscopy and scanning Kelvin probe. *Corrosion Science*. 48 (2006) 1193–1208.
- [10] Burns, J.R., Hu, H., Nie, X., Su, J.F., Corrosion of permanent mould cast Mg alloy AJ62 in NaCl solutions. *American Foundry Society*. (2010) Paper No. 10-022.
- [11] Burns, J.R., Hu, H., Nie, X., Han, L., Microstructure influence on the corrosion of permanent mould cast magnesium alloy AJ62 in engine coolant. *Society of Automotive Engineers*. (2010) Paper No. 2010-01-0412.
- [12] Makar, G.L., Kruger, J., Corrosion of magnesium. *International Materials Reviews*. 38 2 (1993) 138-153.
- [13] Han, L., Nie, X., Hu, H., Zhang, Q. Influence of electrolytic plasma oxidation coating on tensile behaviour of die-cast AM50 alloy subjected to salt corrosion. *International Journal of Modern Physics B*. 23 6-7 (2009) 960-965.
- [14] Song, G., Atrens, A., Understanding magnesium corrosion a framework for improved alloy performance. *Advanced Engineering Materials*. 5 12 (2003) 837-858.
- [15] Burns, J.R., Han, L., Hu, H., Nie, X., Effects of section thicknesses on tensile properties of permanent mould cast magnesium alloy AJ62. *Magnesium Technology 2010, The Minerals, Metals, and Materials Society*. (2010) 367-371.
- [16] Han, L., Burns, J.R., Sun, Z., Hu, H., Unpublished work. *University of Windsor*. (2009).
- [17] Flemings, M.C., *Solidification Processing*. McGraw Hill. USA. 1974.
- [18] Halder, E., Exner, H.E., Coarsening of secondary dendrite arms in a temperature gradient. *Acta Metallurgica*. 36 7 (1988) 1665-1668.
- [19] Kattamis, T.Z., Holmberg, U.T., Flemings, M.C. Influence of coarsening on dendrite arm spacing and grain size of magnesium-zinc alloy. *Journal of the Institute of Metals*. 95 (1967) 343-347.
- [20] Kasprzak, W., Sokolowski, J.H., Sahoo, M., Dobrzanski, L.A., Thermal characteristics of the AM50 magnesium alloy. *Journal of Achievements in Materials and Manufacturing Engineering*. 29 2 (2008) 179-182.

- [21] Burns, J.R., Previously unpublished work from Chapter 5. University of Windsor. (2010)
- [22] Dowling, N.E., Mechanical behaviour of materials: engineering methods for deformation, fracture, and fatigue, 3rd Ed. Pearson Education, Inc. New Jersey, USA. 2007.
- [23] Jayalakshmi, S., Kailas, S.V., Seshan, S., Kim, K.B., Fleury, E., Tensile strength and fracture toughness of two magnesium matrix composites. *Journal of Ceramic Processing Research*. 7 3 (2006) 261-265.

CHAPTER 7

CONCLUSIONS

7.1 REVIEW OF OBJECTIVES

As it was stated in Chapter 1, the main objective of this thesis was to evaluate and determine mechanical and electrochemical properties of PM cast AJ62 independently, and correlate them to microstructure development that takes place during solidification. In the preceding chapters, experimental results were discussed for PM cast AJ62 in the following areas: microstructure influence on mechanical properties; corrosion of solidified microstructures in NaCl solution; effects of microstructure on corrosion in engine coolant; effect of inhibitor and chloride concentration in an electrolyte; and mechanical properties of corroded microstructures.

7.2 SUMMARY OF OBSERVED RESULTS

The results presented in the previous chapters successfully highlight the effect of various solidified PM cast AJ62 microstructures in the context of mechanical and corrosion properties. This chapter will summarise that work by revisiting the key points from each chapter.

7.2.1 Mechanical Properties of Solidified AJ62 [1]

The characteristics of the permanent mould cast AJ62 microstructure prominently affected by casting section thickness include coarseness, cell boundary continuity, and distribution of intermetallics.

In terms of constituent phases, the microstructure of the permanent mould cast AJ62 alloy does not vary from that observed for other casting processes: α -Mg makes up

the matrix; eutectic Al_4Sr appears at the cell boundaries; and globule Al-Mn particles are common within the matrix.

The section thickness plays a large role in the mechanical performance of permanent mould cast AJ62. Most notable is the reduction by over 30 % in elongation from 4 mm thicknesses to 20 mm.

The well-noted transition from ductile to brittle fracture among specimens of increasing casting thickness can be attributed to the cell size and intermetallic distribution.

7.2.2 Corrosion of Solidified AJ62 in NaCl Solutions [2]

The finer microstructure of the 4 mm section had good intermetallic continuity for providing a barrier to corrosion. Reduction in cathodic sites on the order of 50 % could limit the micro-galvanic effect of the 20 mm section.

Results generated with the use of weaker NaCl solutions support existing theories that suggest a finer microstructure is more desirable to resist corrosion. However, little variation in the microstructure response to polarization can be observed. This variation also becomes significantly smaller with increased chloride concentration.

Unstable passivation response to anodic polarization deteriorates significantly with increased chloride concentration for the coarser microstructure.

A buildup of corrosion products on the tested surface is visible with an unaided eye. These deposits most likely consist of Mg and O, while traces of other elements are possible.

The corrosion morphology shows preferential corrosion of α grains when viewing normal to the surface. This is more evident for the coarser microstructure since the finer microstructure corroded via a surface preparation influenced pattern.

Replacement of α cells with corrosion product deposits can be observed below the corroded surface and suggests preferential dissolution and boundary spalling as the likely mechanisms of mass loss.

The recommendations that have been made are to develop: a better understanding of the PM cast AJ62 elevated temperature mechanical performance, and an account of PM cast AJ62 corrosion behaviour using experimentation such as mass loss due to immersion corrosion.

7.2.3 Corrosion of Solidified AJ62 in Engine Coolant [3]

The study has shown that the corrosion of permanent mould cast AJ62 in engine coolant intensifies with increases in casting thickness. Also, while the corrosion of the alloy does continue with prolonged exposure to engine coolant, the initial corrosion during the first week is responsible for the majority of the mass loss. This is particularly true for the thicker casting sections.

Initial corrosion may proceed according to reactions that govern the corrosion of the alloy in water as most engine coolants contain notable amounts of water. Hydrogen evolution and corrosion product deposits can be seen for a period following submersion into the coolant suggesting that this may be the case.

After this period but prior to one week of exposure, all specimen surfaces had developed a dark appearance. In combination with the reduction in hydrogen evolution this suggests the stabilization of a passive film most likely attributed to or accelerated by chemical inhibitors in the coolant.

Polarization testing of the extreme thicknesses indicated that corrosion behaviour of the alloy varies significantly with microstructure in the coolant. However, it may not

relate to the corrosion properties exhibited after passive film stabilization on the magnesium rich cells.

7.2.4 Effect of Chlorides and Inhibitors on Corrosion of Solidified AJ62

It has been clearly presented that finer microstructures have a significant advantage over their coarser counterparts in terms of corrosion. This advantage includes reduced current density for ion exchange as well as less negative open circuit potentials.

For exposure to environments where the electrolytic medium is uncontrolled, *i.e.*, external vehicular applications, developing a finer microstructure via thin sections, greater cooling rates, or some thermal treatment would be beneficial. These efforts are, however, undermined should the corrosive environment include a significant chloride concentration. Therefore, the resources required in developing a desirable microstructure should be weighed against the achievable corrosion resistance.

Other methods of corrosion resistance might include coating technologies for such applications. Depending on the type of coating, microstructure of the substrate may influence the performance of the coating. Thus in most circumstances some attempt to generate a fine microstructure should be made for application in uncontrolled environments.

In a controlled environment where the corrosive medium is a commercial engine coolant, chloride concentrations are low but anodic inhibitors make metallurgical considerations unappreciable in terms of ion exchange current. So the other two considerations are left: corrosion potential and polarization.

Achieving a fine structure reduces the galvanic driving forces significantly with respect to the coarser microstructure. If there is a cathodic surface in the coolant that

leads to severe galvanic corrosion a finer microstructure becomes more desirable. Meanwhile, the coarser microstructure passivating more easily with the help of the chemical additions in the coolant is desirable as well. It should be remembered, though, that passivation could lead to unexpected results in local, small, trapped volumes of electrolyte. This liability and the galvanic considerations ultimately lead to the recommendation of some effort in reducing SDAS for components exposed to coolant as well.

7.2.5 Influence of Corrosion on Mechanical Properties of AJ62

Samples were successfully corroded and parameters were chosen for the corrosion portion of the combined corrosion and mechanical response evaluation. The chosen sample showed pits having up to 250 μm radii. Specimens were then corroded and subsequently measured and pulled.

Engineering stress-strain curves pointed out that corrosion of specimens leads to a marked reduction in achievable elongation. Two theories based on widely accepted concepts, stress intensification and area reduction, do not necessarily explain the premature failure of the corroded specimens without consideration of pre-existing sub-surface defects apparent on the fracture surface.

Oxides forming in what appears to be an opened casting defect indicate that premature failure of corroded thick sections may be three-fold. Thick sections in PM AJ62 (i) fail in a brittle manner, (ii) have more large internal defects inherent to the processing, and (iii) suffer greater corrosion because of their microstructure. All of these conditions together allow for crack initiation by way of internal void and corrosion pit interaction. This interaction is unique to the combination of casting parameters, corrosion parameters, and alloy used in this study. As a recommendation, fine

microstructure is suggested for PM AJ62 regardless whether service life requires resistance to mechanical loading, corrosion, or a combination thereof.

7.3 FINAL RECOMMENDATIONS

In all of the preceding work, it can be seen that the finer of the observed microstructures is dominant when considering PM cast AJ62 mechanical and electrochemical properties. This fine microstructure is the product of a faster cooling rate and offers the recommendation that the casting process should be designed to target rapid solidification, when possible, for improved PM cast AJ62 properties.

7.4 REFERENCES

- [1] Burns, J.R., Han, L., Hu, H., Nie, X., Effects of section thicknesses on tensile properties of permanent mould cast magnesium alloy AJ62. Magnesium Technology 2010, The Minerals, Metals, and Materials Society. (2010) 367-371.
- [2] Burns, J.R., Hu, H., Nie, X., Su, J.F., Corrosion of permanent mould cast Mg alloy AJ62 in NaCl solutions. American Foundry Society. (2010) Paper No. 10-022.
- [3] Burns, J.R., Hu, H., Nie, X., Han, L., Microstructure influence on the corrosion of permanent mould cast magnesium alloy AJ62 in engine coolant. Society of Automotive Engineers. (2010) Paper No. 2010-01-0412.

APPENDIX A – CALCULATIONS FROM SECTION 6.3.3

Calculation for stress intensification of 0.25 mm radius semi-circle

Given: $a=0.00025$ m; $t=0.006$ m (6 mm thickness); $b=0.01$ m (half of 20 mm width assuming crack in the middle); and $S=110$ MPa.

$$f_a = \left(1.04 + 0.2017 \left(\frac{a}{t} \right)^2 - 0.1061 \left(\frac{a}{t} \right)^4 \right) \left(1.1 + 0.35 \left(\frac{a}{t} \right)^2 \right)$$

$$f_a = \left(1.04 + 0.2017 \left(\frac{0.00025}{0.006} \right)^2 - 0.1061 \left(\frac{0.00025}{0.006} \right)^4 \right) \left(1.1 + 0.35 \left(\frac{0.00025}{0.006} \right)^2 \right)$$

$$f_a = 0.911$$

$$f_w = \sqrt{\sec \left(\frac{\pi a}{2b} \sqrt{\frac{a}{t}} \right)}$$

$$f_w = \sqrt{\sec \left(\frac{\pi(0.00025)}{2(0.01)} \sqrt{\frac{0.00025}{0.006}} \right)}$$

$$f_w = 1.250$$

$$F = f_a f_w \frac{2}{\pi}$$

$$F = 0.911 \cdot 1.250 \cdot \frac{2}{\pi}$$

$$F = 0.725$$

$$K = FS\sqrt{\pi a}$$

$$K = 0.725 \cdot 110 \sqrt{\pi \cdot 0.00025}$$

$$K = 2.24 \text{ MPa/m}^{0.5}$$

Calculation for stress correction from reduced area

Given: $a=0.00025$ m; $A=0.020-0.006=0.00012$ m²; $N=10$; and $S=110$ MPa

$$A_{actual} = A - N \frac{\pi a^2}{2}$$

$$A_{actual} = 0.00012 - 10 \cdot \frac{\pi \cdot 0.00025^2}{2}$$

$$A_{actual} = 119E - 06 \text{ m}$$

$$S_{actual} = S \cdot \frac{A}{A_{actual}}$$

$$S_{actual} = 110 \cdot \frac{0.000120}{0.000119}$$

$$S_{actual} = 111 \text{ MPa}$$

Calculation for stress intensification of 1.25 mm radius semi-circle

Given: $a=0.00125$ m; $t=0.006$ m (6 mm thickness); $b=0.01$ m (half of 20 mm width assuming crack in the middle); and $S=110$ MPa.

$$f_a = \left(1.04 + 0.2017 \left(\frac{a}{t} \right)^2 - 0.1061 \left(\frac{a}{t} \right)^4 \right) \left(1.1 + 0.35 \left(\frac{a}{t} \right)^2 \right)$$

$$f_a = \left(1.04 + 0.2017 \left(\frac{0.00125}{0.006} \right)^2 - 0.1061 \left(\frac{0.00125}{0.006} \right)^4 \right) \left(1.1 + 0.35 \left(\frac{0.00125}{0.006} \right)^2 \right)$$

$$f_a = 0.906$$

$$f_w = \sqrt{\sec\left(\frac{\pi a}{2b} \sqrt{\frac{a}{t}}\right)}$$

$$f_w = \sqrt{\sec\left(\frac{\pi(0.00125)}{2(0.01)} \sqrt{\frac{0.00125}{0.006}}\right)}$$

$$f_w = 1.217$$

$$F = f_a f_w \frac{2}{\pi}$$

$$F = 0.906 \cdot 1.217 \cdot \frac{2}{\pi}$$

$$F = 0.702$$

$$K = FS\sqrt{\pi a}$$

$$K = 0.702 \cdot 110 \sqrt{\pi \cdot 0.00125}$$

$$K = 4.84 \text{ MPa/m}^{0.5}$$

APPENDIX B – COPYRIGHT RELEASES FOR PREVIOUSLY PUBLISHED MANUSCRIPTS

TMS copyright permissions

From:	Bob Makowski <makowski@tms.org>
Subject:	FW: Publication Permission Request
Date:	Mon, 5 Apr 2010 15:01:09 -0400
To:	"burnss@uwindsor.ca" <burnss@uwindsor.ca>

Dear Mr. Burns,

Thank you for contacting TMS with your request for permission for inclusion of the paper "Effects of Section Thicknesses on Tensile Properties of Permanent Mould Cast Magnesium Alloy AJ62" by Jonathan Burns, LiHong Han, Henry Hu, and Xueyuan Nie that was published in the Magnesium Technology 2010 Proceedings in your Master's thesis entitled "Tensile Behaviour and Microstructure of Permanent Mould Cast Magnesium Alloy AJ62 Subject to Corrosion". Permission is granted provided that a full citation or the original work from the Magnesium Technology 2010 proceedings is included. Thank you for your interest and participation in TMS Publications.

Best regards,

Robert A. Makowski

TMS Director of Publications Development

The Minerals, Metals & Materials Society

184 Thorn Hill Road

Warrendale, PA 15086

Telephone: 724-776-9000, extension 217

Fax: 724-776-3770

E-mail: <makowski@tms.org>

AFS copyright permissions

From:	"Laura Moreno" <Laura@afsinc.org>
Subject:	RE: Copyright permissions
Date:	Tue, 6 Jul 2010 09:12:35 -0500
To:	<burnss@uwindsor.ca>
Cc:	"Pam Lassila" <Pam@afsinc.org>

Dear Mr. Burns,

Permission granted. Please note the following: Copyright 2010 American Foundry Society.

Best regards,

Laura Moreno

Director, Special Publications

American Foundry Society

1695 N Penny Lane

Schaumburg, IL 60173

T 800-537-4237

T 847-824-0181 x241

F 847-824-7848

E lmoreno@afsinc.org

SAE copyright permissions

From:	Terri Kelly <terri@sae.org>
Subject:	RE: Copyrights and Permissions
Date:	Wed, 28 Apr 2010 19:00:28 +0000
To:	"burnss@uwindsor.ca" <burnss@uwindsor.ca>

Dear Mr. Burns,

Thank you for requesting permission to reprint material from SAE technical paper 2010-01-0412 – which you authored - in your master's thesis titled "Tensile Behaviour and Microstructure of Permanent Mould Cast Magnesium Alloy AJ62 Subject to Corrosion" for University of Windsor.

Permission is hereby granted, and we request the following credit statement be used: "Reprinted with permission from SAE paper number 2010-01-0412 © 2010 SAE International".

Permission is for this one-time use only. New requests are required for further use of the material. Please contact me if I can be of further assistance.

Regards,

Terri Kelly

Intellectual Property Rights Administrator

SAE International

Phone: 001.724.772.4095; Fax: 001.724.776.9765

E-mail: terri@sae.org

VITA AUCTORIS

NAME: Jonathan Robert Burns
PLACE OF BIRTH: Leamington, Ontario, Canada
YEAR OF BIRTH: 1985
EDUCATION: Leamington District Secondary School,
Leamington, Ontario 1999-2003
University of Windsor, Windsor, Ontario
2003-2008 B.A.Sc.
University of Windsor, Windsor, Ontario
2008-2010 M.A.Sc.